REHABILITATION OF RC INVERTED-T BENTCAP GIRDERS USING ANCHORED CFRP SHEETS

Mukesh Sekar

A Thesis

in

The Department

of

Building, Civil and Environmental Engineering

Presented in Partial Fulfillment of the Requirements

for the Degree of Master of Applied Science (Civil Engineering) at

CONCORDIA UNIVERSITY

Montréal, Québec, Canada

December 2006

Your file Votre référence
ISBN: 978-0-494-28903-7
Our file Notre référence
ISBN: 978-0-494-28903-7

ABSTRACT

REHABILITATION OF RC INVERTED-T BENTCAP GIRDERS USING ANCHORED CFRP SHEETS

Mukesh Sekar

Existing infrastructure includes significant number of reinforced concrete (RC) bridges that are old and designed based on outdated design codes. Inverted-T beams used as bentcap girders that support the bridge's longitudinal precast beams provided a popular structural system of many existing bridges. The structural behaviour of inverted-T beams is different than that of conventional top-loaded beams, due to the fact that the loads are introduced into the bottom flange rather than the top of the beam.

The objective of the present study is to experimentally examine the effectiveness of new rehabilitation techniques using anchored carbon fibre-reinforced polymer (CFRP) sheets to eliminate non-ductile failure mechanisms in hanger, web, and flange zones of RC inverted-T girders, and to analytically evaluate the effect of design variables on the failure mechanisms of FRP-rehabilitated RC inverted-T bentcap bridge girders.

The experimental phase of this study included conducting eight tests on four simply supported RC inverted-T girders before and after rehabilitation. The girders represent a $1/3^{rd}$ scale model of a prototype bentcap girder. The experimental results showed that the proposed new rehabilitation schemes proved to eliminate the non-ductile mechanisms in hanger, web, and flange zones. The rehabilitated girders were able to reach displacement ductility levels of up to 4 and showed an increase in strength up to 20% compared to the control girders.

The analytical phase of this study included conducting a parametric study on the effect of the uncertainties in the design variables on the failure mechanisms of an existing RC inverted-T bridge bentcap girder rehabilitated using externally bonded FRP sheets. The analytical study identified the design variables that are directly- or indirectly-proportional to the required content of FRP wraps that is needed to ensure a ductile response, which is useful for design engineers of rehabilitation schemes that uses externally-bonded FRP sheets.

முகவுரை

தற்போது வட அமெரிக்கா மற்றும் உலகமெங்கும் உள்ள உள்கட்டமைப்பு வசதிகளில் குறிப்பிடத்தக்க அளவு, கம்பியில் உறுதி செய்யப்பட்ட கற்காரை 1970ம் ஆண்டிற்கு முன் உள்ள தர மதிப்பிட்டு நடத்தை நெறி அடிப்படையில் வடிவமைக்கப் பட்டுள்ளது. ஆங்கில எழுத்தான டீ தலைகீழ் வடிவ உத்திரங்கள் பாலங்களின் முன்வார்ப்பு நீள உத்திரங்களை தாங்கி நிற்பது ஒரு பிரபலமான கட்டுமான அமைப்பு ஆகும். ஆங்கில 'டீ'ன் தலைகீழ் வடிவில் அமைக்கப்பட்ட இரும்பு உத்திரங்கள் எப்போதும் பழக்கத்தில் உள்ள மேலே பாரம் ஏற்றும் உத்திரங்களிலிருந்து மாறுபட்ட கட்டுமான தன்மையை வெளிப்படுத்துகிறது. இதில் பாரங்கள் மேல்பாகத்திற்கு பதில் உத்திரத்தின் அடிபாகத்தில் கொடுக்கப்படுகிறது.

இந்த ஆய்வு சக்தி வாய்ந்த உறுதிமிக்க தொழில்நுட்பத்துடன் கூடிய வளைக்க முடியாத கம்பியில் உறுதி செய்யப்பட்ட கருங்கல் கலவையால் செய்யப்பட்ட அசையாத கார்பன் நார் கலந்த பாலிமர் தகடுகள் குறித்த உயர் ஆய்வின் ஒரு பகுதியாகும். இந்த ஆய்வு வளைக்க முடியாத நேரங்களில் ஏற்படும் முறிவை தடுப்பதை குறிக்கோளாக கொண்டதாகும்.

தலைகீழ் வடிவ உத்திரங்கள் அகலம் மற்றும் ஆழத்திற்குண்டான விகிதாசாரம் 2.0 என்ற வகையில் செய்யப்பட்டு சோதனைக்கு உட்படுத்தப்பட்டது. அந்த நேரத்தில் ஒரே மாதிரியாக, முறிவு ஏற்படும் வரை உத்திரத்தின் மீது பாரம் கொடுக்கப்பட்டது. இந்த மாதிரி உத்திரமானது அசலில் மூன்றில் ஒருபாக அளவாகும். இந்த ஆய்வின் முடிவு புணர் நிர்மான திட்ட மற்றும் மறு இடமாற்ற, வளைக்கக் கூடிய குறியீட்டினை அதிகப்படுத்துவதுடன் உத்திரத்தின் எடை சுமக்கும் திறனையும் அதிகப்படுத்துகிறது.

ACKNOWLEDGEMENTS

I would like to express my sincere appreciation to my supervisor, **Dr. Khaled Galal,** professor in the department of Building, Civil and Environmental engineering, Concordia University for his encouragement, patience and endless support throughout the research steps. I believe this research would not have been completed without his sincere guidance, commitment and continuous support. Also, I would like to thank him for the funding provided throughout this research.

Also I would like to thank Structural laboratory technician Mr. Daniel Roy for his help and guidance during the experimental work. Many thanks to Mr. Ali Ahmed for his help with respect to the FE program (ABAQUS).

I would like to thank AMBEX Concrete Technologies for donating concrete and Fyfe Co. for the donating the CFRP sheets used in the current study.

I would like to give my colleagues in the Building, Civil and Environmental Engineering department warm thanks for their support and help whenever asked for.

Special thanks to Mr. Fernando Jr., Mr. Anil Kumar and Ms. K. Sasikala for their help during my research work. Many thanks are extended to all my friends for their support.

In India, I would like to thank my parents and my sisters for their immeasurable support and encouragement in every facet of my life despite the distance.

I offer my respectful obeisances unto the feet of my parents, who instilled the basic will to achieve

என்னுள் இலச்சியத்தை அடையும் நெருப்பை விதைத்த என் அம்மா அப்பாவின் பாதங்களில் விழுந்து சமர்பனம்!

TABLE OF CONTENTS

CHAPTER 5 EXPERIMENTAL RESULTS

LIST OF FIGURES

LIST OF TABLES

LIST OF SYMBOLS

a/t	Shear span-to-depth ratio
A_v	Total cross-sectional area of stirrups
A_s	Total area of longitudinal steel
b_w	Minimum width of cross section over the effective depth
B	Length of bearing pad along edge of flange
B_w	Width of bearing pad perpendicular to girder axis
d	Effective depth of cross section
d_f	Effective depth of flange from centroid of top layer of flange transverse reinforcement to the bottom of the flange reinforcement
e	Distance from face of web to center of bearing pad
E_{fu}	Elastic modulus of FRP in the principle fibre orientation
f'_c	Characteristic concrete compressive strength (MPa)
f_y	Yield strength of reinforcement (MPa)
f_{yv}	Yield strength of stirrups (MPa)
n	Number of FRP layers on one side of the beam
P	Total concentrated load acting on one the girder
PF/V	Punching force-to-shear force ratio
s	Spacing of stirrups
s_{vf}	Spacing of transverse reinforcement
θ	Angle of diagonal crack with respect to the member axis
α	Ratio of flange depth-to-depth of the girder
β	Ratio of flange over hang-to-width of the web
γ	Ratio of the effective depth-to-total girder depth
χ	Ratio of width of the web-to-total girder depth
ε_{fe}	Effective strain
$\varepsilon_{fd}, \varepsilon$	Design value of effective FRP strain
ρ_{vw}	Web transverse reinforcement ratio
ρ_{vf}	Flange transverse reinforcement ratio
ρ_f	Longitudinal steel ratio given
ρ_{FRP}	CFRP reinforcement ratio

CHAPTER 1

INTRODUCTION

1.1 GENERAL

The existing infrastructure in North America and worldwide includes significant number of reinforced concrete (RC) bridges and overpasses that are old and designed based on outdated design codes. The deterioration of such structures has significant economical and life safety impacts. This is evidenced by the increasing number of failures of such bridges (e.g. the collapse of the Laval overpass in Québec (CCE 2006)). Many of these infrastructures require rehabilitation to conform to the current design code provisions, meet the increased demand, enhance the performance, and extend the service life. The inadequacy of structural strength and ductility, and consequently the susceptibility to non-ductile failure mechanisms, are the main sources of the deterioration of RC bridges designed according to old codes. Prior to the enforcement of ductile design philosophy of 1970's, structures were designed on the basis of strength. Once the ultimate strength of a structure is reached, abrupt non-ductile deterioration follows, which results in a brittle failure. Also, events such as steel reinforcement corrosion, spalling of concrete cover, and the decrease in the materials' strength due to fatigue and aging, lead to the acceleration of such inadequacy in strength and ductility capacities of RC bridges.

Inverted-T beams used as bentcap girders that support the bridge's longitudinal precast beams provided a popular structural system of many existing bridges. The structural behaviour of inverted-T beams is different than that of conventional top-loaded

beams, due to the fact that the loads are introduced into the bottom flange rather than the top of the beam. The flange of the inverted-T serves as a shallow shelf to support precast beams while the stem of the inverted-T, rising to the height of the supported beams, provides the needed depth to sustain flexure and shear forces. Early investigations that studied the behaviour of inverted-T beams identified three main categories of non-ductile failure mechanisms depending on location, which are failure in hanger zone, failure in web, and failure in flange.

Recent research studied the upgrade of reinforced concrete (RC) bridge girders using externally bonded fibre-reinforced polymers (FRP) as an alternative for conventional strengthening techniques such as using steel plates, reinforced concrete jackets, or external post-tensioning. Externally bonded FRP reinforcement is an attractive rehabilitation technique due to its tailorable performance characteristics, ease of application, high strength-to-weight ratio, and non-corrosiveness characteristics.

Despite the use of inverted-T beam in several existing parking structures and bridge bentcaps that were designed according to older codes, minimal research attention had been found in the literature in evaluating their strengthening techniques using FRP composites. Most of the previous research activities focused on rehabilitating RC rectangular and regular T-sections.

1.2 OBJECTIVE

The objective of the present study is to experimentally examine the effectiveness of new strengthening techniques using carbon Fibre-reinforced polymer (CFRP) sheets to

eliminate non-ductile failure mechanisms in hanger, web, and flange zones of RC inverted-T girders.

1.3 SCOPE

In order to achieve the study objectives, the scope of the work is as follows:

1. To analytically evaluate the effect of design variables on the failure mechanisms of FRP-rehabilitated RC inverted-T bentcap bridge girders.
2. To experimentally evaluate the efficiency of new rehabilitation techniques using CFRP sheets on strengthening the hanger, shear and punching resisting mechanisms of inverted-T girders.
3. To model the tested RC girders using a commercially available non-linear analysis software to predict their load carrying capacities in comparison with the experimental ones.

CHAPTER 2

LITERATURE SURVEY

2.1 INTRODUCTION

As mentioned in Chapter 1, the objective of the current study is to examine the effectiveness of new rehabilitation techniques using CFRP sheets in eliminating non-ductile failure mechanisms of RC inverted-T girders. Despite the importance of the problem, there has been limited research conducted on the performance of RC inverted-T girders. Although the use of FRP sheets for rehabilitating rectangular and regular T-beams has been investigated extensively, yet there is no study in the available literature explored their application for rehabilitating inverted-T girders. In this chapter, previous research related to the above mentioned areas are briefly reviewed with the highlight on the points related to the current investigations.

2.2 BRIDGE SYSTEMS

Many existing bridges are of the slab-on-girder type system (Figure 2.1 and 2.2). The super structure of such bridge system consists of a concrete slab resting on a set of stringers which are connected together through cross-diaphragms every spacing. The stringers could be steel beam, reinforced concrete or precast prestressed beams. Inverted-T girders act as a support for the stringers in order to transfer the load to the bridge piers. Depending on the number, and location of the pier, inverted-T bentcap girder can be

simply supported, cantilevered over simple supports, or they can be constructed monolithically with columns or piers. They reduce the overall depth of the bridge deck system (i.e. slab, stringer, inverted-T bentcap girder) by avoiding deep rectangular bentcap girders beneath the stringers.

2.2.1 Behaviour of RC inverted-T girders

Inverted-T girders provide a natural and popular structural form to support precast beams. The flange of the inverted-T serves as a shallow shelf to support precast beams while the stem of the inverted-T, rising to the height of the supported beams, provides the needed depth to sustain flexure and shear forces.

The structural behaviour of the inverted-T shape differs from that of the more conventional top-loaded standard T-section in the following ways:

- Loads that are introduced from precast beams into the bottom rather than into the sides or the top of the web must be supported by stirrups acting as hangers to transmit vertical forces into the body of the web.
- Flange reinforcement perpendicular to the web is necessary to deliver flange forces to the hangers in the web.
- Application of flange forces occurs at a greater distance from the centerline of the web, thereby creating greater twisting forces on the web.

The current Canadian highway bridge design code (CHBDC 2000) does not specify design guidelines for the design (or rehabilitation) of inverted-T bentcap girders. Mirza and Furlong (1983) worked on identifying the behaviour of RC inverted beam and categorized 3 modes of failures according to its location; they are hanger, web and flange.

Hanger failures were the failures of stirrups acting as hangers supporting the concentrated loads on the bracket. Web failures involved shear compression or a shear off compression zone. Flange failures were attributed either to shear friction or flexure were accompanied by punching shear contributions longitudinally in the bracket. Figure 2.3 shows the structural actions on Inverted-T girder. Mirza and Furlong (1985) proposed empirical formulas for the design of RC inverted-T girders and different failure mechanisms are explained in the following subsections:

2.2.1.1 Hanger failure of stirrups

It is failure (Figure 2.4) of stirrups acting as hangers in delivering the bracket loads to the upper part of the inverted T-beam web. Failure by excessive yielding of hanger bars at the web-flange junction nearest the concentrated loads that permitted a failure of the bracket or the overall shear failure of the web.

To achieve safe delivery of flange loads into the web, following equation was suggested by Mirza and Furlong (1985),

$$\frac{A_v}{s} = \frac{P - 0.332\sqrt{f_c'}b_f d_f}{f_y\left(B + 2d_f\right)} \qquad [2\text{-}1]$$

In which,

A_v = total cross-sectional area of stirrups that are spaced at spacing's'.

f'_c = Characteristic concrete compressive strength (MPa)

f_y = Yield strength of reinforcement (MPa)

2.2.1.2 Shear compression failure in web

Shear-compression failure (Figure 2.5) is characterized here by the propagation of a diagonal tension crack towards the compression zone of a beam, followed by the eventual crushing-spalling of concrete in the compression zone.

2.2.1.3 Shear off-compression zone in web

The failure (Figure 2.5) that follows the shearing-off of the compression zone along the diagonal crack line represents a failure mode that differs from the shear-compression type of failure. Such a failure occurs only when the web shear span-to-depth ratio is small enough to ensure adequate concrete flexural compression strength in resisting the bending moment developed by the shear force acting through the shear span. For large shear spans, shear-compression failure occurs when flexural compression capacity is reached. Hence, failures due to the diagonal tension and subsequent shearing-off of the compression zone occur in beams with smaller shear span-to-depth ratios than those of beams involving shear-compression failures.

2.2.1.4 Punching flexure failure in bracket

A punching failure (Figure 2.6) involves a diagonal tension separation along a truncated pyramid around a concentrated load. This failure is distinguished here from flexural failure in the bracket by the lack of crushing in the compression zone at the bottom of the bracket. When crushing occurs in the compression zone at the bottom of the bracket, the failure is said to be a flexural failure. With heavy hanger bars and relatively light bracket flexural reinforcement, the secondary compression occurs along

the centerline of the loaded area at the bottom face of the bracket after excessive yielding of the transverse flexural steel in the bracket. With the light hanger steel and relatively heavy bracket flexural bars, a punching type of failure occurs without the secondary compression failure.

The flange should be deep enough to prevent punching shear failure. This can be achieved by satisfying the following equation proposed by Mirza and Furlong (1985) for effective flange depth (d_f) from the top face of the flange to the top of the bottom layer of transverse reinforcement in the flange.

$$0.332\sqrt{f_c'}\,(B_p+2d_f) \geq P \qquad [2\text{-}2]$$

In which,

$B_p = B+2B_w$

B = length of bearing pad along edge of flange

B_w = width of bearing pad perpendicular to girder axis

P = Total concentrated load acting on the girder

2.2.1.5 Shear friction failure in bracket

A shear friction failure in inverted T-beams occurs when the concrete fails by sliding or shearing along the plane represented by the vertical face of the web at the interface of the web and the flange.

The effective depth of flange (d_f) from centroid of top layer of flange transverse reinforcement to the bottom of the flange reinforcement that is required to fulfil shear friction requirements was proposed by Mirza and Furlong (1985) to satisfy the following equation:

$$0.2 f_c' d_f (B + 4e) \geq P \qquad [2\text{-}3]$$

In which,

e = distance from face of web to center of bearing pad

$0.2 f_c'$ = shear strength of concrete resisting shear friction

2.3 STRENGTHENING OF RC BEAMS USING EXTERNALLY BONDED FRP SHEETS

Externally bonded reinforcement for the rehabilitation of concrete components traditionally involved the application of steel plates to the tensile face of structural components for strengthening. However, the use of the steel plates as external reinforcement presented the following disadvantages, (a) Deterioration of the bond at the steel concrete interface from steel corrosion; (b) Difficulty in handling of the plates at the construction site; (c) Increased load demand on the structure; (d) Restrictions on length of steel plates due to weight (Karbhari and Seible 2000; Traiantafillou and Plevris 1991). In order to develop an alternative to bonding of steel plates, the use of FRP composites for strengthening RC structures was first investigated at Swiss Federal Laboratory for Materials Testing and Research (EMPA) where tests on RC beams strengthened with CFRP plates were conducted in 1984 (Teng et al. 2003).

FRP materials are lightweight, noncorrosive, and exhibit high tensile strength (ACI 2002) and can be tailored to performance requirements via volume fraction control and/or fiber orientation on the matrix to obtain maximum efficiency (Karbhari and Seible 2000). FRP composites are available in a variety of forms ranging from factory-made laminates to dry fabrics that can conform to the geometry of the structure before adding resin (ACI 2002; Teng et al. 2003).

FRP composite materials possess important qualities, which suggest immense potential to application of civil structures. As such, the replacement of externally bonded steel plates with externally bonded FRP composites has been the focus of many researches in the recent past to repair, strengthen, and retrofit RC structures (Teng et al. 2003). FRP composites possess the following characteristics, which provide advantages in terms of materials properties and use in field applications, (a) High strength-to-weight and stiffness-to-weight ratios, (2) Enhanced fatigue life, (3) Corrosion Resistance, (4) Potential lower life cycle costs (Karbhari and Zhao 2000). In addition, the lightweight nature of the materials and ease of application make for an attractive for construction purposes.

A rehabilitation strategy, such as flexural strengthening of a RC bridge deck with CFRP composites, can be performed without interference of the intended function of the structure; i.e., no interference with traffic. Although, significant advantages are realized with FRP composites for bridge strengthening and repair, questions regarding quality and durability of FRP composites at the material level remain as well as the effect of FRP materials degradation on the long-term response of the rehabilitated component. It should be noted, however, the current codes for conventional materials don not provide an explicit method for incorporation of materials degradation and hence this in itself is a major contribution.

2.4 CONTRIBUTION OF MATERIALS TO SHEAR CAPACITY

2.4.1 Concrete and steel

One hundred years ago, the Swiss engineer Ritter published his famous paper on shear in reinforced concrete (Ritter 1899). His "45° truss model" became the basis of many building codes in North America and around the world. Ritter's model assumed that after cracking of the concrete, the behaviour of a reinforced concrete beam becomes analogous to that of a truss with a top longitudinal concrete chord, a bottom longitudinal steel chord, vertical steel ties, and diagonal concrete struts inclined at 45°. The models also assumed that the diagonally cracked concrete cannot resist tension and thus eliminated the need for diagonal tension members' perpendicular to the concrete struts. The shear force was assumed to be resisted by forces in the transverse steel, commonly referred to as the steel contribution (V_s). For the usual case of transverse reinforcement which is at 90° to the longitudinal reinforcement,

$$V_s = \frac{A_v f_y d_v}{s} \qquad [2\text{-}4]$$

Over the past 100 years, thousands of tests have been conducted to study the shear behaviour of reinforced and prestressed concrete beams. These experiments studied the effects of the numerous parameters that affect the shear behaviour, such as the concrete compressive strength, the amount and distribution of transverse and longitudinal reinforcement, prestressing, span to depth ratio, beam size (size effects), and the magnitude of coexisting bending moments and axial loads. Based on the experimental results, many semi-empirical modifications have been proposed to improve Ritter's 45° truss model. The main modification has been the addition of a semi-empirical concrete

contribution term (V_c) to the steel contribution term (V_s) in the equation for total shear resistance. To account for the effects of the parameters affecting the shear strength, this traditional method includes different expressions and numerous attached restrictions for the calculation of the concrete contribution factor V_c.

As in the tradition approach, the concrete contribution to the shear strength is related to square root of the concrete compressive strength ($\sqrt{f_c'}$). Thus,

$$V_c = \beta\sqrt{f_c'}b_w d_v \qquad [2\text{-}5]$$

2.4.2 Contribution of FRP to shear capacity

FRPs were first used as external reinforcement to strengthen reinforced concrete beams at the Swiss Federal Laboratories for Materials Testing and Research (EMPA) (Meier 1992). The research conducted by Meier et al. examined the effectiveness of epoxy bonding thin CFRP plates to the underside of reinforced concrete beams. Flexural strengthening of reinforced concrete member with external epoxy-bonded FRP laminates has been studied in detail by researchers at several institutions, including EMPA, the German Institute for Structural Materials, Building construction, and Fire Protection (IBMB), the Massachusetts Institute of Technology, and the University of Arizona (Meier 1992). These studies have examined both the short-term and the long-term performance of reinforced concrete beams strengthened by carbon, glass, or aramid FRP epoxy-bonded laminates. Among the topics investigated was the static, creep and fatigue behaviour, the effect of various types of adhesives and composite materials on the response, the use of pretensioned laminates, the behaviour under fire and the development of design procedures based on reliability theory. The results obtained through such investigations have proved that the FRP-strengthening technique is highly

efficient and effective, especially when the FRP materials are made using carbon fibres (CFRP), and have led to hundred of applications worldwide.

Triantafillou and Plevris (1991) investigated the collapse mechanism of post-strengthened beams strengthened by FRP sheets. The strain compatibility method, concepts of fracture mechanics and a model of FRP peeling-off mechanism were used to develop a systematic approach to the study of the behaviour of FRP bonded beams. The assumptions in the analytical model were the same as those of An et. al (1991), which were similar to the classical theories of reinforced concrete members subjected to flexure. FRP strengthened beams were assumed to fail in several flexural modes and the pertinent strength equations were developed.

Uji (1992), tested reinforced concrete beams strengthened in shear with wrapped-around carbon fabrics and CFRP laminates bonded to the vertical sides. Eight concrete beams (100 mm x 200 mm x 1300 mm), consisting of 2-16 mm diameter bars in tension and compression, and 6 mm diameter stirrups at 70 mm spacing (shear reinforcement of 0.81%) were used. His model for the FRP contribution to shear capacity is based on rather arbitrarily defined FRP-concrete bonding interfaces, which during peeling-off of the fabrics, carry average shear stresses determined by experiments (to be about 1.3 MPa). The upper limit to the FRP contribution is given by its tensile strength. He concluded that CFRP stirrups carry greater shear force than calculated from the ratio of the cross-sectional area of CFRP stirrups and the internal stirrups.

The work of Al-Sulaimani et al. (1994), dealt with shear strengthening using fiberglass plate bonding (FGPB) techniques. Their model for the contribution of composites to shear capacity is based on the assumption of FRP-concrete interfaces

which carry average shear stresses during peeling-off equal to 0.8 MPa and 1.2 MPa for the case of plates and strips, respectively.

Chajes et al. (1995) carried out extensive series of experiments on reinforced concrete beams strengthened using composites with various types of fibres, namely glass, aramid, and carbon. He tested twelve reinforced concrete T-beams to study the effect of using externally applied composite fabric as a method of increasing beam shear capacity. Three different types of composite were used in the study so that the effects of the fabric modulus of elasticity and tensile strength could be examined. The selection of the adhesive was based on the results of pull-off tests using 25 mm wide fabric bonded to a concrete specimen. Test results for eight beams strengthened for shear were compared with the corresponding results for the four control beams. De-bonding of the fabric from concrete did not occur in any of the tests. The behaviour of the strengthened beams was similar to that exhibited by the control beams both before and after cracking. Before cracking in the beam occurred, recorded strains in the fabric were very low. However, after cracking, the fabric strains increased significantly until failure occurred. The test results indicated that externally bonded composite fabric increased the ultimate shear strength by 60 to 150%. An analytical method was presented for predicting the ultimate shear capacity of beams strengthened with bonded composite. In this work, the FRP contribution to shear capacity is modeled in analogy with steel stirrups and assumes a limiting FRP strain, which was determined by experiments to be approximately equal to 0.005.

Chaallal et al. (1998) proposed a model by assuming that the bonded FRP contributes to the shear capacity in the same way as that of internal steel shear

reinforcement. Also he did some work on debonding and found that tensile strength of the FRP can always be fully utilized if there is a sufficiently long bond length.

At another research effort, Triantafillou (1998) report on strengthening of reinforced concrete beams in shear using epoxy-bonded composite materials in the form of laminates or fabrics and based on limit states, the design of FRP-strengthened members can be treated in analogy with the design of internal shear reinforcement, provided that an effective FRP strain is used in the formulation. He concluded that the effectiveness of the technique increases almost linearly with the FRP axial rigidity and reaches a maximum, beyond which it varies very little.

Triantafillou (1998) and Triantafillou and Antonopoulos (2000) demonstrated that when the concrete member reaches its shear capacity, the external FRP is stretched in the principle fibre direction up to a strain level, which is, in general, less than the tensile fracture strain (ε_{fu}). This strain is defined as effective strain, (ε_{fe}) to reflect the fact that if it were multiplied by the FRP elastic modulus in the principal fibre direction, (E_f), and the available FRP cross sectional area, it could provide the total force carried by the FRP at shear failure of the element.

According to the model of Triantafillou (1998), the external FRP reinforcement may be treated in analogy to the internal steel (accepting that the FRP carries only normal stresses in the principle FRP material direction), assuming that at the ultimate limit state in shear (concrete diagonal tension) the FRP develops as effective strain in the principal material direction, ε_{fe}. The effective strain ε_{fe} is in general less than the tensile failure strain ε_{fu}. Hence, the FRP contribution to shear capacity, V_{fd}, can be written as,

$$V_{fd} = 0.9.\varepsilon_{fd}, \varepsilon.E_{fu}.\rho.b_w.d(\cot\theta + \cot\alpha)\sin\alpha \qquad [2\text{-}6]$$

Where,

$\varepsilon_{fd}, \varepsilon$ = design value of effective FRP strain

b_w = minimum width of cross section over the effective depth

d = effective depth of cross section

ρ = FRP reinforcement ratio equal to $(2.t_f.\sin\alpha)/b_w$ for continuously bonded shear reinforcement of thickness tf (b_w = minimum width of the concrete cross section over the effective depth), or $(2t_f/b_w)(b_f/s_f)$ for FRP reinforcement in the form of strips or sheets of width b_f at a spacing s_f

E_{fu} = elastic modulus of FRP in the principle fibre orientation

θ = angle of diagonal crack with respect to the member axis, assumed equal to 45°

α = angle between principle fibre orientation and longitudinal axis of member

Triantafillou (1998) observed the effective strain to be a function of the axial rigidity of the FRP sheet ($\rho_f E_f$) and based on experimental results, for several rigidities of FRP sheet a relationship between effective strain and axial rigidity was found as

$$\varepsilon_{fe} = 0.0119 - 0.0205(\rho_f E_f) + 0.0104(\rho_f E_f)^2 \; for \; 0 \le \rho_f E_f \le 1GPa \qquad [2\text{-}7]$$

$$\varepsilon_{fe} = 0.00245 - 0.00065(\rho_f E_f) for \; \rho_f E_f > 1GPa \qquad [2\text{-}8]$$

Based on more experimental data, Khalifa (1998) modified the Triantafillou model based on the observation that $\rho_f E_f$ does not exceed 1.1 GPa in all data. In this

model (effective stress method) to eliminate the effects of various types of FRP sheet, the ratio of effective strain to ultimate strain, R = $\varepsilon_{fe} / \varepsilon_{fu}$, is plotted versus axial rigidity and the best polynomial fit to the data is given by

$$R = 0.5622(\rho_f E_f)^2 - 1.2188(\rho_f E_f) + 0.778 \leq 0.50 \qquad [2\text{-}9]$$

The ratio of the effective strain to ultimate strain, R, may be used as a reduction factor on the ultimate strain. $\varepsilon_{fe} = R\varepsilon_{fu}$

Similarly, Khalifa proposed another equation for reduction factor based on bond mechanism between the CFRP sheet and the concrete which is given by,

$$R = \frac{0.0042(f_c')^{2/3} w_{fe}}{(E_f t_f)^{0.58} \varepsilon_{fu} d_f} \qquad [2\text{-}10]$$

By experience and common practice, the upper limit of the reduction factor is taken as 0.5 and the governing value of R is then the lowest result among the two methods.

With the available experimental results Triantafillou (2000) suggests that debonding is not likely to dominate in the case of fully wrapped CFRP. If debonding is not dominant, the effective strain appears to depend on the type of FRP due to the very different fracture strain of materials used. Using his above statement he had generated the best fit power-type expressions for the available test data. Which are given by

Premature shear failure due to debonding

$$\varepsilon_{fe} = 0.65\left(\frac{f_c^{2/3}}{E_f \rho_f}\right)^{0.3} x10^{-3} \qquad [2\text{-}11]$$

Shear failure combined with or followed by CFRP fracture

$$\frac{\varepsilon_{fe}}{\varepsilon_{fu}} = 0.17\left(\frac{f_c^{2/3}}{E_f \rho_f}\right)^{0.3} \qquad [2\text{-}12]$$

Based on a rational bond strength model between FRP and concrete, Chen (2003) developed a model for debonding failures in FRP shear strengthened beams. This model explicitly recognizes the non-uniform stress distribution in the FRP along a crack as determined by the bond strength between FRP strips and concrete. According to the author the FRP contribution to shear capacity is expressed as

$$V_{frp} = 2 f_{frp,e} t_{frp} w_{frp} \frac{h_{frp,e}(\cot\theta + \cot\beta)\sin\beta}{s_{frp}} \qquad [2\text{-}13]$$

Taken the non-uniformity of stresses in the FRP intersected by the critical shear crack into consideration, the effective or average stress in the FRP at the ultimate limit state $f_{frp,e}$, was defined as

$$f_{frp,e} = D_{frp}\sigma_{frp,\max} \qquad [2\text{-}14]$$

In which $\sigma_{frp,\max}$ is the maximum stress in the FRP and D_{frp} is termed as the stress distribution factor which is defined as

$$D_{frp} = \frac{\int_{zt}^{zb} \sigma_{frp,z}\, dz}{h_{frp,e}\sigma_{frp,\max}} \qquad [2\text{-}15]$$

Where $\sigma_{frp,z}$ is the stress in the FRP at the ultimate limit state at the location where the intersecting critical shear crack is at a coordinate *z*.

2.5 SUMMARY

In this chapter, the behaviour of existing RC inverted-T girder is reviewed. The development in strengthening of rectangular and regular-T RC beams using externally bonded FRP sheets is surveyed. The literature review indicates that the behaviour of FRP-rehabilitated inverted-T girders need to be explored due to the fact that the loads acting from the stringers on the inverted-T girder flanges will change the load path and behaviour of the inverted-T girder compared to that of the conventional top loaded ones.

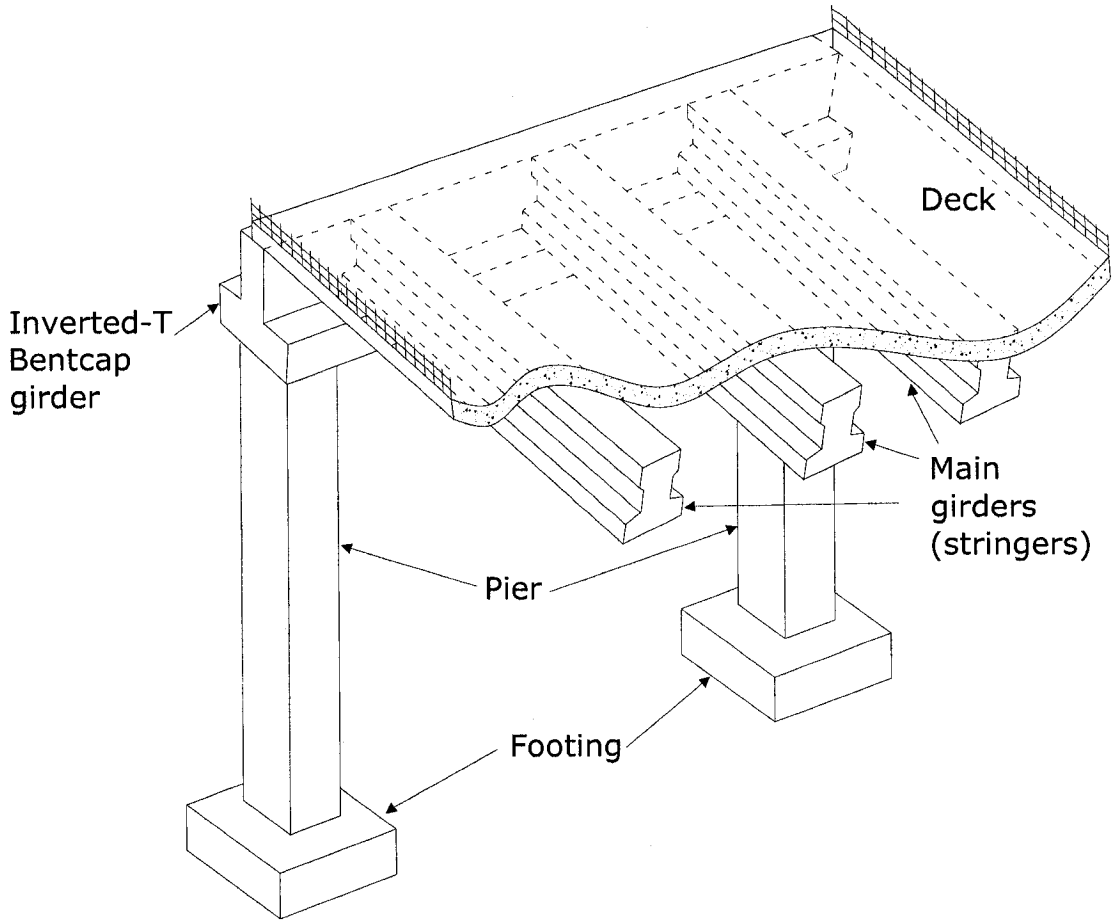

Figure 2.1 Structural system of an inverted-T bentcap girder

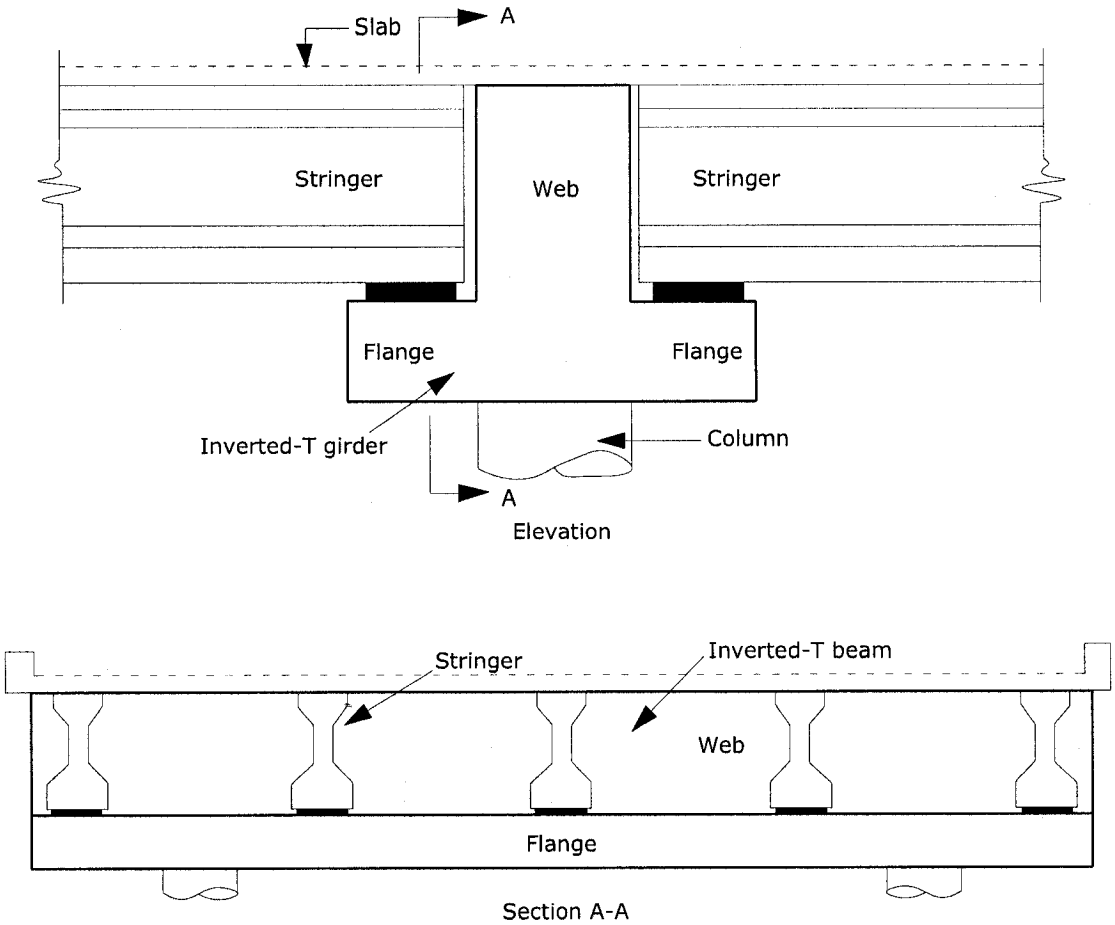

Figure 2.2 Inverted-T girder bentcap

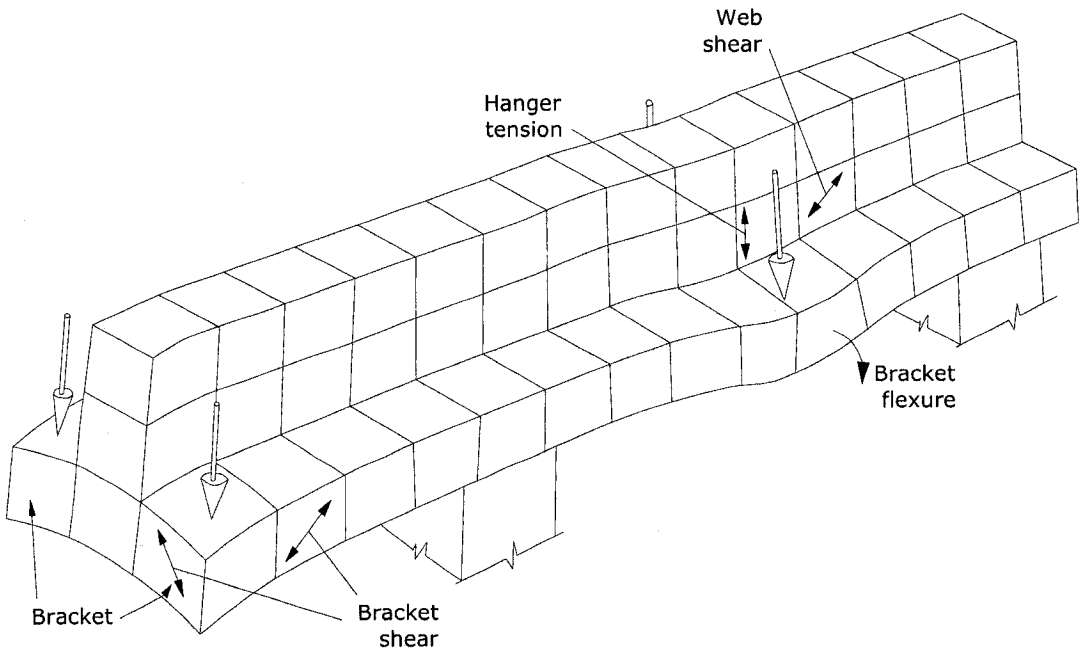

Figure 2.3 Structural actions on Inverted-T girder

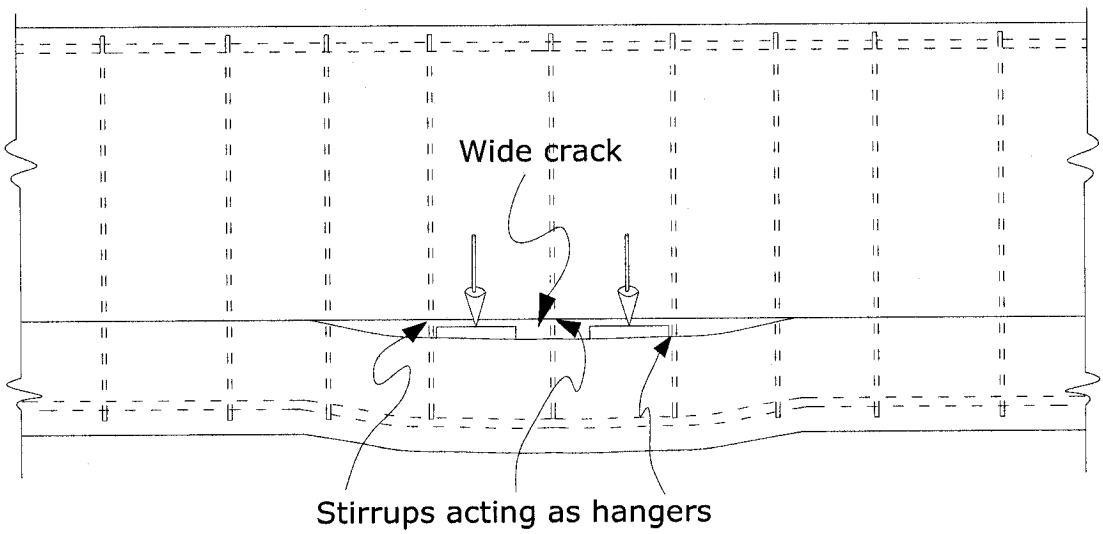

Figure 2.4 Hanger failure mode

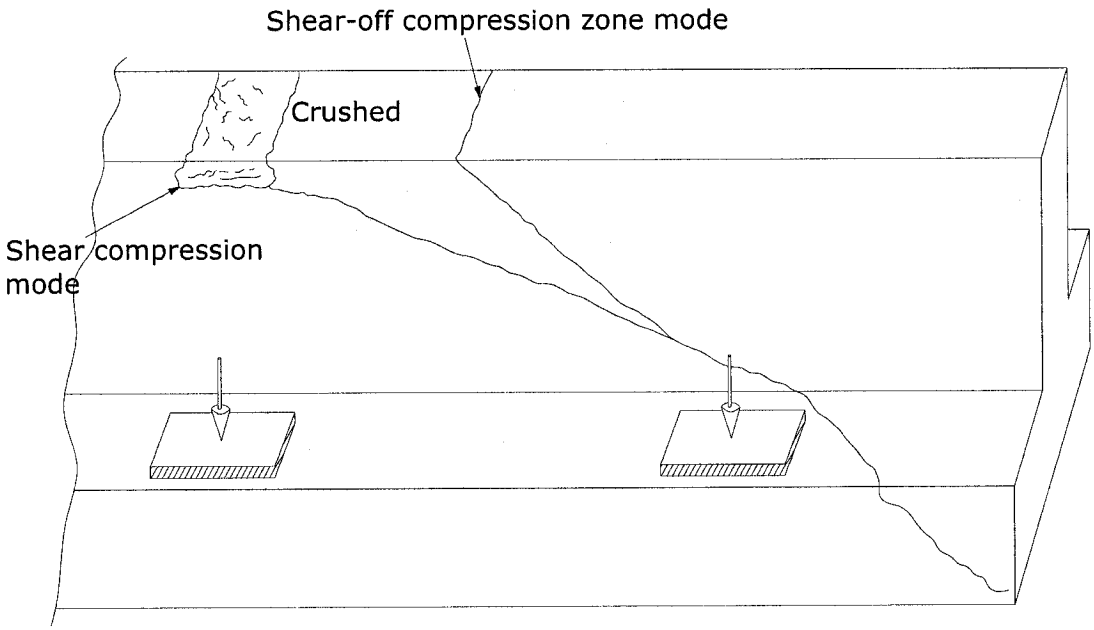

Figure 2.5 Typical shear compression and shear-off compression zone mode

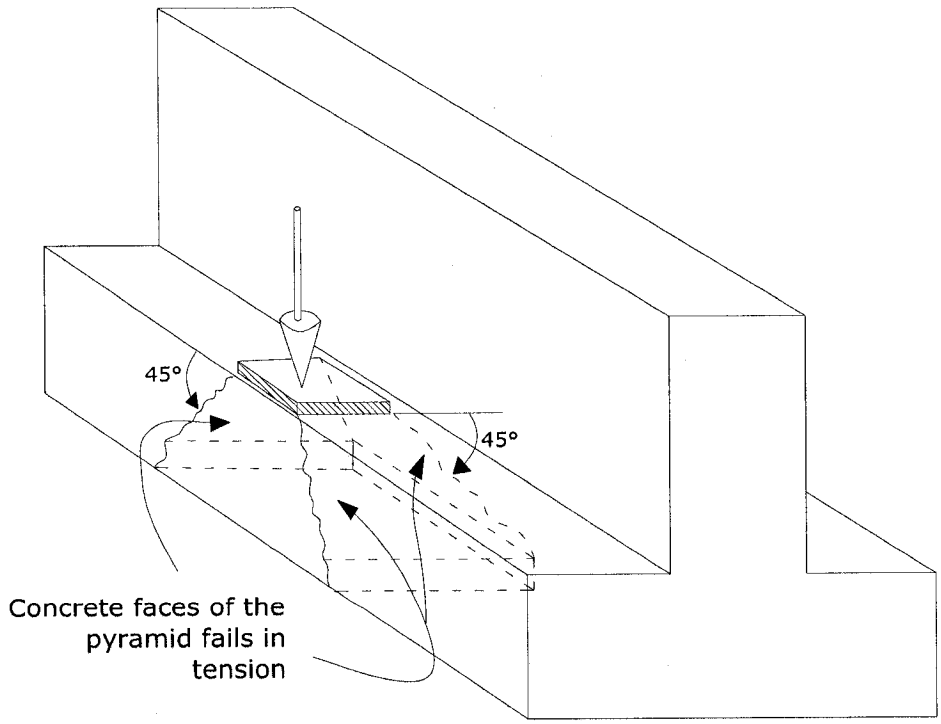

Figure 2.6 Typical punching shear failure mode

CHAPTER 3

EFFECT OF THE DESIGN VARIABLES ON THE FAILURE MECHANISMS OF FRP-REHABILITATED RC INVERTED-T BRIDGE BENTCAP GIRDERS

3.1 INTRODUCTION

The number of existing infrastructures that are in need for rehabilitation is increasing every day. Among these are inverted-T girder bridge bentcap girders that are susceptible to non-ductile failure. Recent research showed that externally bonded fibre-reinforced polymer (FRP) sheets can increase the shear strength of existing bridge girders. Previous research on the in-plane behaviour of RC inverted-T girders identified three main categories of non-ductile failure mechanisms, viz. failure in hanger, failure in web and failure in flange. Figure 3.1 shows an inverted-T bentcap girder with stringers supported on the shelf formed by the flange of the inverted-T. A designer of a rehabilitation scheme using externally bonded FRP sheets for an existing inverted-T girder should develop an understanding of the influence of different factors on the girder's failure mechanisms. Unlike in laboratory-tested girders, designing the required number of FRP sheets to ensure a ductile behaviour by reaching the flexural capacity of the girder of an existing old bridge, might involve several uncertainties in the design variables. These design variables include the mechanical properties of concrete and longitudinal and transverse reinforcements, and the content of the longitudinal, web and flange reinforcements. Other variables that affect the failure mechanism are: cross-

sectional relative dimensions, shear span-to-depth ratio and punching force-to-shear force ratio.

The objective of this chapter is to evaluate the effect of the abovementioned variables on the failure mechanisms of FRP-rehabilitated RC inverted-T girder bridge bentcaps.

3.2 FAILURE MECHANISMS OF FRP-REHABILITATED INVERTED-T GIRDERS

Previous research on RC inverted-T girders (Mirza and Furlong 1985) proposed empirical formulas for the design of regular RC inverted-T girders. The empirical formulas provide limits for the web stirrups acting as hangers to transfer flange forces to the web, the girder web and the design of the flange. In this chapter, these empirical formulas will be simplified to express the shear strength capacity (V/bt) of the girder web in terms of design variables. The expected increase of the shear strength capacity for FRP- rehabilitated girders (due to the use of FRP sheets) is included. Consequently, the effect of varying these design variables on the shear stress capacity and the failure mechanism of FRP-rehabilitated inverted-T girders is studied in this chapter. Table 3.1 and Figure 3.2 show the notations of the design variables that are used in the current study. Design parameters can be grouped in four categories; namely, material properties, cross-sectional geometric properties, reinforcement content ratios, and longitudinal span/load properties. The following sub-sections describe briefly the design formulas (Mirza and Furlong 1985) that govern different failure mechanisms, while equations 3-1 to 3-7 give the corresponding shear strength capacity in terms of the design variables f'_c,

f_{yv}, f_y, χ, β, γ, α, ρ_{vw}, ρ_{vf}, ρ_f, ρ_{FRP}, ρ_{FRP}, and PF/V. Definitions of design variables are described in Table 3.1

3.2.1 Hanger failure mechanism

Forces are transmitted from the flange to the web of the inverted-T girder through web stirrups that are acting as hangers at the vicinity of the stringers. The necessary hangers are governed by (Mirza and Furlong 1985), $\frac{A_v}{s} = \frac{P - 0.332\sqrt{f_c'}b_f d_f}{f_y(B + 2d_f)}$ therefore

$$\frac{V}{bt} = \frac{\rho_{vw} f_{yv}(\beta\chi + 2\alpha) + 0.332 f_c'(1 + 2\beta)\alpha}{(PF/V)_{ratio}} \qquad [3\text{-}1]$$

Where, A_v = total cross-sectional area of stirrups that are spaced at spacing's', B = length of bearing pad along edge of flange, b_f = width of flange and f'_c = compressive strength of concrete.

3.2.2 Shear and flexural failure mechanism

The forces transferred from the flange to the web through the hanger stirrups are then transferred to the supports through web shear and flexure mechanisms. The *nominal shear* capacity of the web is the sum of the contribution from concrete and steel mechanism in accordance with CSA (2004) is given by $\frac{V}{bt} = 0.2\sqrt{f_c'}\gamma + \rho_{vw} f_{yv}\gamma$ [3-2]

The *flexural capacity* of the girder can be evaluated using sectional analysis and expressed in terms of V/bt as, $\frac{V}{bt} = \frac{\rho_f f_y \gamma^2 (1 - (\rho_f f_y)/(2 f_c'\alpha_1))}{(a/t)_{ratio}}$ [3-3]

Where, ρ_f = Longitudinal steel ratio.

3.2.3 Flange failure mechanism

The strength of the flange should be adequate to sustain the punching shear action of the stringer loads applied on the flange. In addition, the flange should be able to resist the shear friction forces at the face of the web caused by the bracket action of the flange.

The *Punching shear* in the flange is governed by (Mirza and Furlong 1985) $0.332\sqrt{f_c'}\,(B_p+2d_f)\,d_f \geq P$ by having d_f shown in Figure 3.2. Where, $B_p = B+2B_w$, B, B_w shown in Figure 3.1; P = Total concentrated load acting on the girder. Thus, the shear strength capacity can be simplified as

$$\frac{V}{bt}=\frac{0.332\sqrt{f_c'}(3\beta+2\gamma\alpha/\chi)\gamma\alpha}{(PF/V)_{ratio}} \qquad [3\text{-}4]$$

The *bracket-type shear friction* in the flange is governed by (Mirza and Furlong 1985)

$0.2f_c'd_f(B+4e)\geq P$

therefore

$$\frac{V}{bt}=\frac{0.2f_c'\alpha\gamma(\beta+2\beta)}{(PF/V)_{ratio}} \qquad [3\text{-}5]$$

Where, $0.2f_c'$ = shear strength of concrete resisting shear friction.

The *transverse reinforcement required to satisfy shear friction* in the flange is governed by (Mirza and Furlong 1985) $\mu\, A_{vf} f_y \geq P$ therefore

$$\frac{V}{bt}=\frac{\mu\rho_{vf}\alpha(\beta+2\beta)f_{yv}}{(PF/V)_{ratio}} \qquad [3\text{-}6]$$

Where, μ = co-efficient of sliding friction taken as 1.4 for normal weight concrete.

The *flange transverse reinforcement required to resist flexural tension* is governed by (Mirza and Furlong 1985) $0.8\, d_f A_{sf} f_y \geq Pe$ therefore

$$\frac{V}{bt}=\frac{5.6\alpha^2\rho_{vf}\chi\ f_{yv}}{(PF/V)_{ratio}} \qquad [3\text{-}7]$$

Where, $0.8\ d_f$ = effective distance between centroid of compression and centroid of tension for calculating flexural reinforcement in flange.

3.2.4 FRP wrap contribution

In general, the nominal shear capacity, V, of a RC beam rehabilitated with FRP composites results from the contributions of three mechanisms, namely, concrete V_c, transverse steel V_s, and FRP V_f.

$$V = V_c + V_s + V_f \qquad [3\text{-}8]$$

Where the contributions of the concrete V_c and steel V_s mechanisms are shown in equation 3-2.

In this study, the contribution of the FRP wrap of total thickness t_{FRP} to the shear mechanism V_f is taken as that provided by ACI (2002),

$$V_f = \frac{A_{fv} f_{fe} (\sin\alpha + \cos\alpha) d_f}{s_f} \qquad [3\text{-}9]$$

Where, $A_{fv} = 2nt_f w_f$ and $f_{fe} = \varepsilon_{fe} E_f$

$$\frac{V_f}{bt} = \rho_{FRP}\, \varepsilon_{fe}\, \gamma\ f_{yv} \qquad [3\text{-}10]$$

Where, $\rho_{FRP} = 2t_f E_f / bf_{yv}$, ε_{fe} = effective strain in FRP, n = number of FRP layers on one side of the beam and t_f= thickness of one layer of FRP.

3.3 EFFECT OF DESIGN VARIABLES ON THE FAILURE MECHANISMS OF FRP-REHABILITATED RC INVERTED-T GIRDERS

From the above mentioned formulations, it is shown that the shear strength capacity V/bt of FRP-rehabilitated RC inverted-T girder depends on thirteen variables that control the failure mechanisms as grouped in Table 3.1. In order to study the effect of these design variables on the failure mechanisms of inverted-T girder, a typical RC inverted-T girder with specific properties as shown in Table 3.2a-3.2d is considered; hence the effect of changing these properties is evaluated.

As an example, Figure 3.3 shows the effect of changing the web transverse reinforcement ratio (ρ_{vw}) on the shear strength capacity V/bt due to different mechanisms. From the figure, it can be seen that an un-rehabilitated inverted-T girder (with the studied properties) is expected to have a non-ductile failure mechanism (due to punching shear). In order to ensure a ductile behaviour, the shear strength capacity V/bt of non-ductile mechanisms should exceed that of flexural failure. This can be achieved by rehabilitating the girder using FRP sheets. Figure 3.4 shows the effect of varying ρ_{vw} on V/bt due to different mechanism after strengthening with 1.5% of ρ_{FRP}. From the figure, it can be seen that the FRP increased the shear strength capacity of non-ductile mechanisms, thus the girder is expected to have a ductile failure through its flexure mechanisms.

In the following sections, a factor of safety index that relates the non-ductile capacity-to-flexural capacity ratio of the girder is used to evaluate the effect of the design variables on the failure mechanisms. This non-ductile capacity-to-flexural capacity ratio is indicated by the ratio of X/Y as shown in figures 3.3 and 3.4. Thus, if the non-ductile

capacity-to-flexural capacity ratio is less than 1 (e.g. unrehabilitated girder, Figure 3.3), a non-ductile failure is expected, while a ductile flexure failure is expected if this ratio exceeds 1 (e.g. rehabilitated girder, Figure 3.4). Higher values of non-ductile capacity-to-flexure capacity ratio represent the factor of safety against non-ductile failure. On the other hand, this ratio also represents the degree of allowance for the increase in the flexural capacity of the inverted-T girder (e.g. by rehabilitating it using longitudinal FRP sheets, strips or rebars) without reaching its non-ductile failure capacity.

3.3.1 Effect of reinforcement content

Figures 3.5 to 3.7 show the effect of variation of the reinforcement ratios on the non-ductile capacity-to-flexure capacity ratio. Figure 3.5 shows that increasing the web reinforcement ratio, ρ_{vw}, of the studied girder did not change the mode of failure, which was governed by punching failure mechanism. Rehabilitating the studied girder with FRP sheets increased the shear strength capacity, V/bt, of non-ductile mechanisms such that the non-ductile capacity-to-flexural capacity ratio reached about 1.92 for ρ_{FRP} = 1.5%.

Figure 3.6 shows that increasing the flange reinforcement content, ρ_{vf}, up to 0.63% increases the V/bt capacity of the shear friction failure in flange, while the failure mechanism is governed by punching failure mechanism beyond that ratio. Strengthening with ρ_{FRP} up to 1.5% shows increase in V/bt capacity as well as change in failure mechanism from non-ductile to ductile by eliminating both punching and shear friction failure mechanisms of the studied girder.

Figure 3.7 shows that increase in longitudinal steel content, ρ_f, decreases the non-ductile capacity-to-flexure capacity ratio. This is attributed to the increase in the V/bt capacity that corresponds to flexure mechanism. Increasing ρ_{FRP} beyond 0.5% increases the non-ductile capacity to flexure capacity ratio.

3.3.2 Effect of material properties

Figured 3.8 to 3.10 show the effect of variation of the material properties on the non-ductile capacity-to-flexure capacity ratio. Figure 3.8 shows that for the studied girder, the section behaves in a non-ductile manner for the concrete strength less than 45 MPa. For this section, it can be seen that an over estimation of a 10 MPa in the concrete strength f'_c results in an under estimation of the necessary ρ_{FRP} by 0.1% for a targeted non-ductile capacity-to-flexure capacity ratio. Figure 3.9 shows that, for the studied section, the variation in estimating f_{yv} (to be 300 MPa or 500 MPa) did not have an effect on the mode of failure for the existing girder, nor the non-ductile capacity-to-flexure capacity ratio of FRP rehabilitated girders.

Figure 3.10 shows that an under estimation of the yield strength of longitudinal reinforcement, f_y, to be 300 MPa results in an under estimation of the necessary ρ_{FRP} by 0.5% for a targeted non-ductile capacity- to-flexure capacity ratio.

3.3.3 Effect of span geometry

Figure 3.11 shows that increasing the shear span-to-depth ratio $(a/t)_{ratio}$ of the studied girder results in a more ductile failure mechanism. On the other hand, for girders

with low $(a/t)_{ratio}$, rehabilitating the girder with FRP increases its non-ductile capacity-to-flexure-capacity ratio.

Figure 3.12 shows the effect if variation of punching force-to-shear force ratio $(PF/V)_{ratio}$ on the non-ductile capacity-to-flexure capacity ratio. From the figure, it can be seen that inverted-T girder that have structural systems with higher punching force-to-shear force ratio $(PF/V)_{ratio}$ are expected to have low non-ductile capacity-to-flexure capacity ratios. Rehabilitating the girder using FRP increases its non-ductile capacity-to-flexure capacity ratio.

3.3.4 Effect of cross-sectional geometry

From Figures 3.13 and 3.14, it can be seen that increasing the flange dimensions, i.e. flange width and height, reduces the possibility of non-ductile mechanism without altering the girder's flexure capacity, thus increases the non-ductile capacity-to-flexure capacity ratio.

On the other hand, an under estimate of the effective depth-to-total depth ratio, γ, (Figure 3.15) by 5% results in under estimation of the necessary ρ_{FRP} by 0.25% for a targeted non-ductile capacity-to-flexure capacity ratio.

3.4 SUMMARY

The effect of eleven variables that control the failure mechanism of FRP-rehabilitated RC inverted-T girders is evaluated. The variables are grouped into four categories, namely, material properties, cross-sectional geometry, reinforcement content and span geometry. Different failure mechanisms are represented by their shear strength capacity V/bt.

The failure mechanisms are based on existing model. In order to study the effect of variables, the ratio of the non-ductile shear strength capacity to the shear capacity that corresponds to flexure failure of the girder is considered. Thus, if the non-ductile capacity-to-flexural capacity ratio is less than 1, a non-ductile failure is expected, while a ductile flexure failure is expected if this ratio exceeds 1. The higher the non-ductile capacity-to-flexure capacity ratio, the higher the factor of safety against non-ductile failure and the higher possibility to increase the flexural strength of the girder.

1. For targeted non-ductile capacity-to-flexure capacity, the required content of FRP wraps increases with the increase of Yield strength of reinforcement (f_y), Ratio of the effective depth-to-total girder depth (γ), Longitudinal steel ratio (ρ_f) and Punching force-to-shear force ratio $(PF/V)_{ratio}$.

2. For targeted non-ductile capacity-to-flexure capacity, the required content of FRP wraps increases with the decrease of Characteristic concrete compressive strength (f'_c), Ratio of flange over hang-to-width of the web (β), Ratio of flange depth-to-depth of the girder (α), Web transverse reinforcement ratio (ρ_{vw}), Flange transverse reinforcement ratio (ρ_{vf}) and Shear span-to-depth ratio $(a/t)_{ratio}$.

Table 3.1 Studied variables that affect the failure mechanism of inverted-T girder

Category	Variable	Definition
Material properties	f'_c	Characteristic concrete compressive strength (MPa)
	f_{yv}	Yield strength of stirrups (MPa)
	f_y	Yield strength of reinforcement (MPa)
Cross-sectional geometry	χ	Ratio of width of the web-to-total girder depth
	β	Ratio of flange over hang-to-width of the web
	γ	Ratio of the effective depth-to-total girder depth
	α	Ratio of flange depth-to-depth of the girder
Reinforcement content	ρ_{vw}	Web transverse reinforcement ratio given by A_v/bs, where A_v= total area of stirrups, b = width of web and s = spacing of stirrups
	ρ_{vf}	Flange transverse reinforcement ratio given by $A_{vf}/\alpha t s_{vf}$, where A_{vf}=All transverse reinforcement within the longitudinal distance 2e each side of the bearing pad, s_{vf} = Spacing of transverse reinf., e and t refer Fig.2
	ρ_f	Longitudinal steel ratio given by $A_s/b\gamma t$, where A_s = Total area of longitudinal steel
	ρ_{FRP}	CFRP content given by $2t_fE_f/bf_{yv}$ where t_f = total thickness of FRP sheets in one side of the girder and E_f = tensile modulus of the fiber sheets
Span geometry	a/t	Shear span-to-depth ratio
	PF/V	Punching force-to-shear force ratio

Table 3.2a Properties of the studied RC inverted-T girder (Material)

Variable	f'_c (MPa)	f_{yv} (MPa)	f_y (MPa)
Value	40	400	400

Table 3.2b Properties of the studied RC inverted-T girder (Cross-sectional geometry)

Variable	χ	β	γ	α
Value	0.3	0.8	0.9	0.3

Table 3.2c Properties of the studied RC inverted-T girder (Reinforcement content)

Variable	ρ_{vw} (%)	ρ_{vf} (%)	ρ_f (%)	ρ_{FRP} (%)
Value	1	0.85	2	0

Table 3.2d Properties of the studied RC inverted-T girder (Span geometry)

Variable	a/t	PF/V
Value	2.5	1

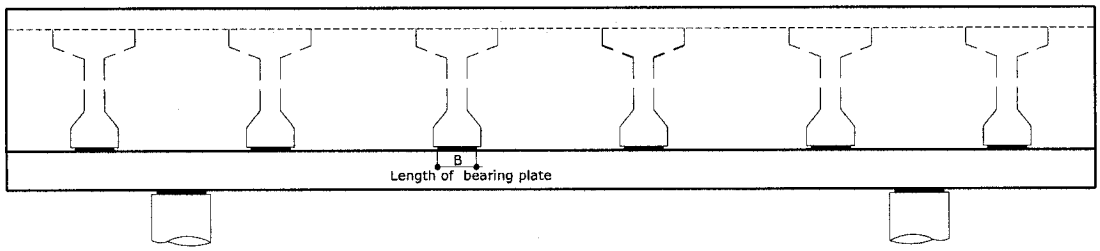

Elevation

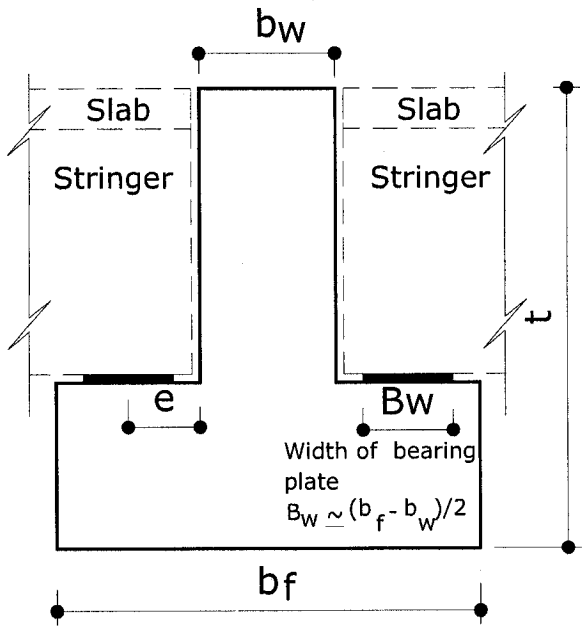

Cross-section

Figure 3.1 Inverted-T bentcap girder

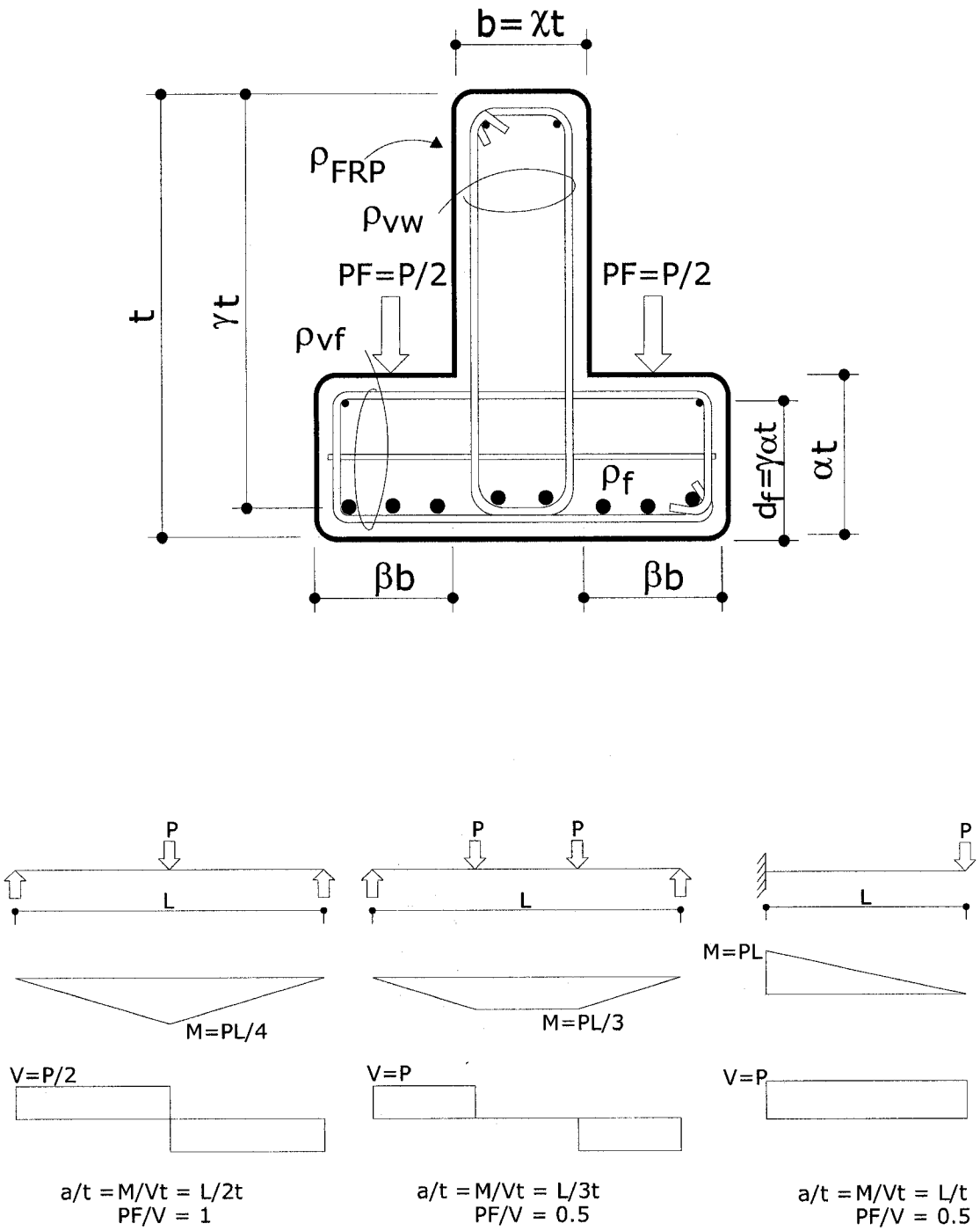

Figure 3.2 Notations of the design variables for inverted-T girder

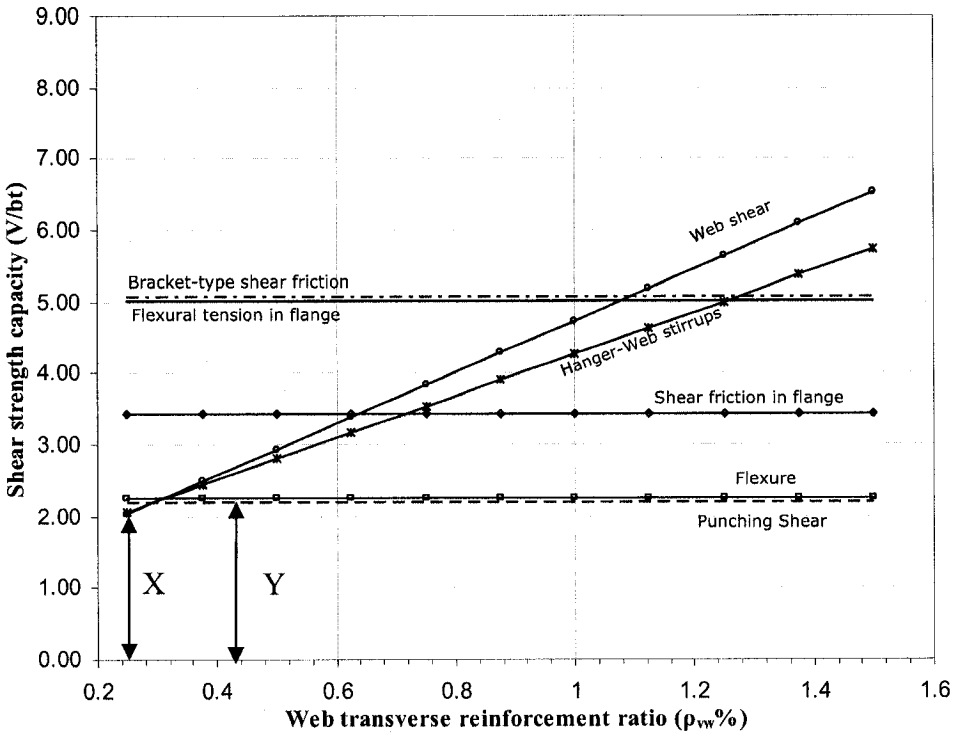

Figure 3.3 Influence of ρ_{vw} on V/bt

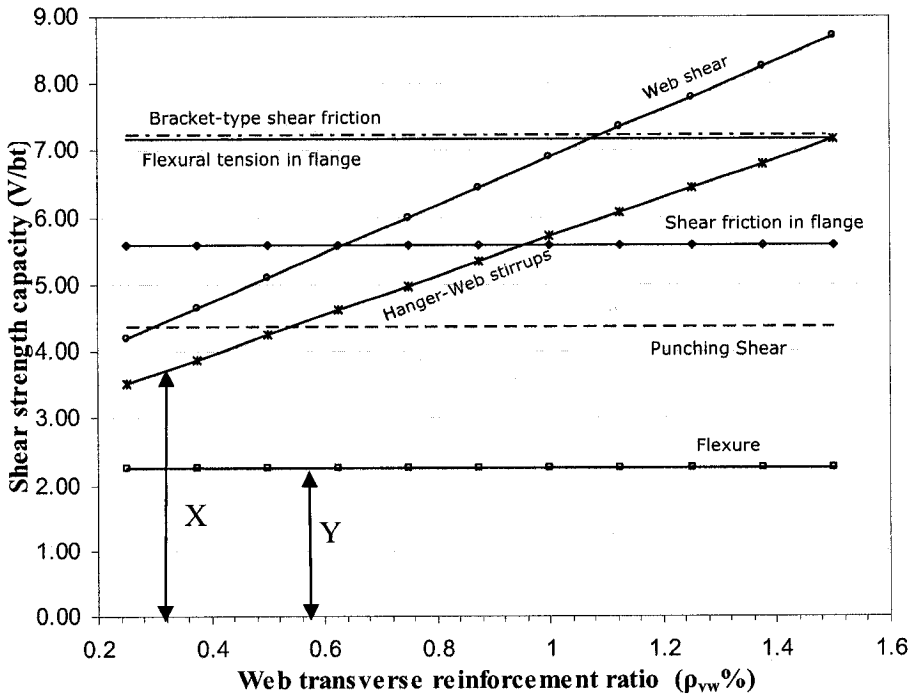

Figure 3.4 Influence of ρ_{vw} with 1.5%of ρ_{frp} on V/bt

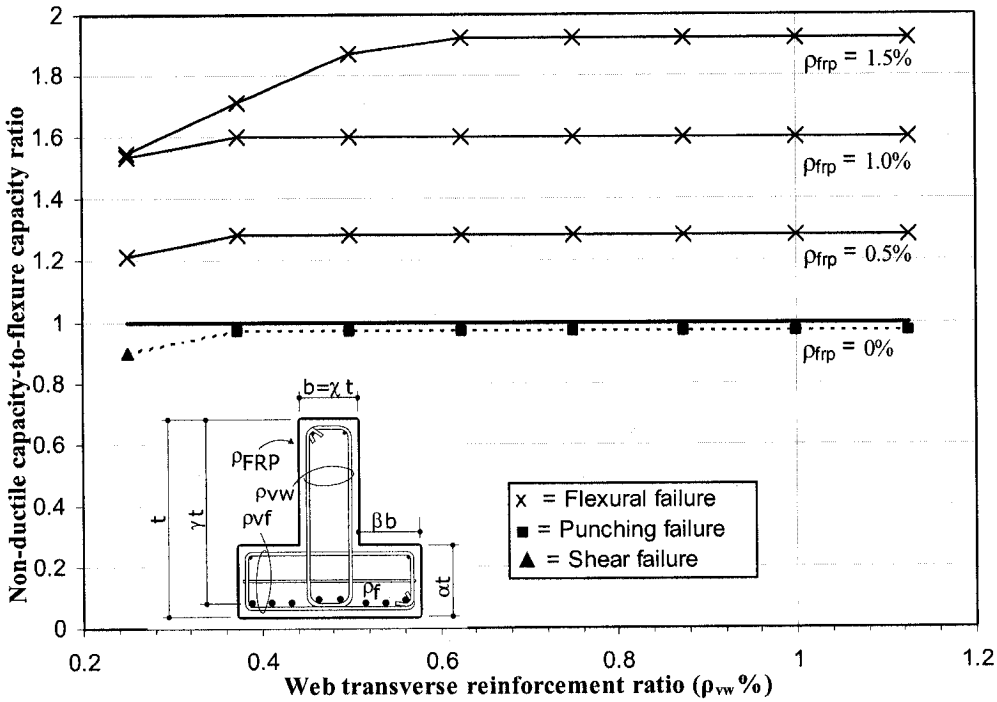

Figure 3.5 Influence of ρ_{vw} on the non ductile capacity-to-flexural capacity ratio

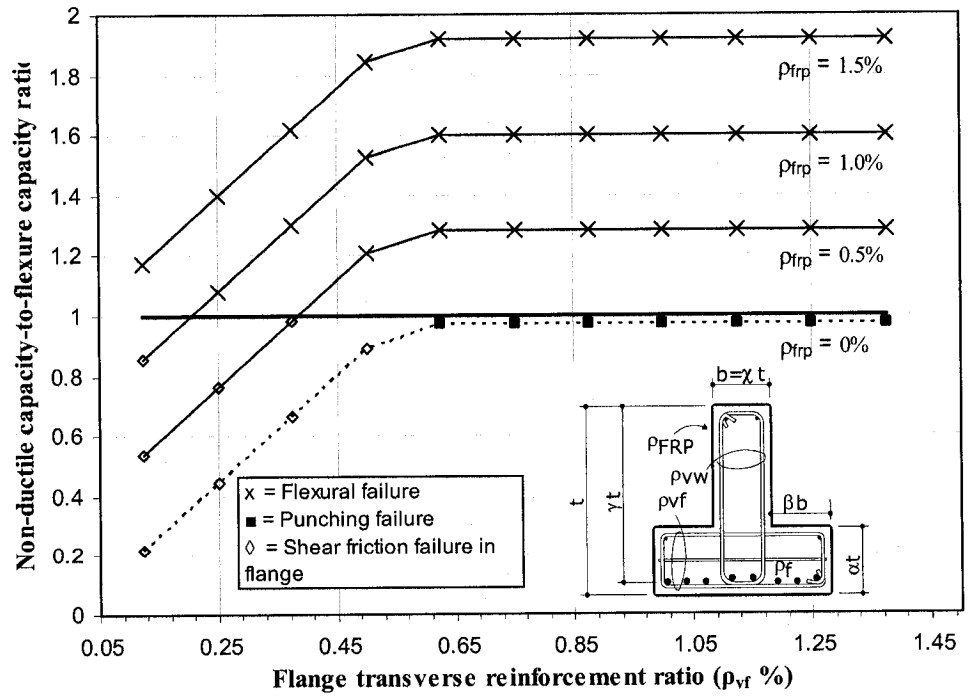

Figure 3.6 Influence of ρ_{vf} on the non ductile capacity-to-flexural capacity ratio

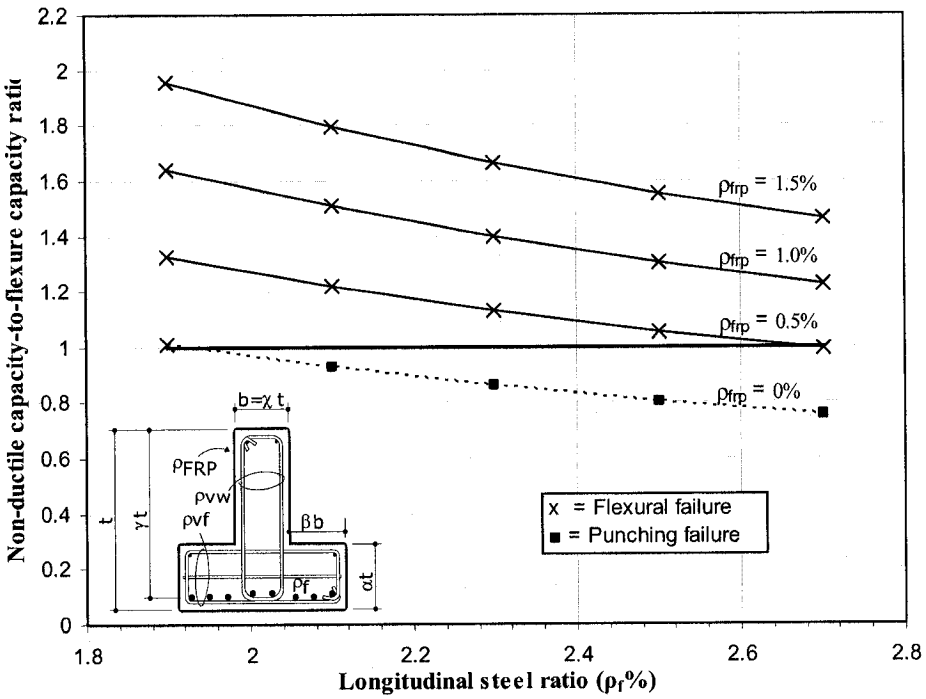

Figure 3.7 Influence of ρ_f on the non ductile capacity-to-flexural capacity ratio

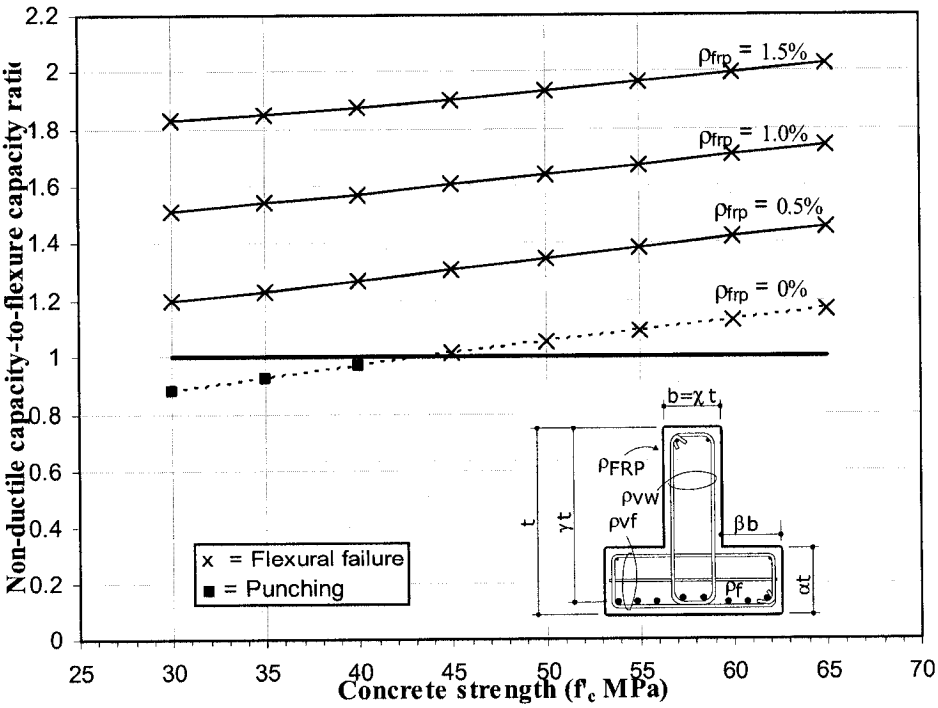

Figure 3.8 Influence of f'_c on the non ductile capacity-to-flexural capacity ratio

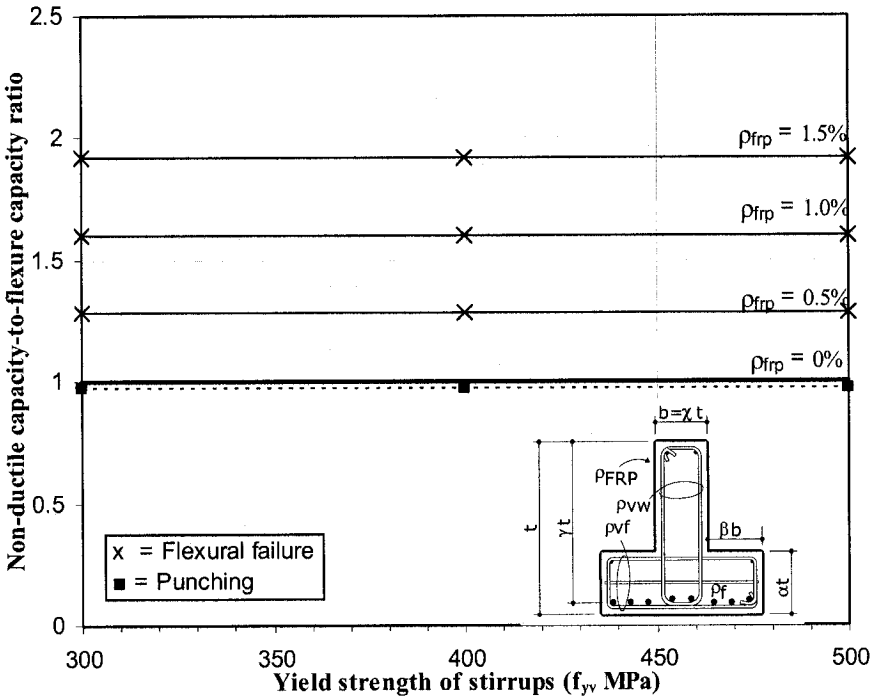

Figure 3.9 Influence of f_{yv} on the non ductile capacity-to-flexural capacity ratio

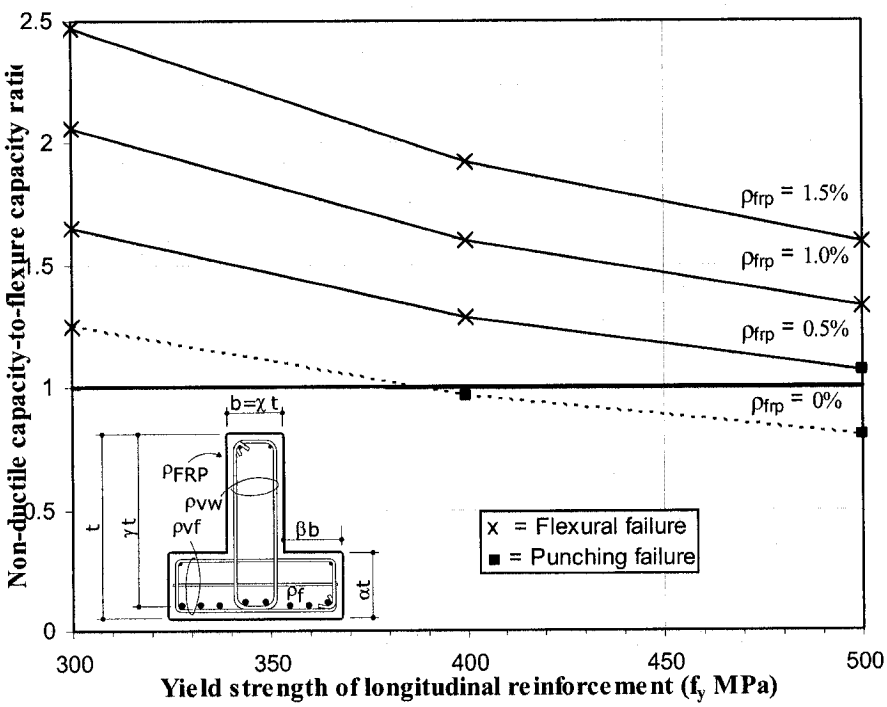

Figure 3.10 Influence of f_y on the non ductile capacity-to-flexural capacity ratio

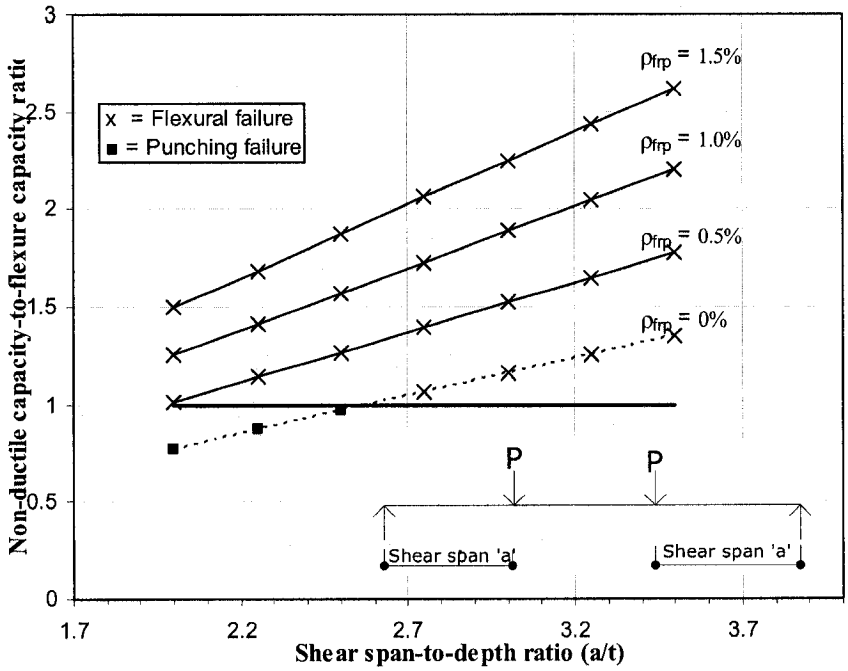

Figure 3.11 Influence of $(a/t)_{ratio}$ on the non ductile capacity-to-flexural capacity ratio

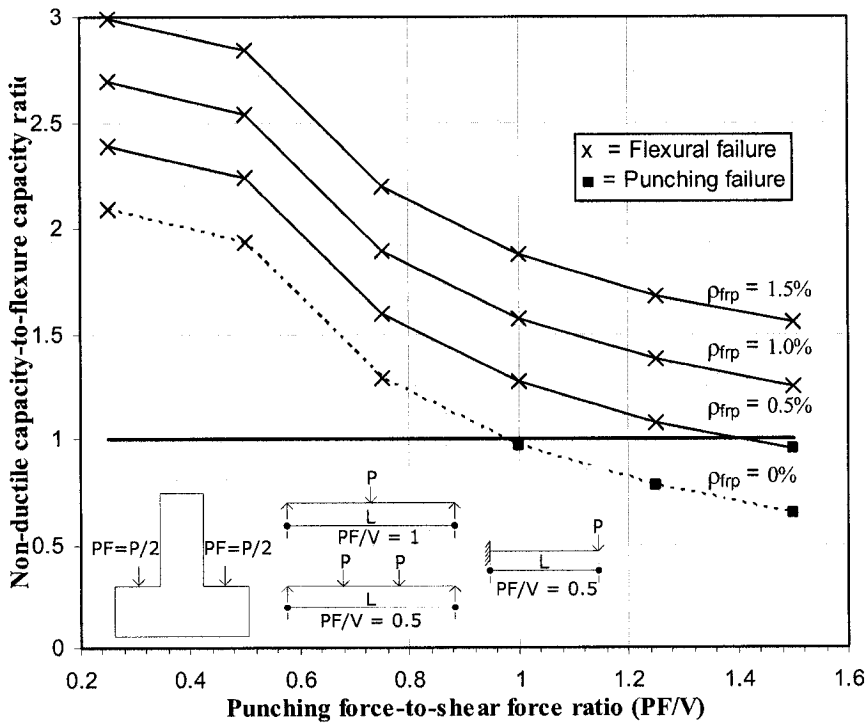

Figure 3.12 Influence of $(PF/SF)_{ratio}$ on the non ductile capacity-to-flexural capacity ratio

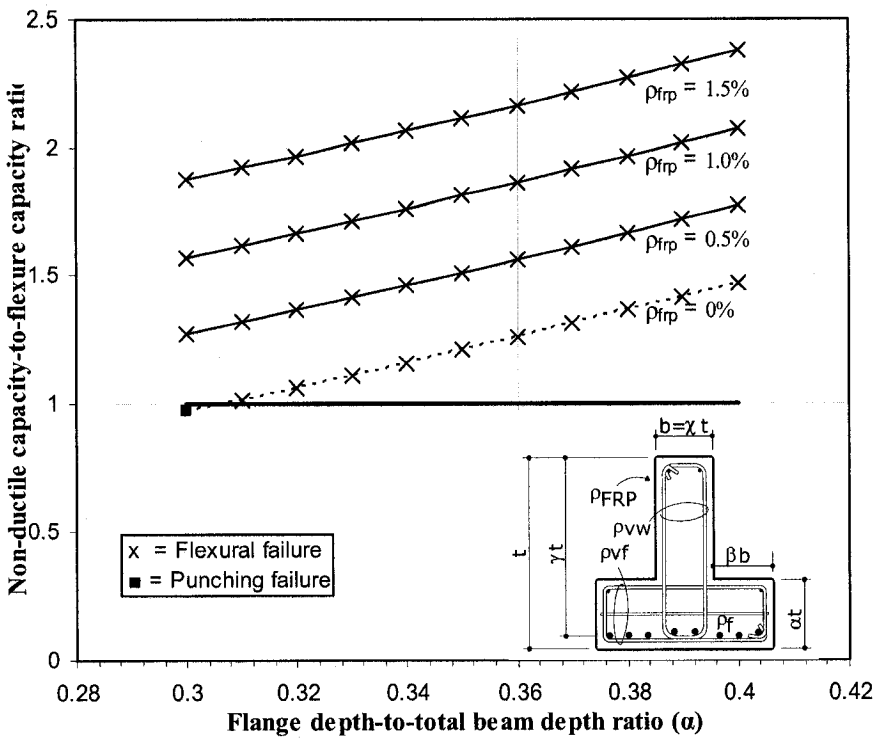

Figure 3.13 Influence of α on the non ductile capacity-to-flexural capacity ratio

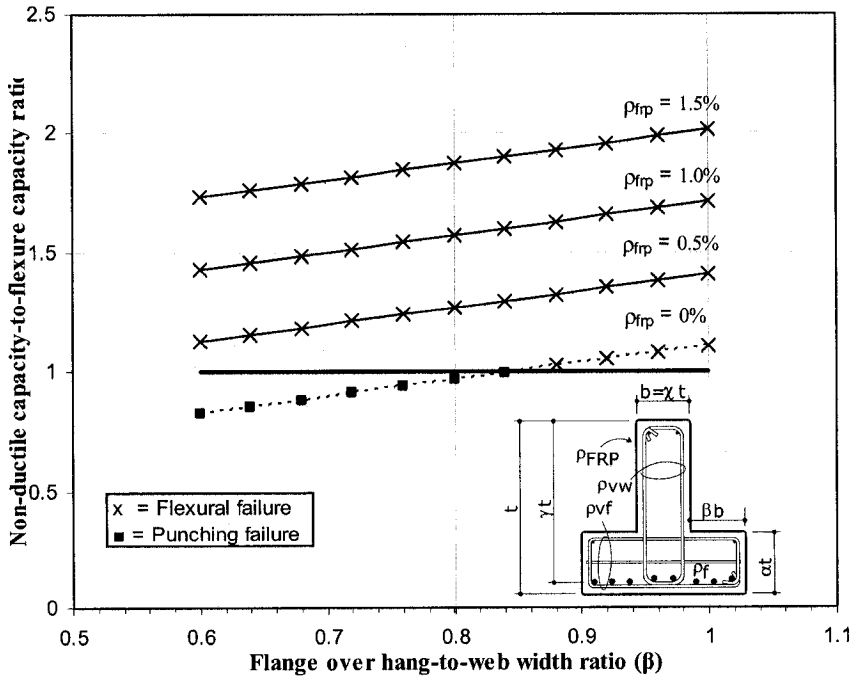

Figure 3.14 Influence of β on the non ductile capacity-to-flexural capacity ratio

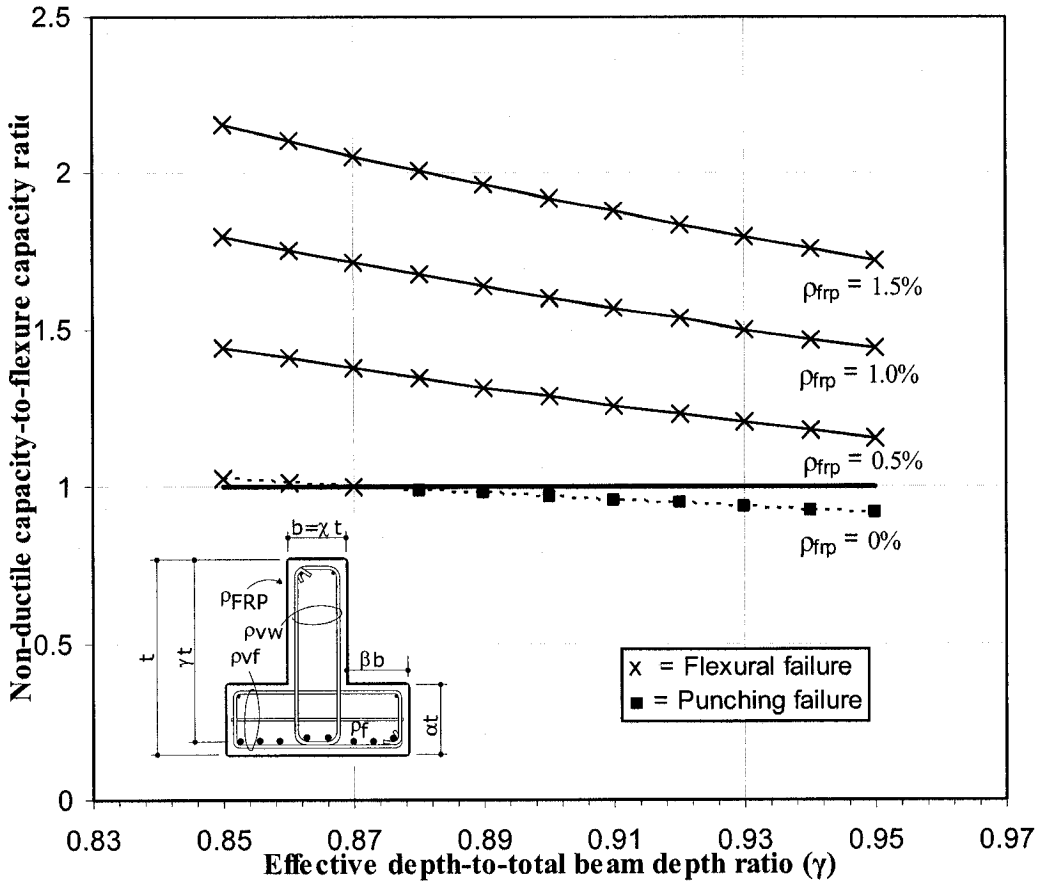

Figure 3.15 Influence of γ on the non ductile capacity-to-flexural capacity ratio

CHAPTER 4

EXPERIMENTAL PROGRAM

4.1 GENERAL

The objective of the experimental program is to investigate the use of externally bonded carbon fibre-reinforced polymer (CFRP) composite in strengthening existing reinforced concrete (RC) inverted-T bentcap bridge girders to eliminate non-ductile failure mechanisms on hanger, web and flange. Eight tests were conducted on four inverted-T scaled girders to asses the effectiveness of the proposed strengthening schemes for the studied failure mechanisms. The control girders were subjected to increasing incremental load up to the first sign of non-ductile mechanism, while the rehabilitated specimens where tested up to failure. All girders had the same concrete dimensions, with the difference among them being the reinforcement content. In the following sections, the full details of the experimental program are presented.

4.2 TEST SETUP

The girders were tested under 4-point loading system as shown in Figure 4.1 except for girder IT-G1 which was tested under 3-point loading. The girders were tested under increasing monotonic load up to failure. Cement grout was used between the base plate of the loading frame and the top surface of the flange to level the unevenness in the

concrete surface and to ensure uniform pressure. After each loading increment, all visible cracks were marked. The loads, deflections and strains were continuously recorded during the test by means of a 40-channel data acquisition system.

4.3 TEST SPECIMENS

All tested girders were identical in size and proportion, with the only difference being the reinforcement content in hanger, web shear and punching zones. Figures 4.2-4.4 shows the dimensions and details of reinforcement of the control girders and its corresponding test profile. The tested girders represent a $1/3^{rd}$ scale prototype of RC inverted-T bridge bentcap girders. The girders are simply supported over the span of 3000 mm (10′) with a height of 610 mm (24″), flange width of 560 mm (22″), flange height of 220 mm (8.6″) and web width of 180 mm (7″). The control girders are designated as IT-G# while the girders rehabilitated using CFRP sheets are designated as IT-G#R

A total of four girders were cast to study the behaviour of various parameters influencing the failure criteria of the girder and the possibility of eliminating them. The control girders were designed to satisfy the minimum reinforcement requirements according to the ACI (1968) code providing negligible capacities in hanger, web-shear and punching zones for girders G1&G2, G3 and G4, respectively. The longitudinal bottom reinforcement was identical for all tested girders. Eight 20 mm diameter bars ($\rho_f = 2.3\%$) were used for the flexural reinforcement, while two 10 mm bars are placed at the top of the flange. Rectangular closed stirrups made of 10 mm diameter bars were used

for web reinforcement. 10 mm diameter bars (flexural reinforcement for bracket action of the flange) were used for reinforcement in flange. Supplementary flange horizontal bar of 10 mm diameter were placed at mid-height of the flange. This arrangement of reinforcement was selected to simulate those of inverted-T bentcap bridge girders constructed before 1970's.

4.3.1 Specimens IT-G1 and IT-G2

Figure 4.2 shows the dimensions, reinforcement details of girders IT-G1 and IT-G2 and their test profile. Both specimens have the same dimensions and reinforcement contents. The specimens have minimum reinforcement content in the web-shear and hanger zones. Spacing of web and flange reinforcements were 305 mm and 102 mm, respectively. Two 10 mm steel bars were used as compression reinforcement placed on top of the web. The difference between the two specimens is the shear span-to-depth ratio (M/Vd). Specimen IT-G1 was subjected to one axis of loading at its midspan, while specimen IT-G2 was subjected to two axes of loading that are 400 mm apart. The shear span-to-depth ratio was 2.5 and 2.0 for specimens IT-G1 and IT-G2, respectively.

4.3.2 Specimen IT-G3

The objective of this control specimen was to determine the feasibility of web-shear strengthening of inverted-T girders using CFRP sheets. The girder had minimum shear reinforcement content, with 10 mm stirrups spaced at 305 mm. In order to avoid the possibility of failure in hanger or in flange, the reinforcement spacing in the hanger and

punching zones was decreased to 51 mm up to 370 mm on both sides from center of the girder. Figure 4.3 shows the dimensions, details of reinforcement and test profile of specimen IT-G3.

4.3.3 Specimen IT-G4

In this specimen, punching shear behaviour of the flanges of the girder was studied therefore, the girder had high shear and hanger reinforcement contents (10M @ 102 mm and 10M @ 51 mm, respectively) as shown in Figure 4.4. The reinforcement content in the punching zone was reduced by increasing the spacing of the flange reinforcement from 51 mm to 102 mm. Figure 4.4 show the girder IT-G4 test profile.

4.3.4 Specimen IT-G1R

A new rehabilitation scheme using CFRP sheets was used for girder IT-G1R in order to eliminate the non-ductile failure in the web (shear-compression) and hanger failure mechanisms observed in girder IT-G2 (that has the same loading condition). The girder is rehabilitated using 3 layers of Tyfo® SCH-11UP carbon fibre sheets (Fyfe 2005). The difficulties in proposing an FRP-rehabilitation scheme for inverted-T girders compared to regular rectangular, or even T-girders is the presence of the bottom flange and the inaccessibility at the locations of the loading points (i.e. stringers), which prevents wrapping the FRP sheets around the bottom side of the stringer beam. Therefore, in order to ensure that the FRP sheets will not peel off the concrete at high stress levels,

FRP sheets were anchored to concrete. Figure 4.5 shows the rehabilitation scheme of the girder.

Figures 4.6(a) shows the cross section of the rehabilitation scheme at locations away from the loading plates (section A-A). Holes with depth of 3″ were pre-drilled in the girder's web and flange to allow for anchoring using 3/8″ threaded rods after applying FRP sheets. At the connection between the web and the flange, concave grout with a radius of 30 mm is used in order to allow for the smooth transition of stresses in the FRP sheet from the web to the flange. A 6 mm thick curved angle plate that is anchored to concrete is used to clamp the FRP in position as shown in the figure.

Figure 4.6(b) shows the cross section of the rehabilitation scheme at locations of loading plates (section B-B). At these locations, the FRP sheets cannot extend to the top of the flange. Another anchoring technique to anchor the FRP on the web of the girder to concrete was used. Two 3″ deep pre-drilled holes and CFRP fan-type anchors or fibre anchors were used to transfer the stresses from the FRP to the girder as shown in the figure.

The CFRP sheets were bonded to the test girders according to the instructions provided by the manufacturer (Fyfe 2005). Angle grinder was used to chamfer the girder edges to a radius of 25 mm to avoid stress concentration as well as any irregularities on the surface of the girders. Composite sheets were cut to the required length. The two components of the epoxy were thoroughly mixed using a mixing paddle and electric drill motor. A thin coat of epoxy was applied to the top surface of the concrete girders in the area where strips were to be applied, as well as to the bonding side of the composite sheets using roller. The strips were then applied to the epoxy-coated concrete girder

surface and rolled out with a roller to ensure proper bonding. Figure 4.10 shows the elevation of the rehabilitated girder IT-G1R before test.

4.3.5 Specimen IT-G2R

In this specimen, another rehabilitation scheme was examined to eliminate the non-ductile failure in the web (shear-compression) and hanger failure mechanism observed in girder IT-G2 as shown in Figure 4.7. The girder was rehabilitated using 3 layers of CFRP sheets that has an inverted ⊔ shape over the web portion of the girder along the web shear zones and at the locations of the loading plates. The CFRP sheets were anchored to the girder using 3″ threaded rods that are drilled to the girder. Washers were used with the threaded rods near the supports and 2″x1″x2/8″ steel plates were used as washers near the loading points. Flange portion of the girder were also wrapped completely beneath and anchored on the top of the flange.

In the zones adjacent to the loading plates (that represents stringer of a bridge), the girder was fully wrapped with CFRP. In an attempt for avoiding peeling of the CFRP at the connection between the web and the flange due to the outward resultant of the tensile forces in the FRP sheets, anchored curved angle plates (similar to those shown in Figure 4.6(a)) were used in the zones adjacent to the loading plates. Figure 4.8 shows the cross-section of the rehabilitation scheme at sections A-A and B-B.

4.3.6 Specimen IT-G3R

A rehabilitation scheme as shown in Figure 4.9 was used for girder IT-G3R in order to eliminate the web-shear failure mechanism of girder IT-G3. The girder was rehabilitated using 3 layers of CFRP sheets with an inverted ⊔ shape in the web-shear zones. Since there were no signs of delamination of CFRP sheets in the girder IT-G2R near the supports, in this scheme it was decided to use anchors using 3/8″ threaded rods only up to a distance equal to the girders height, h (610 mm), from the loading point. At the connection between the web and the flange, 6″ curved angle plate were used similar to IT-G1R.

4.3.7 Specimen IT-G4R

Based on the failure mechanism of IT-G4 the rehabilitation scheme for girder IT-G4R shown in Figure 4.10 was proposed to eliminate punching shear failure in the flanges and to increase the compression capacity of the web by confining the compression zone in the pure flexure region between the loading points (i.e. web-compression zone). To eliminate punching failure mechanism in the flange, 3 layers of CFRP sheets that has a ⊏ shape were wrapped around the two flanges of the girder. In order to transfer the stresses from the CFRP wrap to the web of the girder, fibre anchors that were sandwiched between the layers of the CFRP wrap on both sides of the flange were embedded a distance of 3″ into the web as shown in Figure 4.15. In order to ensure that CFRP sheets at the bottom side of the flange will not peel off the concrete at high stress level, CFRP sheets were anchored to the concrete using 3/8″ threaded rods. To

increase the compression capacity of the web of the girder, 3 layers of CFRP sheets that has an inverted ⊔ shape were wrapped over the web up to the edges of loading frame and were anchored with threaded rods.

4.4 MATERIALS

4.4.1 Steel reinforcement

The flexural reinforcement used as tension (bottom) reinforcement consisted of 20M (19.5 mm nominal diameter) with cross-sectional area of 300 mm^2 deformed steel rebars. 10M rebars (11.3 mm nominal diameter) with cross-sectional area of 100 mm^2 were used for other reinforcement in the web and flanges. Samples of the rebars were tested to obtain their tensile stress-strain relationship. The tested rebars had an average yield strain of 2100 microstrain, yield stress of 440 MPa and modulus of elasticity of 200 GPa.

4.4.2 Concrete

Ready mix concrete was ordered from the plant and was delivered to the laboratory. Concrete with specified compressive strength f'_c = 30 MPa, slump of 125 mm, which provided adequate concrete workability during the concrete casting in the forms and maximum aggregate size of 20 mm was ordered from the ready mix plant. During casting, a total of 15 concrete cylinders (100x200 mm) were cast and cured under the same conditions as the test girders. The curing consisted of moist curing by covering

the whole girder with burlap. Three cylinders were tested after 7, 14, and 28 days and another three were tested on the day of testing of the girders commenced. Table 4.1 shows the results for the concrete compressive and tensile strengths at 28 days of the tested girders.

4.4.3 CFRP Sheets

The girder is rehabilitated using Tyfo® SCH-11UP unidirectional carbon fibre sheets (Fyfe 2005) which was delivered in rolls and a two-component epoxy resin which is mixed and applied to the fibres to form the composite material. The carbon fibres are characterized by a very high tensile strength, a linearly elastic stress-strain relationship up to failure, and a modulus of elasticity slightly higher than that of steel. Table 4.2a shows the typical dry fibre properties while Table 4.2b shows the composite gross laminate properties as provided by the supplies (Fyfe 2005).

4.5 CONSTRUCTION OF THE TESTED GIRDERS

4.5.1 Preparation of formwork

Two formworks were manufactured from 12.5 mm thick wood in order to fabricate two girders per pour. Formworks were braced at the top and sides in order to prevent any lateral movement or change in dimensions during casting. The inner sides of the wood sheets were coated by a thin layer of wax oil to facilitate their removal after pouring concrete.

4.5.2 Preparation of reinforcing cages

All rebars were cut to proper length and stirrups were shop bent and were assembled in the laboratory. Electrical strain gauges were placed at selected locations on the steel bars on flexural reinforcement, stirrups, and on the flange reinforcement. Before installing strain gauges, the ribs on the steel surface were removed using angle grinder. Then the surface was smoothened with different grits of sand paper. The prepared surface was cleaned with acetone and treated with metal conditioner and finally with neutralizer. The strain gauges and the terminals were attached on the cleaned surface using specified adhesives. Gauges were then soldered to lead wires. Each gauge was checked for proper resistance and against short-circuiting. The gauges were waterproofed by polyurethane coating before being covered with a strain gauge protective putty. The whole area was then covered with an insulating tape. All reinforcements are properly arranged on a supports and tied at intersections using tie wires. The cage was then placed in the wooden form with seats providing proper cover on all sides. Figure 4.11 shows the wooden forms with steel cage before pouring concrete.

4.5.3 Casting and curing

The specimens were cast with the flange facing upwards. Concrete was placed into the form directly from a chute on the ready-mix concrete truck. Electric vibrator was used to vibrate the concrete into proper position. The top surface was then trowelled to a smooth surface. 15 cylinders were cast simultaneously with each specimen and were cured along the side the specimens to determine the concrete compressive strength at the

time of testing. After the concrete had set, specimens and cylinders were covered with burlap and moistened regularly. Figure 4.12 shows specimens after pouring concrete.

4.6 GIRDER INSTRUMENTATION

The strain in the stirrups and the distribution of strain in the CFRP sheets were monitored using electrical resistance strain gauges with a 5 mm gauge length. Deflections were also measured at various locations. During each test, load, displacement and strain readings were recorded in parallel using the data acquisition system at a rate of 1 sample per second.

4.6.1 Deflections

Vertical deflections were measured at various locations along the span as shown in the Figure 4.1. Each specimen was instrumented with 9 Linear Variable Displacement Transducers (LVDT) ranging from 50 mm to 100 mm capacity depending on the monitored location.

4.6.2 Strains

Strains in the longitudinal reinforcement and stirrups in the web and flanges were measured by means of 5 mm electrical strain gauges. Typical locations of the strain gauges are shown in Figure 4.13. Each specimen had 29 strain gauges, out of which 8 were placed on the longitudinal reinforcement at the centre and at $1/4^{th}$ positions. 8 strain

gauges were put on web reinforcement to trace their strain in the shear zone of the girder. The strains in the hanger zone were traced by having 6 strain gauges on the hanger reinforcement near the loading plates. 7 strain gauges were used to capture the strains in the steel reinforcement in the flanges of the girder.

The key to a successful and optimal usage of strain gauges in strengthening and rehabilitation is effectively determining optimal placement of the sensors that are capable of capturing the critical strains in the CFRP sheets. Figure 4.14(a-d) shows the locations of the strain gauges on the CFRP sheets for girders to monitor the strain at critical locations.

4.7 COMPARISON OF TESTED GIRDERS

Figure 4.15 shows a comparison between the 8 tests conducted on the inverted-T bentcap girders. From the figure, the following can be evaluated.

1. Effect of changing the shear-span-to-depth from 2.5 to 2.0 on the behaviour of existing non-ductile inverted-T girders (by comparing IT-G1 to IT-G2).
2. Effect of increasing the reinforcement in the hanger and punching zones on the behaviour of existing non-ductile inverted-T girders (by comparing girders IT-G3 to IT-G2).
3. Effect of increasing the web reinforcement in the hanger and shear zones on the behaviour of existing non-ductile inverted-T girders (by comparing girders IT-G4 to IT-G2).

4. Effectiveness of two different FRP-rehabilitation techniques on the response of existing non-ductile inverted-T girders (by comparing IT-G1R and IT-G2R to IT-G2).

5. Effectiveness of a proposed FRP-rehabilitation technique to strengthen the web-shear resistance of existing inverted-T girders (by comparing IT-G3R to IT-G3).

6. Effectiveness of a proposed FRP-rehabilitation technique to strengthen the punching and compressive resistance of existing inverted-T girders (by comparing IT-G4R to IT-G4).

Table 4.1 Concrete compressive and tensile strengths at 28 days of the tested girders

Specimen	f'_c (MPa)	f_t (MPa)
IT-G1	32	3.32
IT-G2	31	3.27
IT-G3	33	3.34
IT-G4	33.5	3.33
IT-G1R	32.7	3.29
IT-G2R	31.6	3.20
IT-G3R	33.5	3.37
IT-G4R	33.9	3.32

Table 4.2a Typical dry fibre properties (as provided by the supplier Fyfe 2005)

Property	Typical test value
Tensile strength	3.79 GPa
Tensile modulus	230 GPa
Ultimate elongation	1.7%
Density	1.74 gm/cm^3
Weight per sq.yd	298 gm/m^2
Fibre thickness	0.127mm

Table 4.2b Composite gross laminate properties (as provided by the supplier Fyfe 2005)

Property	ASTM method	Typical test value
Ultimate tensile strength in primary fiber direction	D-3039	1062 MPa
Elongation at break	D-3039	1.05%
Tensile modulus	D-3039	102 GPa
Ultimate tensile strength 90° to primary fiber	D-3039	0
Laminate thickness	-	0.25 mm

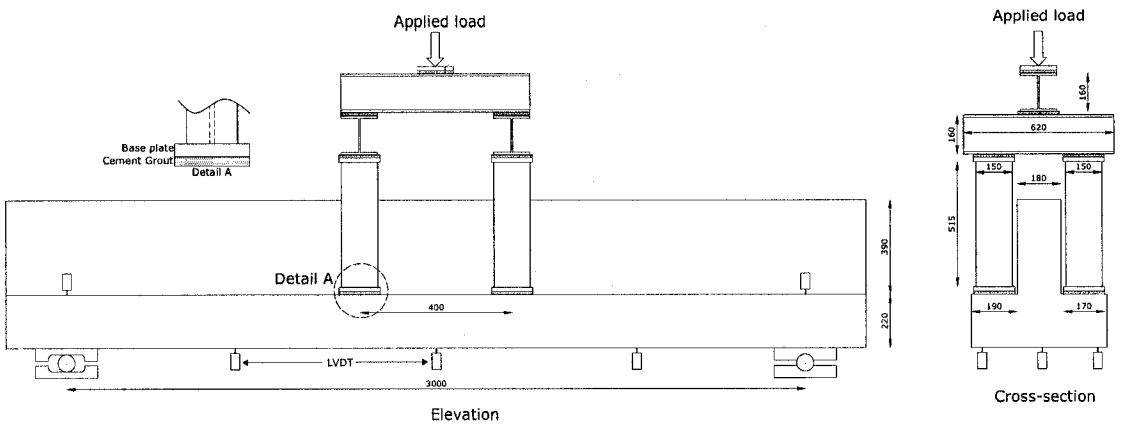

Figure 4.1 Schematic of test setup

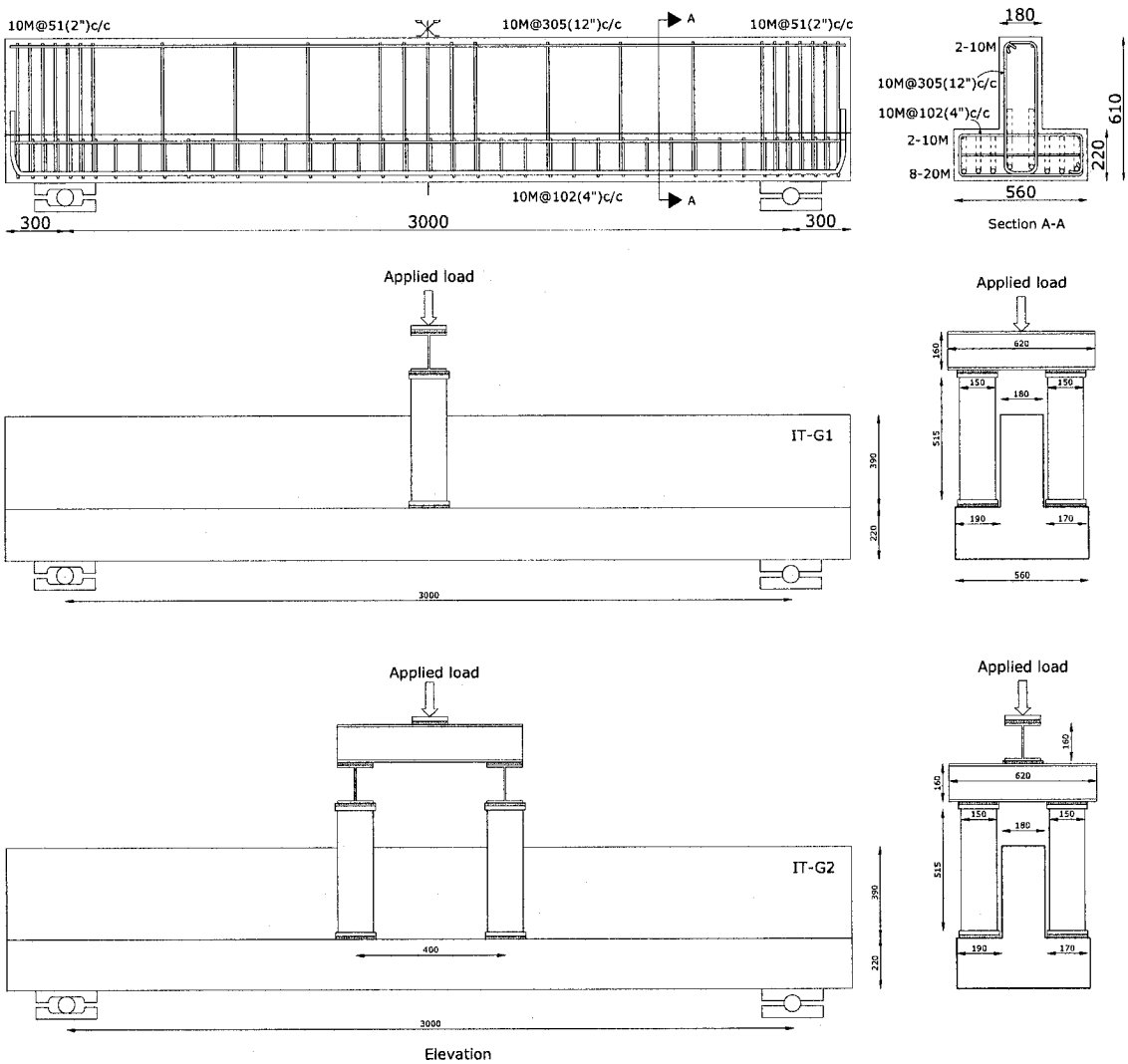

Figure 4.2 Dimensions, details of reinforcement and test profile for girder IT-G1 and IT-G2

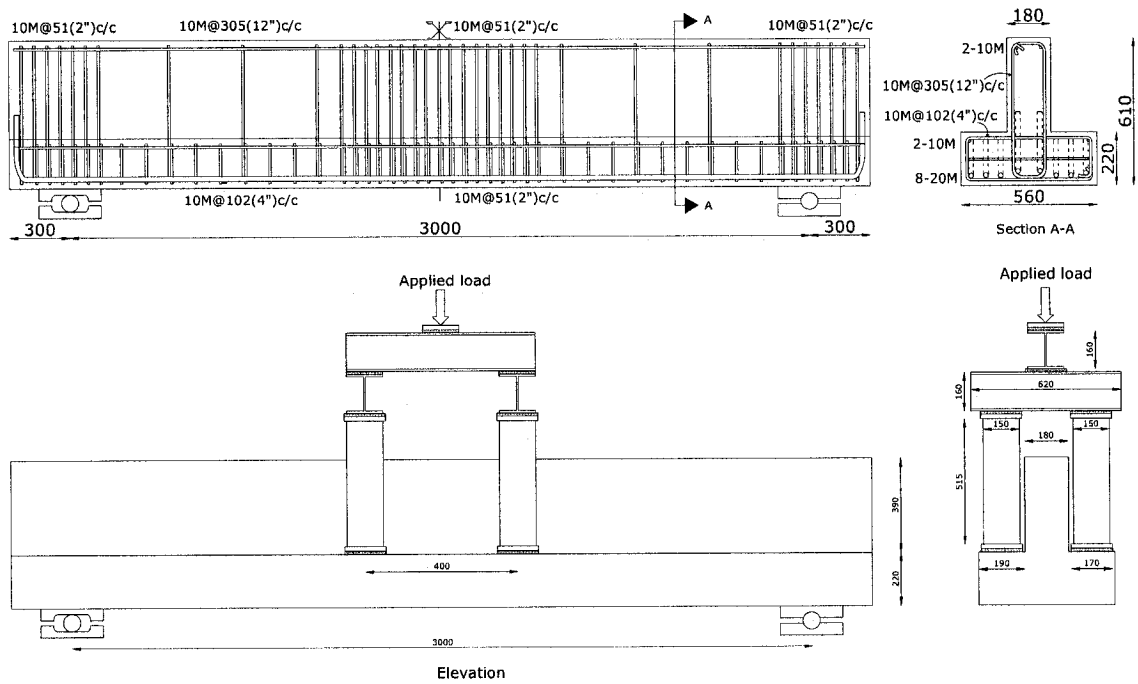

Figure 4.3 Dimensions, details of reinforcement and test profile for girder IT-G3

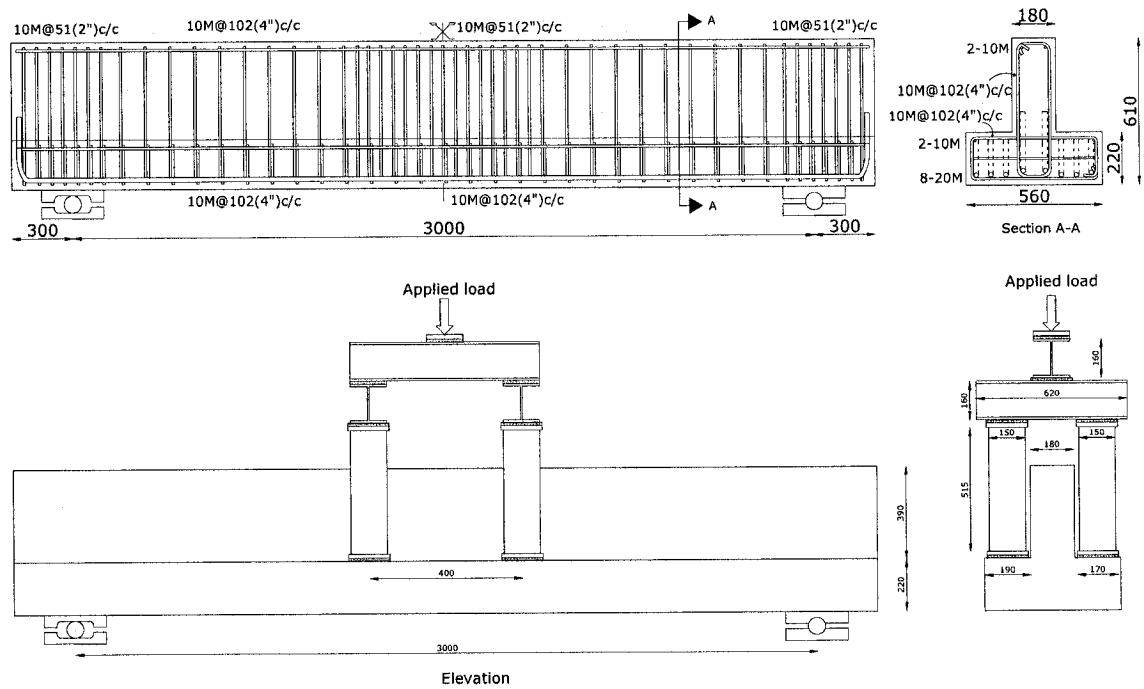

Figure 4.4 Dimensions, details of reinforcement and test profile for girder IT-G4

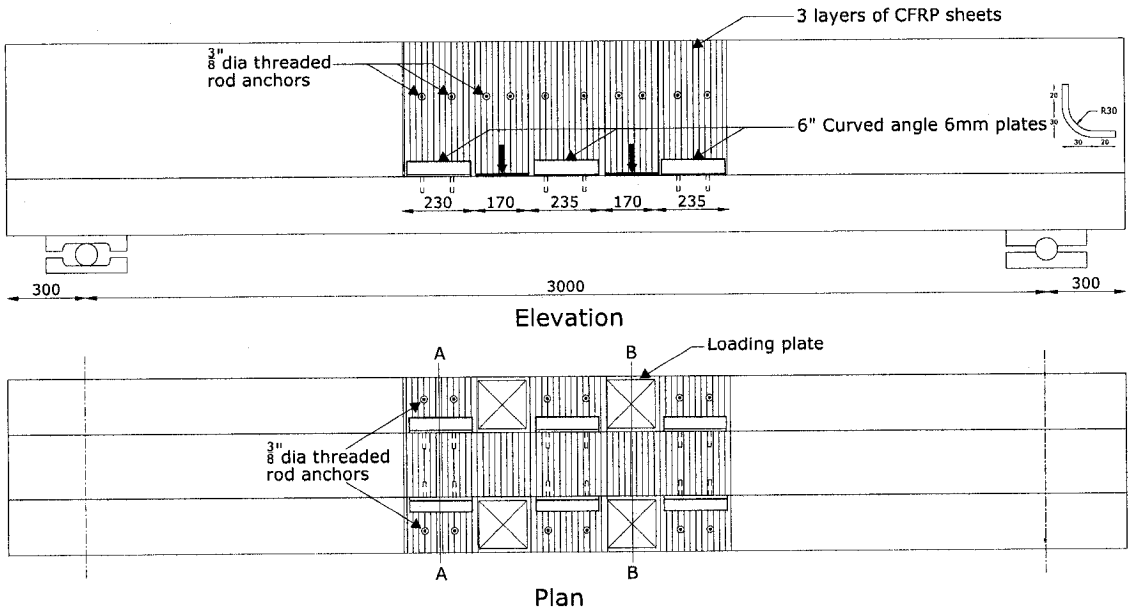

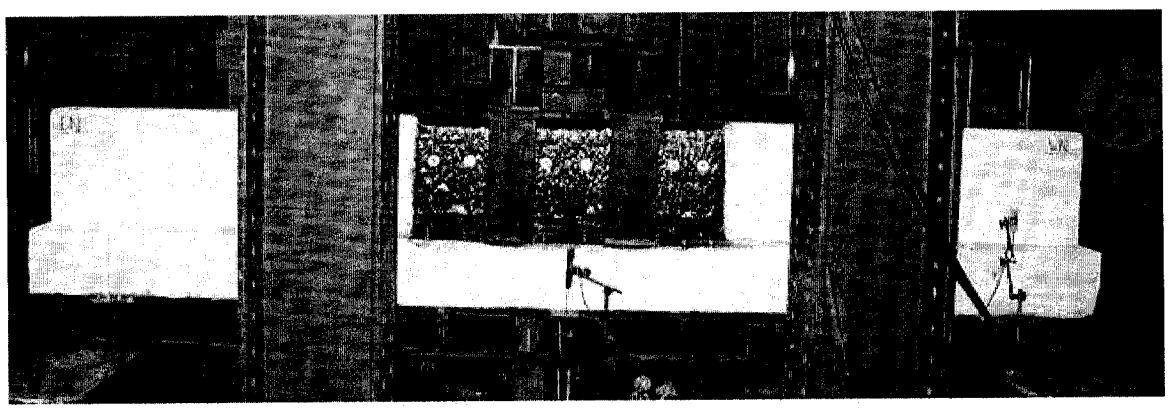

Figure 4.5 Rehabilitation scheme of girder IT-G1R

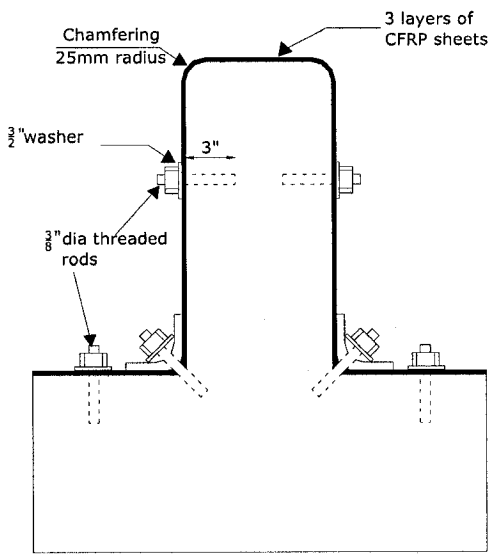

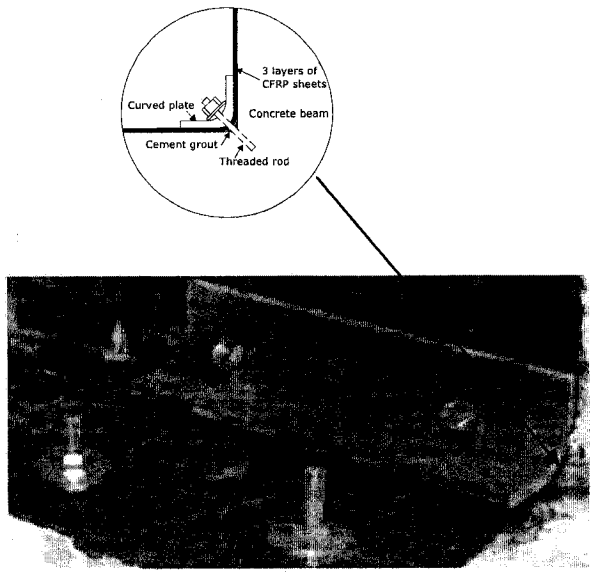

Curved angle plate and anchor

(a) Cross-section at A-A

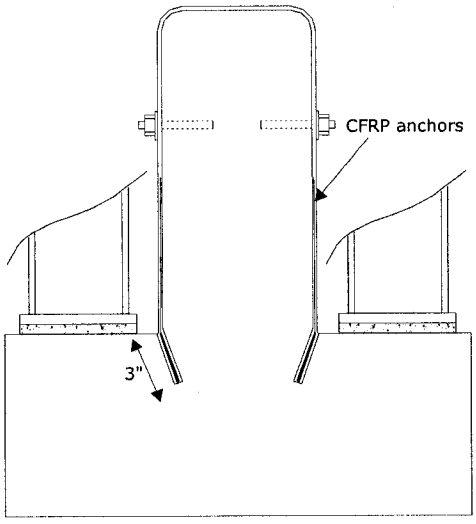

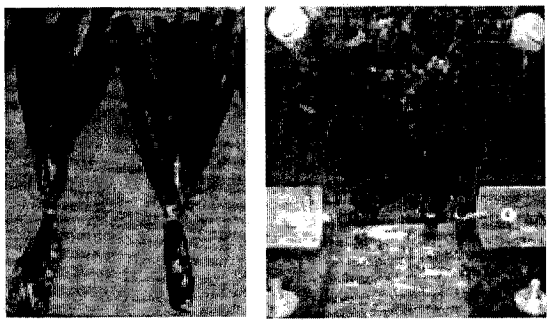

CFRP anchors

(b) Cross-section at B-B

Figure 4.6 Anchoring techniques used in girder IT-G1R at (a) Cross-section A-A, and (b) Cross-section B-B

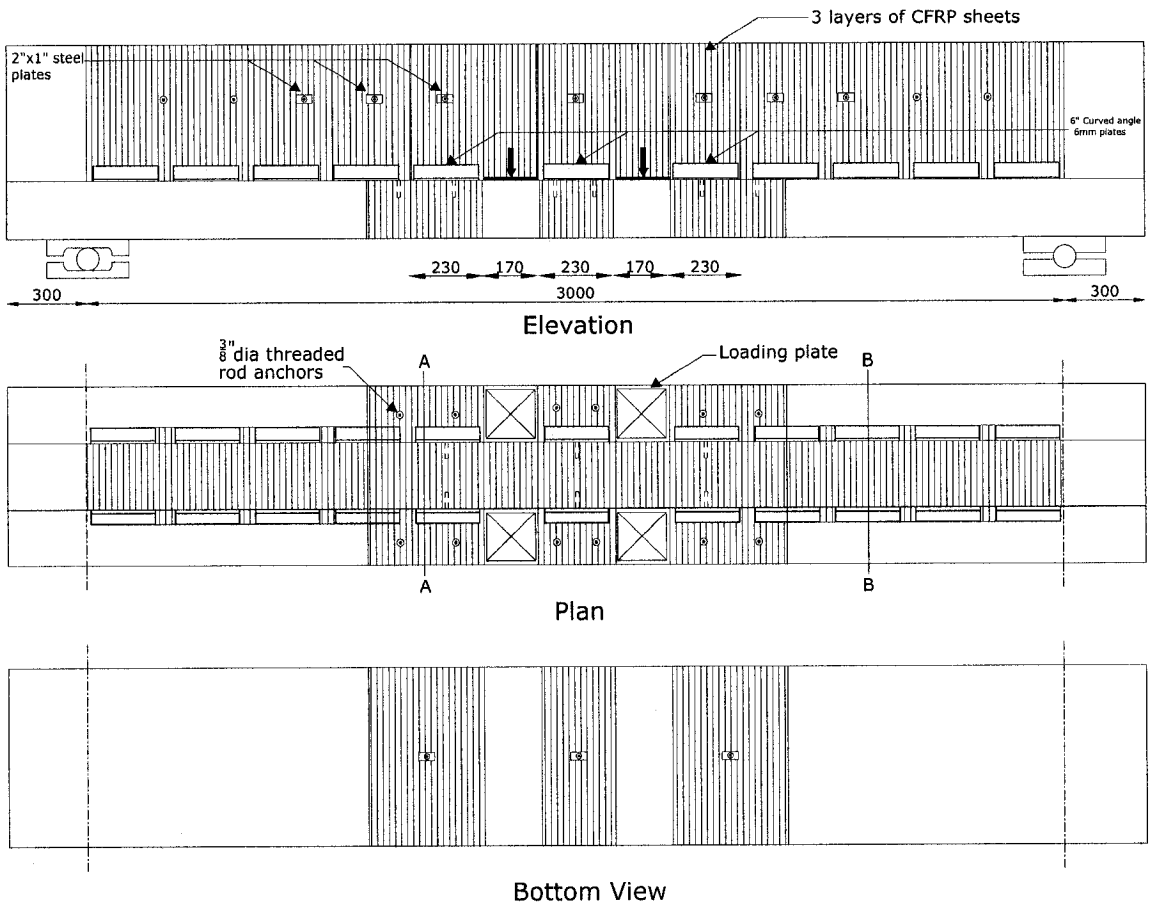

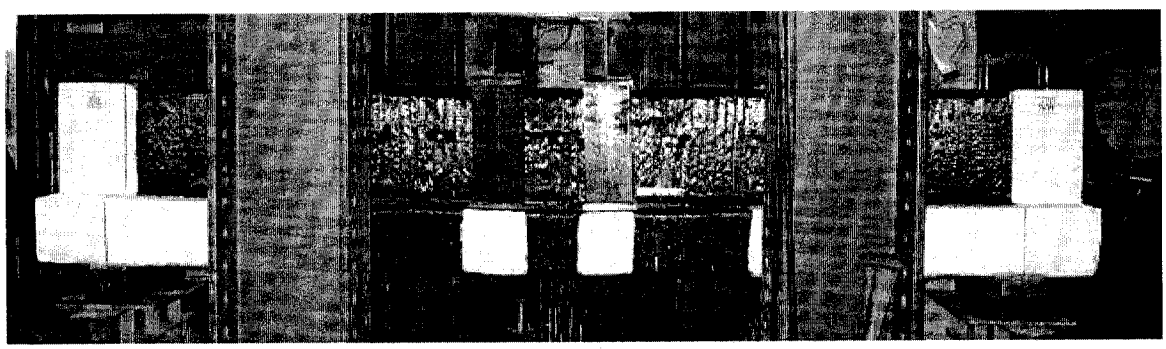

Figure 4.7 Rehabilitation scheme of girder IT-G2R

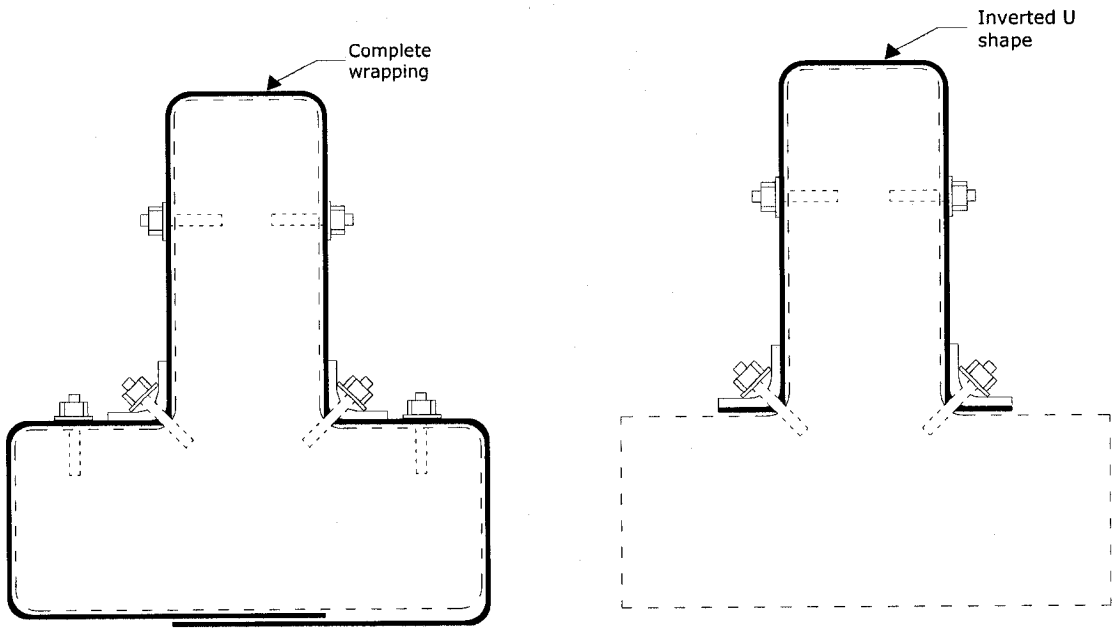

(a) Cross-section at A-A **(b) Cross-section at B-B**

Figure 4.8 Anchoring techniques used in girder IT-G2R at (a) Cross-section A-A, and (b) Cross-section B-B

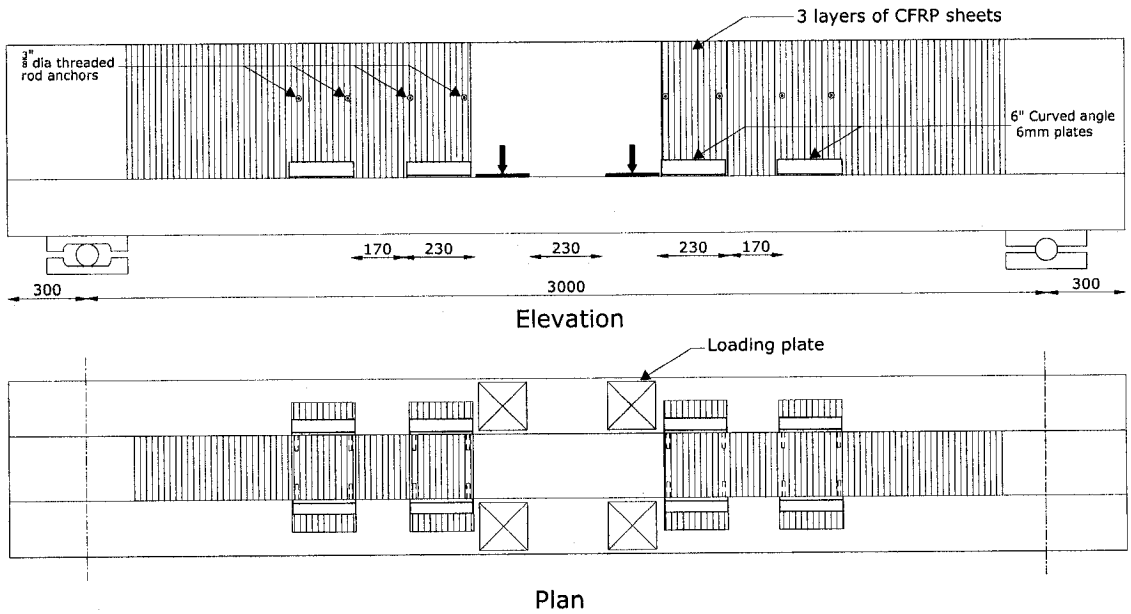

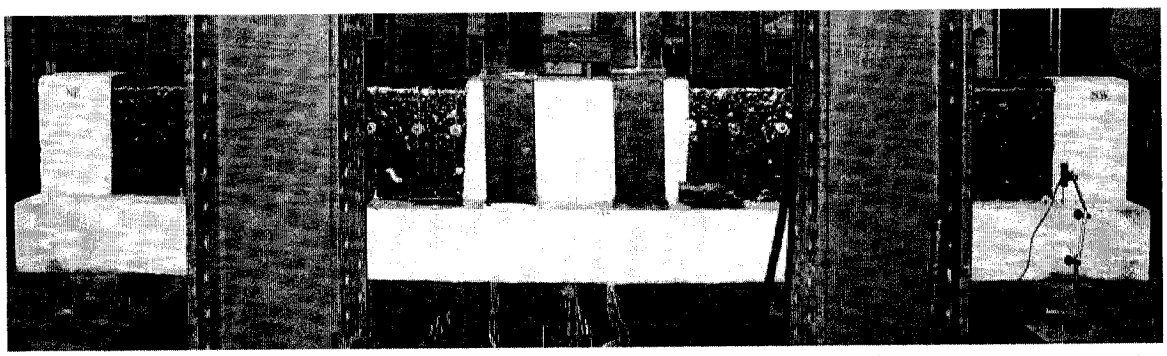

Figure 4.9 Rehabilitation scheme of girder IT-G3R

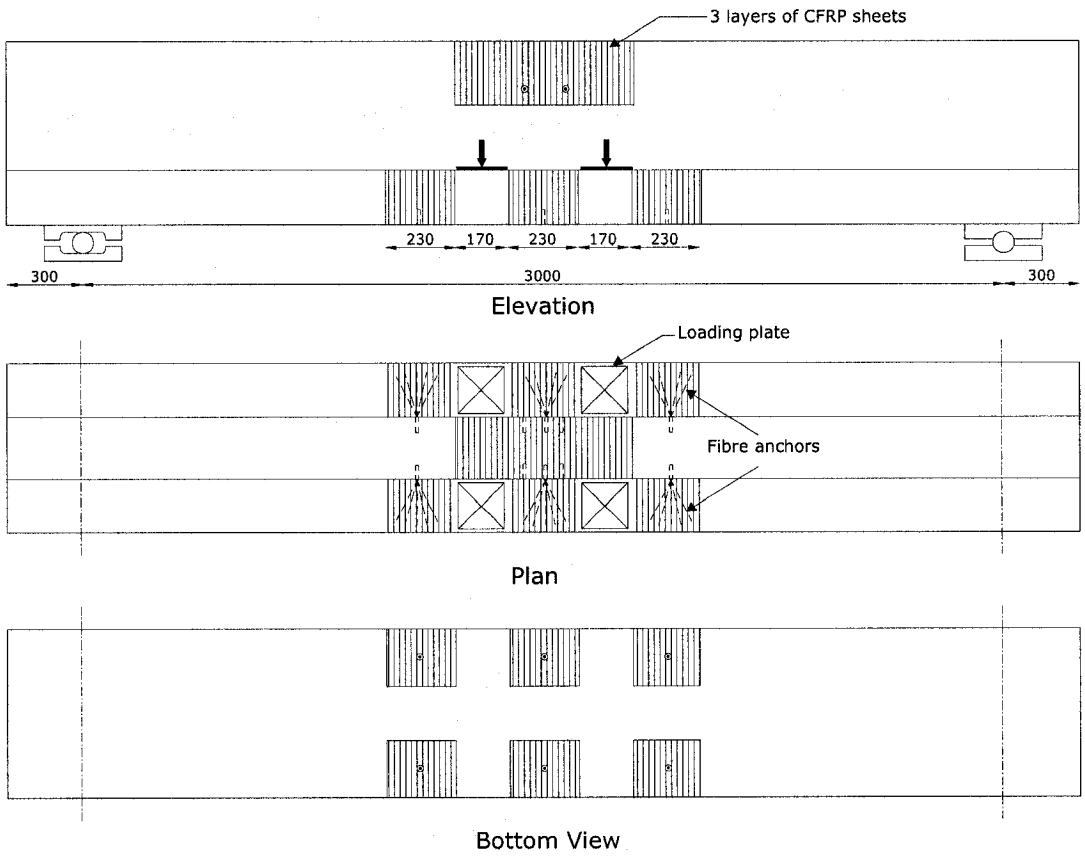

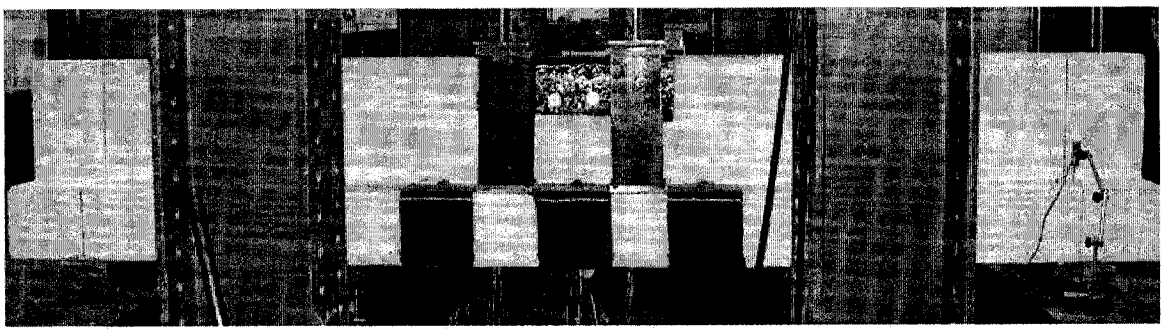

Figure 4.10 Rehabilitation scheme of girder IT-G4R

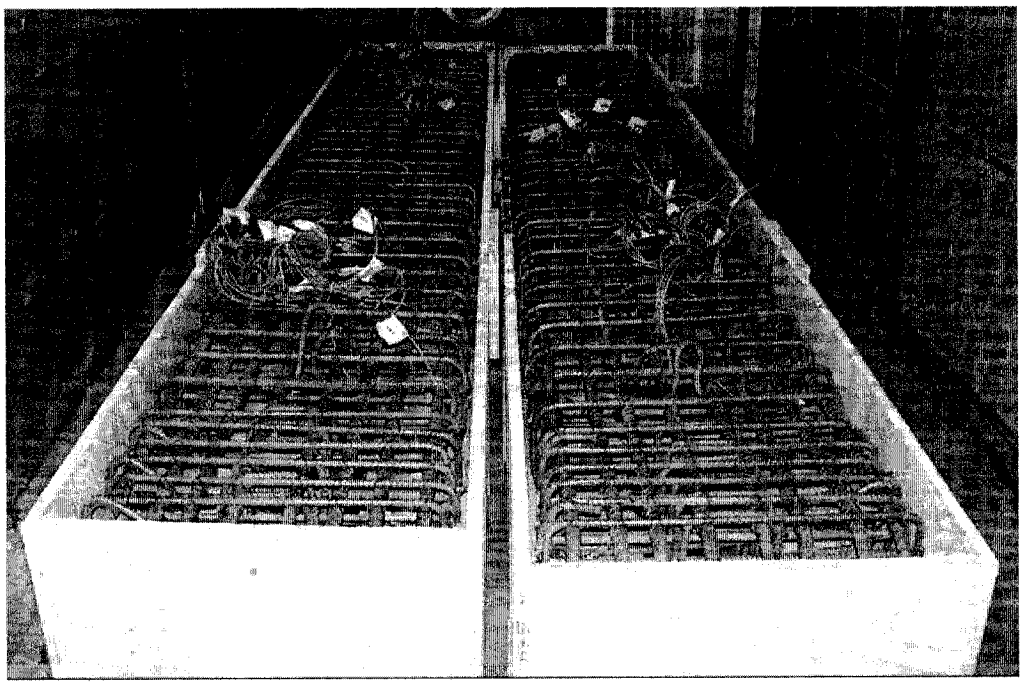

Figure 4.11 Wooden forms with steel cage before pouring concrete

Figure 4.12 Concrete after pouring concrete

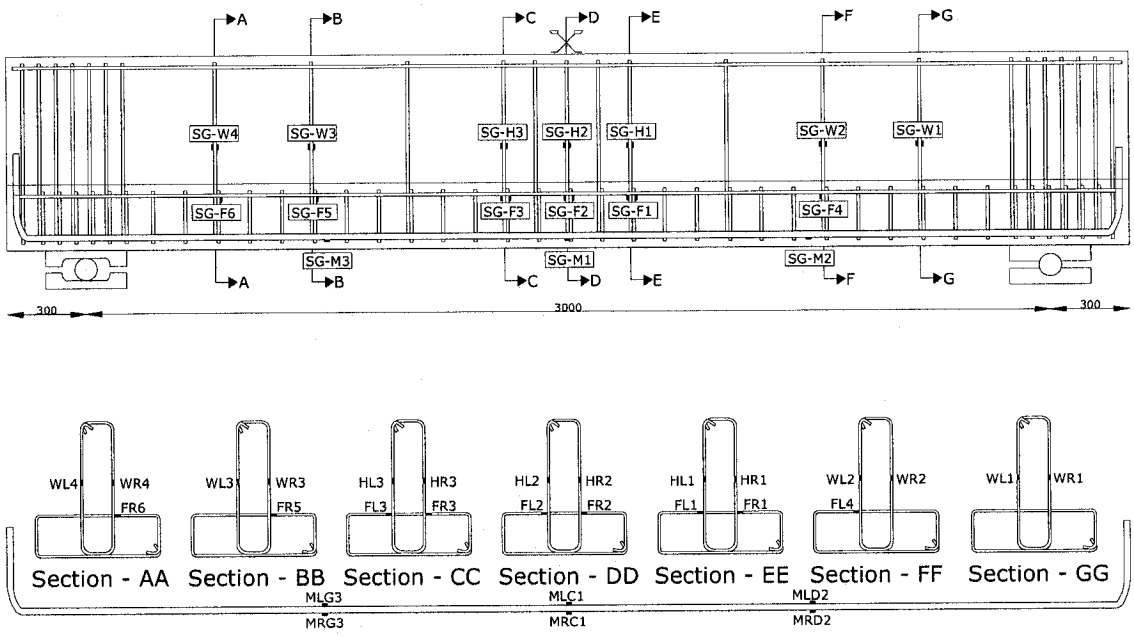

Figure 4.13 Typical locations of strain gauges in the tested girders

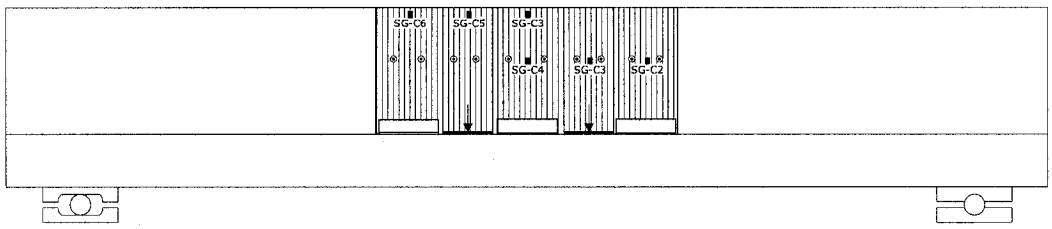

(a) Girder IT-G1R

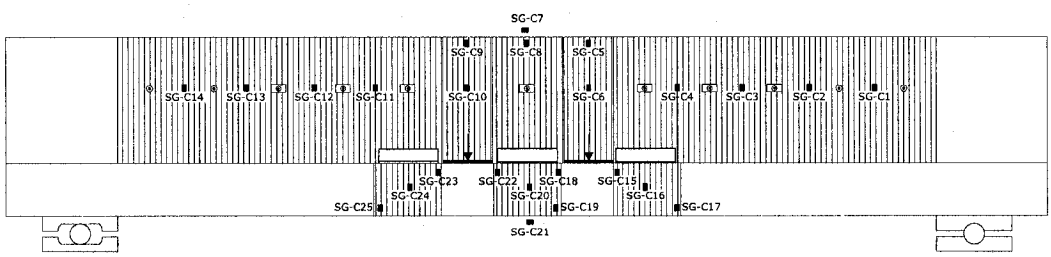

(b) Girder IT-G2R

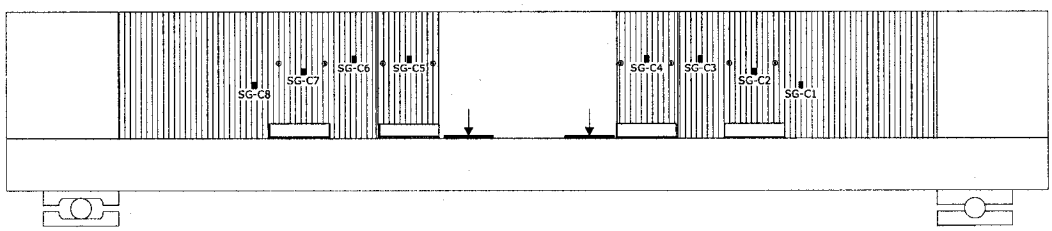

(c) Girder IT-G3R

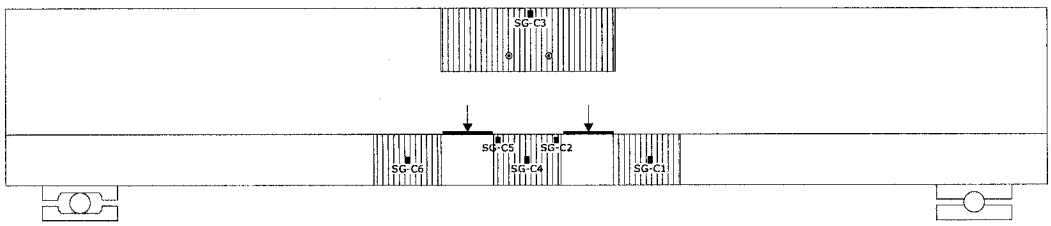

(d) Girder IT-G4R

Figure 4.14 Locations of the strain gauges on the CFRP sheets for girders IT-G1R to IT-G4R

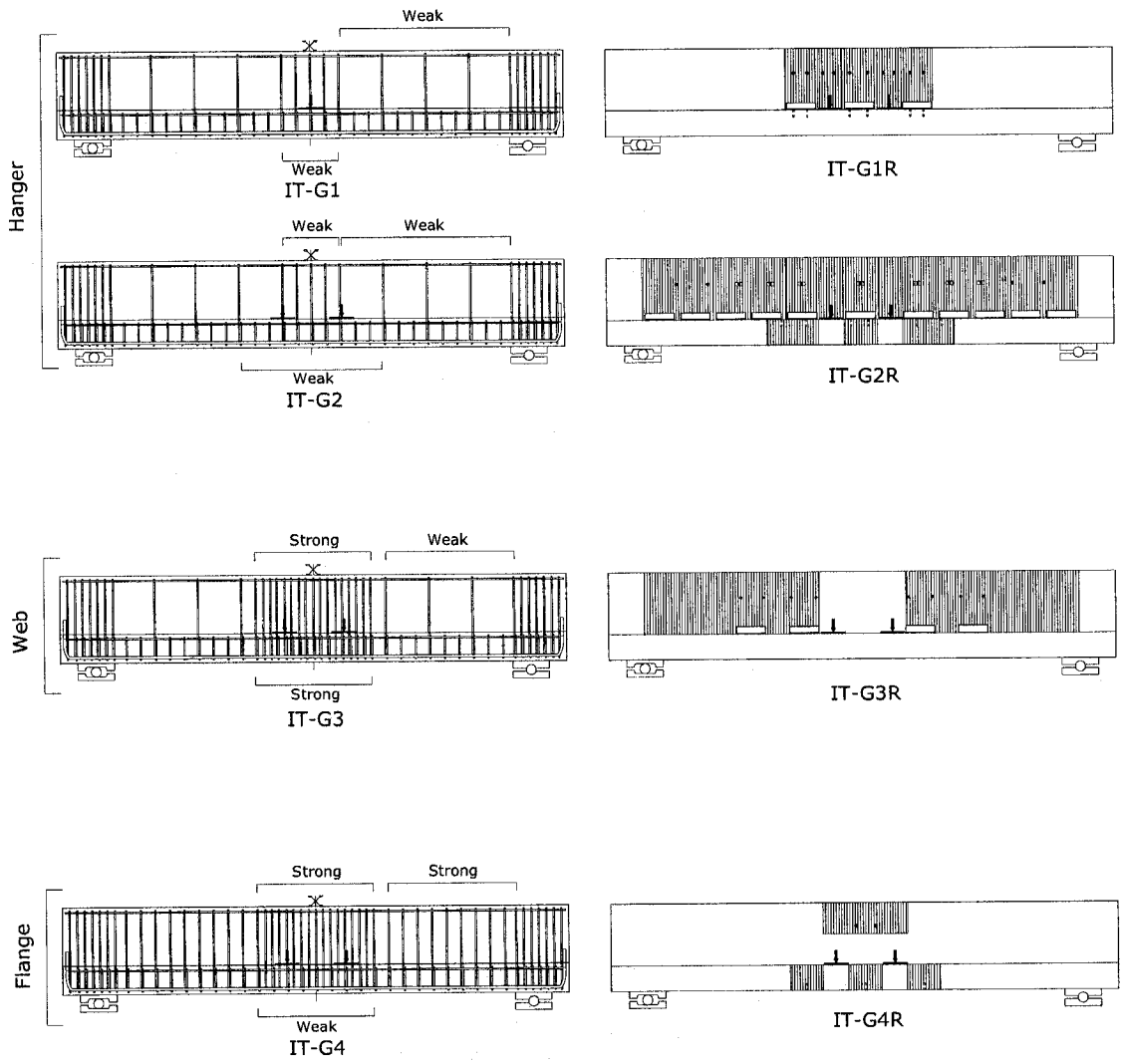

Figure 4.15 Comparison between the 8 tests conducted on the inverted-T bentcap girder models

CHAPTER 5

EXPERIMENTAL RESULTS

5.1 GENERAL

Eight tests were conducted on four reinforced concrete (RC) inverted-T girders to study the use of externally bonded carbon fibre reinforced polymer (CFRP) composite sheets in eliminating their non-ductile failure mechanisms. Four tests were conducted on the girders and four tests were conducted on girders after rehabilitation. The tested girders were subjected to 4-point load applied monotonically in seven tests, while the girder IT-G1 was subjected to 3-point loading. The girders were subjected to incrementally increasing load up to failure. During the test, the complete behaviour of each girder was monitored, including the strains in the steel reinforcements and in the CFRP sheet. In addition, the displacements at different locations along the girder were recorded by linear voltage deferential transducers (LVDT). The crack patterns were manually traced. In this chapter, the test data and experimental results are discussed. The experimental result includes the load-deflection relationships, strain along the CFRP sheets and the gain in strength for rehabilitated girders. The following three sections describe the rehabilitation of non-ductile failure mechanisms of inverted-T girders in hanger, web, and flange.

5.2 REHABILITATION OF HANGER ZONE

Four tests were conducted on two RC inverted-T girders that have minimum hanger reinforcement. Control girders IT-G1 and IT-G2 have the same reinforcement contents. Girder IT-G1 was tested in 3-point loading, while girder IT-G2 was tested in 4-point loading. Rehabilitated girders IT-G1R and IT-G2R have two different rehabilitation schemes and were tested in 4-point loading. The following subsections show the test results of the four tests.

5.2.1 Behaviour of control specimen IT-G1

Figure 5.1 shows the girder IT-G1 before test. First flexure crack was noticed at load of 150 kN. Shear cracks initiated near the supports and propagated through the flange and web at angles between 45 to 50°. The inclinations of the shear cracks decreased as the cracks were propagating towards the middle zone of the girder. At failure, horizontal cracks were developed in the flexure zone. The horizontal cracks are attributed to the high tensile strains along the vertical plane due to the nature of loading of inverted-T girder at its bottom flange which creates a hanger mechanism in the web. The horizontal cracks along with the inclined shear cracks formed a shear-compression failure mechanism.

Figure 5.2 shows the load versus mid-span deflection of girder IT-G1. The girder failed at load of 595 kN in a non-ductile manner. The vertical displacement at mid-span of the girder was approximately 10 mm. Figure 5.3 shows the complete crack pattern through out the girder on the various planes of the girder, where F denotes the location of

failure on the girder. It can be noticed that apart from the shear cracks on the girder, minor cracks were scattered all along the girder on the flange portion. These cracks are attributed to the bracket action of the flange. Figure 5.4 shows the deflected shape of the girder at various performance levels, i.e. cracking of concrete, yielding of longitudinal reinforcement, maximum load, and ultimate deflection. The deflected shape should be theoretically symmetrical but in some cases it is not. This could be due to the rounding off errors in the LVDTs. Figure 5.5 shows the elevation of the girder IT-G1 after failure.

5.2.2 Behaviour of control specimen IT-G2

Girder IT-G2 was tested in 4-point loading with a shear span-to-depth ratio (M/Vt) of 2, which is less than that of girder IT-G1 (M/Vt = 2.5), that was tested in 3-point loading. Figure 5.6 shows the girder IT-G2 before test. Behaviour of the control specimen IT-G2 was very similar to that of the specimen IT-G1. But due to change in loading system, the girder failed due to yielding of reinforcement in the hanger zone. Figure 5.7 shows the load versus mid-span deflection of girder IT-G2. Figure 5.8 shows the elevation of the girder IT-G2 after failure.

5.2.3 Behaviour of rehabilitated girder IT-G1R

Figure 5.9 shows the rehabilitated girder IT-G1R before test. Compared to girder IT-G2, girder IT-G1R behaved in a more ductile manner. The girder failed at load of 585 kN. Even though at failure, wide cracks under the loading plates were obvious but the girder failed after reaching its full flexural capacity. No signs of peeling-off the FRP

were noticed. Minor local tear of FRP sheets at the top of the girder was noticed at failure. This could be attributed to high stresses in FRP at failure load. Figure 5.10 shows rehabilitated girder IT-G1R at failure.

5.2.3.1 Load-deflection relationship

Figure 5.11 shows the load versus mid-span deflection of girders IT-G1R and IT-G2. From the figure, it can be seen that the control specimen IT-G2 failed in a non-ductile manner in the hanger zone after the girder reached its hanger capacity. The control specimen had a mid-span displacement of 12 mm when it reached its peak load capacity of 460 kN. On the other hand, the rehabilitated specimen IT-G1R using the proposed rehabilitation scheme had a higher load carrying capacity of 585 kN and behaved in a more ductile manner. The rehabilitated girder had a yield displacement of 12 mm that corresponds to the load of 520 kN. At failure, the rehabilitated girder had a mid-span deflection of 50 mm that corresponds to displacement ductility of approximately 4. The rehabilitation scheme was successful in eliminating the shear-compression web failure as well as hanger failure mechanism. The rehabilitated girder failed due to punching shear in the flange.

The deflected shapes of the girder at various performance levels are shown in Figure 5.12. The deflected shape shows good symmetry and follows the expected pattern.

5.2.3.2 Strain in web stirrups

Figure 5.13 show that load-strain relationship for the web stirrups. SG-W1 and SG-W2 represent the measured strain in the vertical stirrups in the shear-dominated zone of the girder. SG-H1 and SG-H2 represent the measured strains in the vertical stirrups that act as hangers at the loading points of the girder. From the figure it can be seen that the strains of the web and hanger stirrups of the control specimen exceeded the yield strain. The high strains in SG-W1 and SG-W2 resulted in shear cracks in the web that propagated and got connected to the horizontal cracks at the loading points (due to high strains in SG-H1 and SG-H2) and resulted in a shear-compression failure. Rehabilitating the inverted-T girder using CFRP sheets reduced the strains in the hanger stirrups, while the strain in the web stirrup SG-W1 still exceeded the yield strain. This implies that the rehabilitated scheme was successful in eliminating the hanger mechanism that resulted in the compression shear failure.

5.2.3.3 Strain in FRP

5 mm strain gauges were used to measure the distribution of strain along the principal fibres of the CFRP sheets. The maximum measured strain reached only a strain of 1000 με which is less than the ultimate strain of the used CFRP (0.01mm/mm) as provided by the supplier. Although this low strain might imply that less FRP sheets would have been used for the rehabilitation of the girder, yet there were signs of FRP tier at the horizontal top part of the web near failure, which indicated that higher strains occurred at other locations in the FRP sheets. It can also be noted that the maximum

measured strains were not recorded by the strain gauges SG-C5 and SG-C3 on hanger zone on the web due to the loading on the flange, they were recorded by the gauge SG-C3 which is at the top of the girder due to the high compression forces due to the flexure that cause higher strains to develop.

5.2.4 Behaviour of rehabilitated girder IT-G2R

The objective of this rehabilitation scheme was to look at the possibility of using CFRP sheets for hanger, shear and punching strength upgrade. Figure 5.14 shows the rehabilitated girder before test. Girder was loaded monotonically up to the failure of the girder. As the load was increased in increments of 25 kN, stretching noises of the CFRP sheets were heard right after 415 kN, the girder started to deflect noticeably. At higher loads more cracks were formed in the vicinity of the loading plates. As the load increased, cracks developed near the loading plates gradually became inclined towards the bottom of the girder. Since the girder was rehabilitated for punching shear, the cracks formed away from the rehabilitated zone under the loading plate as shown in Figure 5.15 (a).

After the girder reached a load of 475 kN, a rapid decrease in load carrying capacity is noticed. The load carrying capacity of the rehabilitated girder was increased by only 3% compared to that of the control specimen IT-G2. Careful examination of the girder after failure revealed that the anchoring technique of the CFRP sheets using curved steel angles at the web-flange intersection in the hanger zone has came out and debonding of the CFRP sheets in the hanger zone were the main causes of the girder

failure. There was no sign of peeling off or tensile rupture of CFRP sheets was noticed on the web portion of the girder but it was bulged in the compression zone because of the highly strained concrete in the compression zone of the girder. Due to the bulging, the anchors that were used to the anchor the CFRP sheets to the web of the girder near the loading points were dislocated as shown in Figure 5.15 (b). Figure 5.16 shows the rehabilitated girder at failure.

5.2.4.1 Load-deflection relationship

Figure 5.17 shows the mid span load-deflection curve for the rehabilitated girder IT-G2R and control girder IT-G2. It can be seen that the girder has a low stiffness but resulted in increase in the displacement ductility index when compared to that of un-rehabilitated specimen. The girder showed good yield plateau with a ductility index of 1.8. Figure 5.18 shows the deflected pattern at various load levels.

5.2.4.2 Strain in FRP

Strains on FRP were measured for girder IT-G2R in shear dominated zone, hanger zone and punching zone. It was noticed that the anchored CFRP wrap did not develop significant strains. The maximum recorded strain on the CFRP sheets was 3000 $\mu\varepsilon$ in the punching zone. This is less than the ultimate strain capacity of the laminate.

5.3 REHABILITATION OF WEB ZONE

Two tests were conducted on a RC inverted-T girder that has minimum shear reinforcement in the web shear zone. Girder IT-G3 was tested as a control specimen, while girder IT-G3R tested after being rehabilitated with CFRP sheets. The following subsections show the results of the two tests.

5.3.1 Behaviour of control specimen IT-G3

Figure 5.19 shows the girder IT-G3 before test. Concrete reached its modulus of rupture at 115 kN when a flexural crack appeared in the constant moment region. At 225 kN, cracks were formed near the loading plates and shear cracks initiated near the supports at around 300 kN and propagated through the flange and web at angles between 45 - 50°. Due to the sufficient reinforcement content in the hanger zone, no horizontal cracks on the face of the web between the two load points were observed. As the load increased, the shear cracks in the web propagated towards the middle of the girder. Minor cracks were scattered all along the girder. At approximately 500 kN, the monitored strains of the stirrups in shear dominated zone showed that they were approaching the yield strain.

Upon increasing load, other flexural cracks appeared in other locations between the load points in N-S directions. As the load was increasing, cracks became wider but no further increase in crack length was observed. At 508 kN, web stirrups yielded without increase in load carrying capacity. Formation of wide diagonal shear cracks at the web portion of the girder was the causes of failure.

Figure 5.20 shows the load versus mid-span deflection of girder IT-G3. Load-deflection curve reveals a non-ductile failure mechanism with the failure load of 508 kN while the analytical capacity of the girder was found to be 540 kN.

Figure 5.21 shows the crack pattern of girder IT-G3 at failure. Several 45° cracks were formed at high load levels on the face of the web can be seen. On flange the cracks were more or less vertical appeared through out the length of the girder.

The deflected shapes of the girder at difference performance levels are shown in Figure 5.22. Figure 5.23 show the close up view of the web portion of girder at failure.

5.3.2 Behaviour of rehabilitated girder IT-G3R

Figure 5.24 show the girder before test. The girder was loaded gradually with 25 kN increments. Some stretching noise was heard at the initial stages of loading. Due to the presence of FRP, the shear cracks remained tight and impending of shear failure did not take place. Upon increase in loading minor cracks were scattered all along the girder in the zone not rehabilitated. Upon increase in loading, the girder continued to carry load until failed at 565 kN. The girder failed after reaching its flexural web-compression capacity. There were no signs of delamination of CFRP sheets from the concrete and fully bonded to the concrete at failure. Figure 5.25 show the rehabilitated girder at failure.

5.3.2.1 Load-deflection relationship

Figure 5.26 illustrates load versus mid-span deflection curve of the control and rehabilitated girders. It can be seen that rehabilitated girder failed at a higher load compared to the control specimen. The deflection corresponding to the peak load was approximately 14.5 mm with the ductility index of 1.81. The rehabilitation scheme was successful in eliminating the web-shear failure mechanism.

Figure 5.27 shows the deflected shape of the girder at different load levels. It can be noticed that the FRP controls the deflection of the girder for the same load when compared to the un-rehabilitated girder and the deflected shapes are in accordance with the expected behaviour of the girder

5.3.2.2 Strain in web stirrups

Figure 5.28 shows the load-strain relationship for the web stirrups. SG-W1 and SG-W2 represent the measured strain in the vertical stirrups in the shear-dominated zone of the girder. SG-H1 and SG-H2 represent the measured strains in the vertical stirrups that act as hangers at the loading points of the girder. From the figure it can be seen that the strains of the web stirrups of the control specimen exceeded the yield strain. The high strains in SG-W1 and SG-W2 resulted in shear cracks in the web. But the strains in SG-H1 and SG-H2 were very well below the yield strain which shows that reinforcement provided in the hanger zone was sufficient to transfer the applied load. Therefore high strains in SG-W1 and SG-W2 resulted in a web shear failure. While the rehabilitating the girder with FRP sheets reduced the strain in the shear dominated zone although

exceeding yield strain in SG-W2, but the strain in SG-H1 was close to yield strain and due to the high compressive force, rehabilitated girder failed after reaching flexural web-compression capacity. Therefore the chosen scheme was successful in eliminating shear failure in web.

5.3.2.3 Strain in flange and flexural reinforcement

Figure 5.29 shows that the load-strain relationship for the flange and flexural reinforcement. SG-F1 and SG-F2 are the measured strains in the flange reinforcements where the strain in the flange will be primarily due to the bracket action. SG-M1 represents the measured strain in the flexural reinforcement at the maximum flexural moment location.

Due to high reinforcement content in flange, the recorded strains in SG-F1 and SG-F2 are well below the yield strain. The flexural longitudinal reinforcement reached yield strain (2100με) at a load level of 525 kN.

5.3.2.4 Strain in FRP

Strain in the FRP laminate for various load levels was measured and the maximum strain in the FRP reached was 1400 με which is substantially less than the maximum strain capacity (0.01 mm/mm) of the laminate.

5.4 REHABILITATION OF FLANGE

Two tests were conducted on a RC inverted-T girder that has minimum flange reinforcement in the punching zone. Girder IT-G4 was tested a control specimen, while girder IT-G4R tested after being rehabilitated with CFRP sheets. The following subsections show the results of the two tests.

5.4.1 Behaviour of control specimen IT-G4

Figure 5.30 show the girder IT-G4 before test. The primary objective of testing this girder was to determine the behaviour of CFRP sheets bonded with the girder failed in punching shear. Figure 5.31 shows the load-mid span deflection of IT-G4. As the tensile stress in the flexure zone reached the tensile strength of concrete, the first cracking load was observed at 115 kN. At 225 kN, shear cracks initiated near the loading plates and also near supports which propagated through the flange and to the web. Similar to IT-G3, no horizontal cracks were formed between the two loading points. More minor cracks developed along the girder due to the increase in loading. Web shear cracks stopped progressing and cracks under the loading plates started to widen. At around 515 kN, girder failed due to punching shear with a maximum deflection of 12 mm. The analytical capacity of the girder was 645 kN, while it's failure load was 515 kN.

Figure 5.32 shows the complete crack pattern of girder IT-G4 at failure. Figure 5.33 shows the deflected shapes of the girder at different load levels. The curves are plotted based on the average readings of two LVDT's at each location.

5.4.2 Behaviour of rehabilitated girder IT-G4R

Figure 5.34 shows the rehabilitated girder IT-G4R before test and Figure 5.35 shows the close up view of the rehabilitated scheme. After rehabilitation, the girder was loaded gradually by monitoring the formation of cracks along the girder. As load was increased in increments of 25 kN, minor cracks were scattered along the girder in the zone not rehabilitated. At higher loads, the girder started to deflect more and minor delamination was noticed in the flexural compression zone of the girder, yet the anchoring of the CFRP sheets eliminated the progressive spread of the delamination of the sheet. The girder failed in flexure after significant yield of main reinforcement at the load of 653 kN with the displacement ductility of 4.6. At failure, the sheets remained completely intact and failure occurred outside the strengthened zone. Figure 5.36 shows the rehabilitated girder IT-G4R at failure.

5.4.2.1 Load-deflection relationship

Figure 5.38 shows the load versus mid-span deflection of the tested girders. From the figure it can be seen that the control specimen IT-G4 failed due to non-ductile punching shear failure in the flange with a maximum deflection of 12 mm at a peak load of 515 kN, while the rehabilitated girder IT-G4R behaved in a more ductile manner with a carrying load capacity of 653 kN. The rehabilitated girder had a displacement ductility of approximately 4. This shows that the rehabilitation scheme was successful in eliminating the punching shear failure mechanism.

Figure 5.39 shows the deflected shapes of the girder at different load levels. High curvature in the mid-span region is due to the higher ductility of the girder.

5.4.2.2 Strain in steel

Figure 5.40 shows the load-strain relationship for web stirrups for both control and rehabilitated girder. Since the girder has sufficient reinforcement in shear as well as in hanger zone, strains in those areas are well bellow the yield strain. On the other hand, Figure 5.41 shows the load-strain relation for hanger and flexural reinforcement. Before rehabilitation, reinforcement in the brackets were able to resist the cantilever action of the girder but due to shear in 45° plane along the loading plate resulted in the failure of brackets due to punching. After rehabilitation, strains in steel in the brackets were almost similar when compared to un-rehabilitated specimen. But flexural steel yielded and there is a sudden jump in the strain data which shows that the steel in the flexural zone was yielded. Finally girder reached its flexural capacity and failed at a load of 653 kN in a ductile manner.

5.4.2.3 Strain in FRP

It was observed that the strain produced by the gauge located on the punching zone exhibits more which is because of the high shear stresses near the loading plate at 45° plane when compared to other strain gauges. It was also noticed that the strains in the compression zone also exhibited less strains due to the extra strength given by the FRP. Max strain in the FRP reached was close to 1600 με which is less that the ultimate strain.

This indicates that the FRP reserves more strength and the girder would have carried more load if the failure did not occur outside the strengthened zone. It is also worth mentioning that there were no signs of pullout of the anchors that were used in the punching zone, which indicates that the amount of fibre anchors and their embedded length was sufficient to transfer the stresses from the fibres to the girder.

5.5 COMPARISON BETWEEN THE PREDICTED AND EXPERIMENTAL SHEAR CAPACITIES

Table 5.1 shows that analytically predicted capacities of different mechanism and their corresponding experimental ones of the four rehabilitated girders in kN. Girder IT-G1 that had inadequate hanger and web-shear reinforcement experienced a non-ductile failure mechanism in the hanger zone at a shear capacity of 230 kN. Using 3 layers of anchored CFRP sheets in the hanger zone of girder IT-G1R resulted in increase in its hanger shear capacity. Upon loading the girder to failure, the load-resisting mechanisms of the girder were triggered. From the table, it can be seen that there is a good agreement between the analytically predicted and experimentally recorded behaviour. It should be noted that due to the difficulty of instrumentation, the shear friction mechanisms were not monitored experimentally.

Although girder IT-G2R was rehabilitated such that the FRP would contribute to the shear capacity of the six non-ductile mechanisms, yet the anchoring technique of the CFRP sheets using curved steel angles at the web-flange intersection in the hanger zone did not fully utilised the shear capacity contribution of CFRP sheets. The specimen failed at a load of 475 kN (shear capacity of 237.5 kN) after FRP contributing nearly 155 kN

(V=77.5 kN) more than the initial capacity of the girder in hanger mechanism of 320 kN (V=160 kN). After reaching the load level of 475 kN, the sudden debonding of the CFRP sheets resulted in sudden reduction in the total hanger resistance of the girder which lead to the premature failure of the girder without fully utilizing the contribution of FRP sheets.

Girder IT-G3 that had inadequate web-shear reinforcement experienced a non-ductile shear failure mechanism in the web-shear zone at a shear capacity of 254 kN. Using 3 layers of anchored CFRP sheets in the web-shear zone of girder IT-G3R resulted in an increase in its predicted web-shear capacity and consequently the girder was able to develop a ductile behaviour in flexure. The longitudinal reinforcement of the girder yielded at a load of 525 kN (V=262.5 kN). The girder failed after reaching its flexural web-compression capacity of 565 kN (V=282.5 kN) which is less than the analytically predicted and by about 16%. It should be noted that it is expected the full flexural capacity could have been reached if the web-compression was confined (as was observed in girder IT-G4R).

Girder IT-G4 that had inadequate flange reinforcement experience a non-ductile punching shear failure mechanism in the flange zone at a punching shear capacity of 515 kN (V=275.5 kN). Using 3 layers of anchored CFRP sheets in the punching and web-compression zone resulted in an increase in its predicted shear capacity of five of the six non-ductile mechanisms as shown in Table 5.1. The rehabilitated girder was capable of developing the yielding and ultimate flexural capacities at load levels that are close to the predicted ones.

5.6 FINITE ELEMENT MODELLING

The primary focus of this section was to construct a three-dimensional Finite Element (FE) model that is capable of predicting the load carrying capacity of reinforced concrete inverted-T girders. The FE model was created using the commercially available finite element software ABAQUS® V.6.2. A 3D non-linear model of the RC bridge girder was developed. Modelling the complex behaviour of reinforced concrete elements involves several challenges due to its non-homogeneous and anisotropic nature. The aim of the current model is to use simple models to represent concrete and steel. In this study, the concrete was modelled using 8-node non-linear solid elements in tension and compression, while the steel reinforcement in the reinforced concrete girder is modelled as one-dimensional non-linear strain elements. In order to simulate the failure mechanisms of inverted-T girders, finite element analysis with the concrete damaged plasticity approach (an option in ABAQUS V.6.2) was used.

5.7 MATERIALS

5.7.1 Concrete

Figure 5.42 shows the stress-strain relationships of concrete in compression used to define the material properties of the non-linear model. In compression, the stress-strain curve is taken to be linear up to 30% of the compressive strength of concrete, after which a non-linear relationship represented by a parabola is assumed. In tension, the stress-strain curve for concrete is modelled to be linearly elastic up to the tensile strength of concrete, after which, the concrete cracks and the strength decreases gradually to zero.

Figure 5.43 shows the tensile stress-strain curve of concrete used in model. The stress-strain relationship in compression is similar to the concrete compression softening model proposed by Vecchio and Collins (1986).

Eight node non-linear solid elements are used to model the concrete. The element is defined by eight nodes having three degrees of freedom at each node: translations in the nodal x, y and z directions. The geometry and node locations for this element type are shown in Figure 5.44. Figure 5.45 shows the modelled specimen.

5.7.2 Steel reinforcement

Non-linear uniaxial tension-compression element with three degrees of freedom at each node: translations in the nodal x, y and z directions was used to model the reinforcing rebars. The longitudinal rebars and stirrups were descritized using 2-node straight elements. The geometry and node locations for this element type are shown in Figure 5.46.

Different bar sizes were used in the model to represent those used in the tested specimens. The stress-strain relationships for the steel was assumed to be identical in tension and compression. The yield stress of steel was taken as 400 MPa and the ultimate stress was 600 MPa. The elastic modulus for the steel reinforcement was taken as 200 GPa. Poisson's ratio of 0.3 was used. Figure 5.47 shows the stress-strain relationship used in this study.

Figures 5.48, 5.49 and 5.50 show the modelled reinforcement content for specimens IT-G1, IT-G2, IT-G3 and IT-G4, respectively.

5.8 LOADING, BOUNDARY CONDITIONS AND MODELLING METHODOLOGY

In the experimental program, all the girders were tested in 4-point bending except for the girder IT-G1 tested in 3-point loading. Similarly in finite element models three girders were loaded using 4-point loading systems and one with 3-point loading system. Loads are applied on girders as increasing pressure at the zones of load application and the support was represented as a single line of support. The line of support allows rotations of the nodes and restrains the vertical and lateral displacements. Figure 5.51 shows the finite element model with the loading pattern and boundary conditions.

Due to symmetry and to reduce computation time only one half of the girder was modeled. Since no significant slip between concrete and steel reinforcement was observed in the testing, perfect bond between materials is assumed in this study.

5.9 PREDICTIONS OF LOAD CARRYING CAPACITY

Figure 5.52 shows the comparison between the experimental and finite element model load carrying capacities of the four inverted-T girders. The differences between the predicted load capacities using the FE model and the experimental load capacities are all within 15% for the four tested girders. The over estimation of the load carrying capacities of the tested girders using the FE model by 12.2% to 13.8% can be attributed to ignoring representation of the bond between concrete and steel rebars using interface elements. This could have resulted in a slightly higher analytical stiffness compared to the actual ones.

Table 5.1 Comparison of the predicted and experimental shear capacities (in kN) of the four rehabilitated girders

Failure Mechanisms		IT-G1R				IT-G2R				IT-G3R				IT-G4R			
		Predicted (kN)			Exp. (kN)	Predicted (kN)			Exp. (kN)	Predicted (kN)			Exp. (kN)	Predicted (kN)			Exp. (kN)
		V_c+V_s	V_f	V	V=P/2	V_c+V_s	V_f	V	V=P/2	V_c+V_s	V_f	V	V=P/2	V_c+V_s	V_f	V	V=P/2
Hanger		160	225	775		160	225	385	237.5 F	1025		1025		1025	125	1150	
Web shear		270		270	262.5 Y	270	225	525		270	225	495		565		565	
Flange	**F1**	325		325		325	125	450		325		325		325	125	450	
	F2	705		705		705	125	830		705		705		705	125	830	
	F3	280		280		280	125	405		560		560		280	125	405	
	F4	330		330	275 Y	650	125	775		590		590		330	125	455	
Flexure	**P_c**	51			60 C	51			61 C	51		57.5 C		61		57.5 C	
	P_y	270		270	260 Y	270		270	207.5 Y	270		270	262.5 Y	270		270	255 Y
	P_u	335		335	292.5 F	335		335		335		335	282.5 F	335		335	326.5 F

F1 = Punching shear
F2 = bracket-type shear friction
F3 = transverse reinforcement required to satisfy shear friction
F4 = flange transverse reinforcement required to resist flexural tension
V_f = FRP contribution based on equation 3-9

P_c = Cracking capacity of the girder
P_y = Yielding of the longitudinal reinforcement
P_u = Ultimate flexural capacity of the girder
Exp. = Experimental result
C = Cracking, Y = Yielding; F = Failure

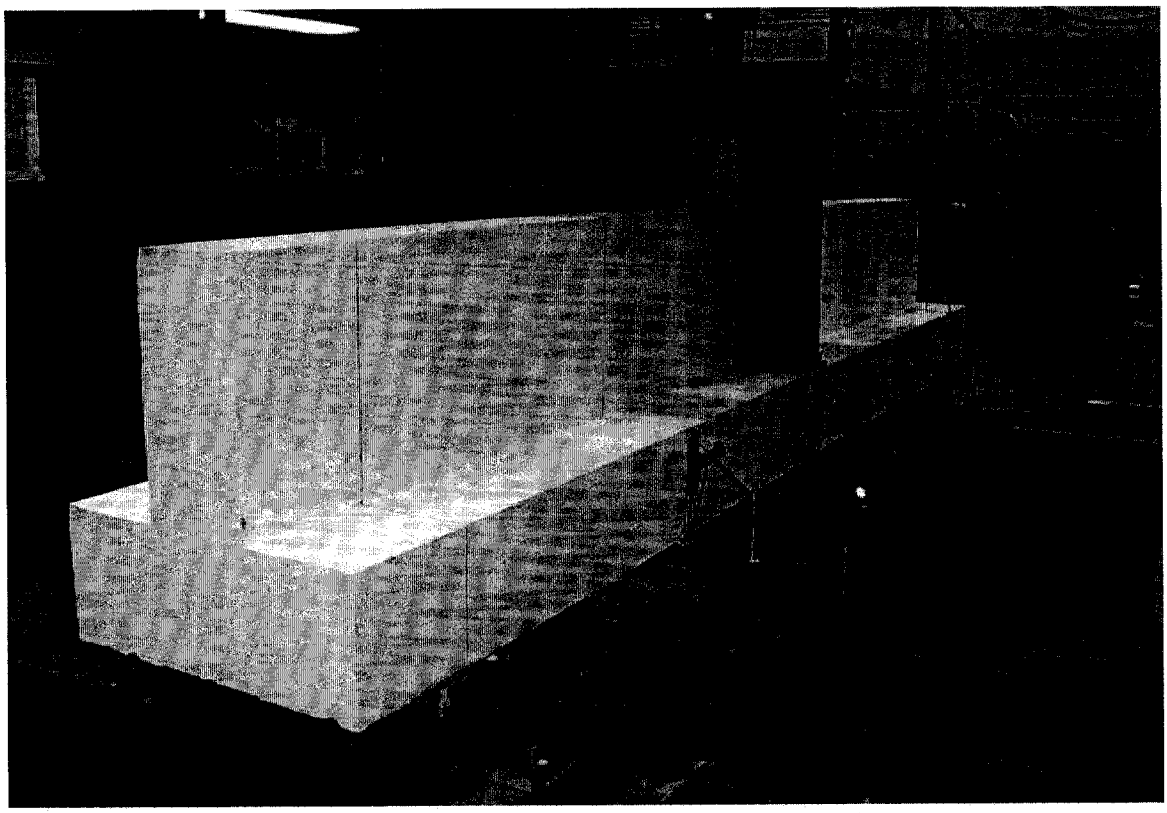

Figure 5.1 Girder IT-G1 before test

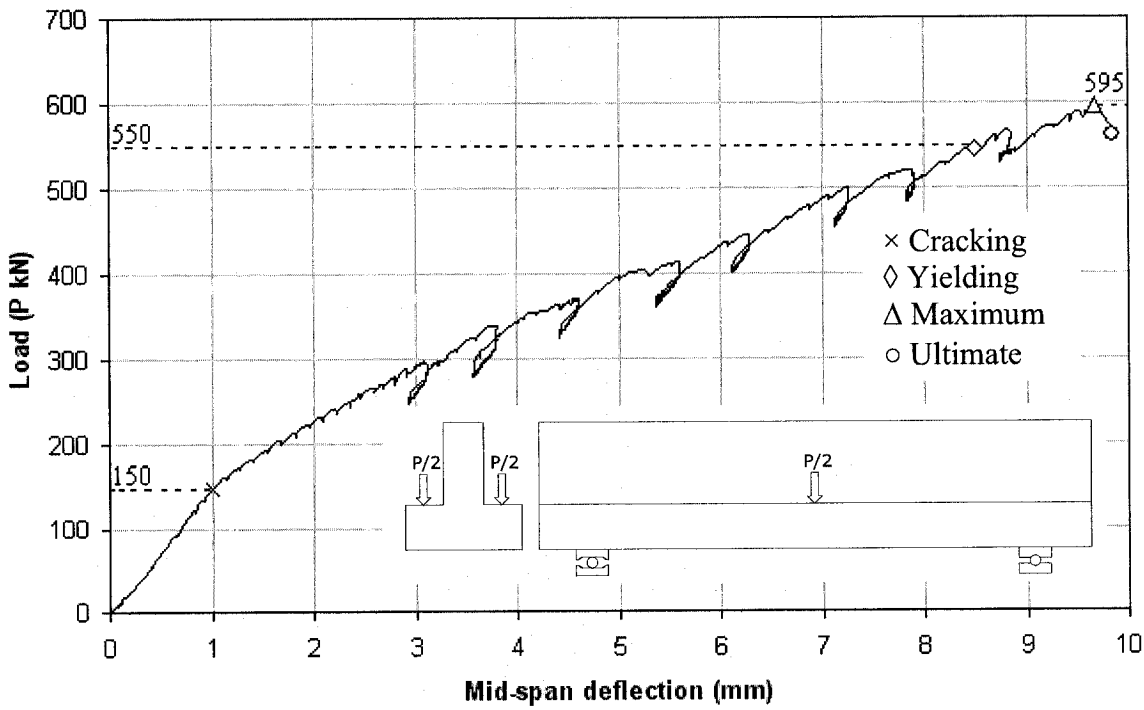

Figure 5.2 Load mid-span deflection of girder IT-G1

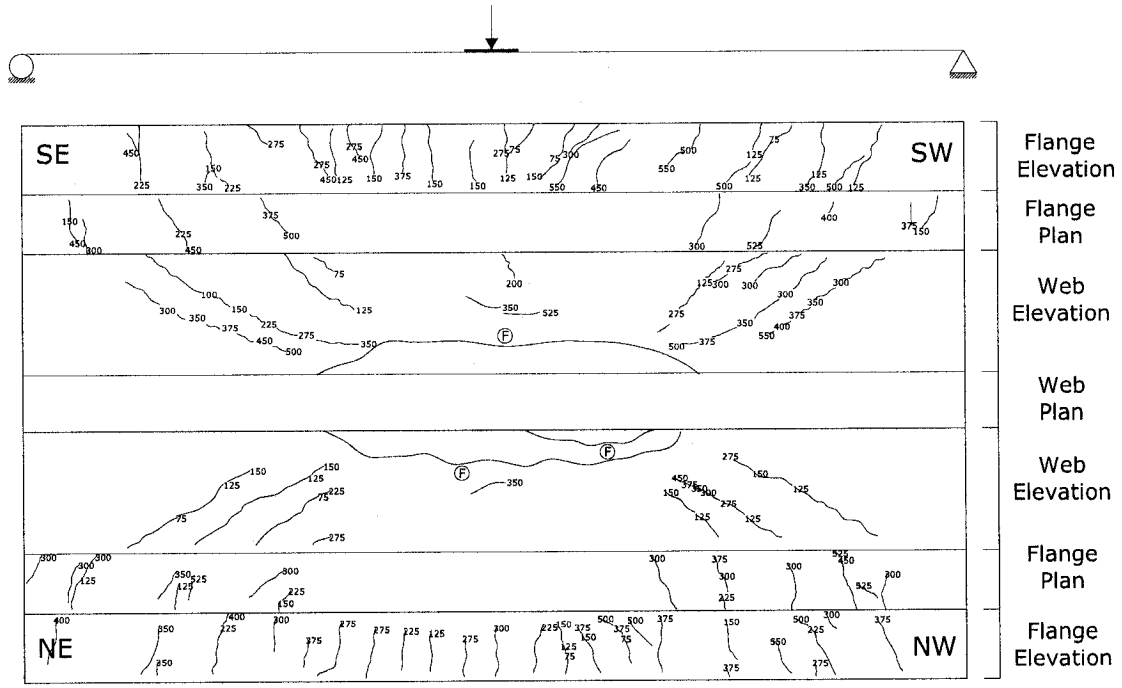

Figure 5.3 Crack pattern of girder IT-G1

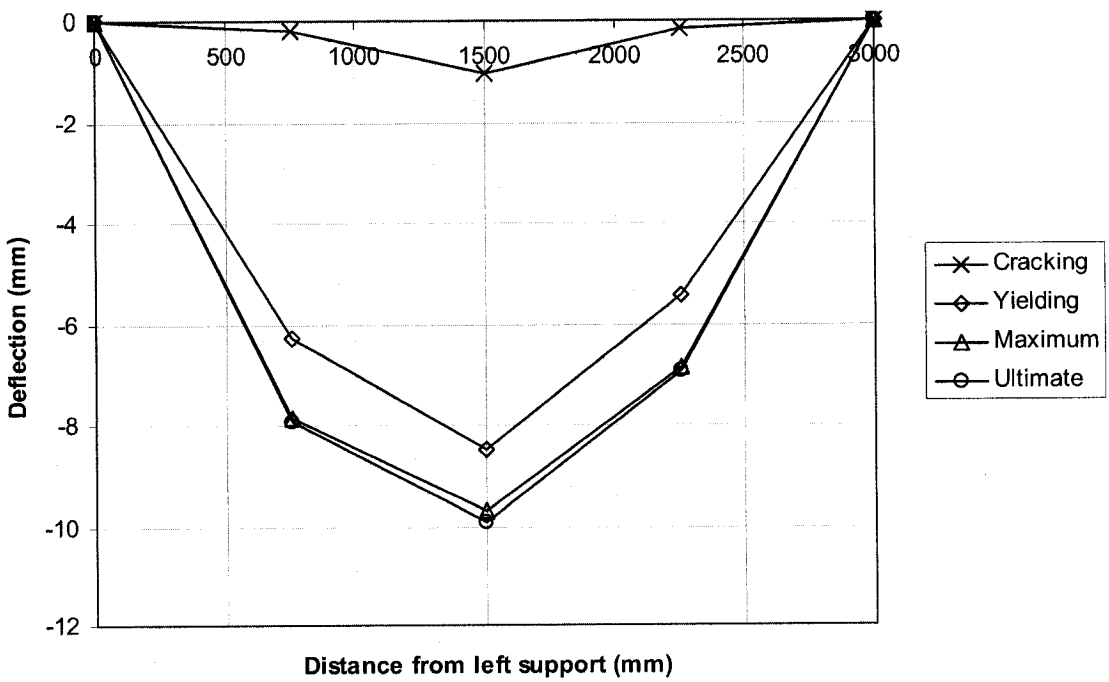

Figure 5.4 Deflected shape of IT-G1 at various performance levels

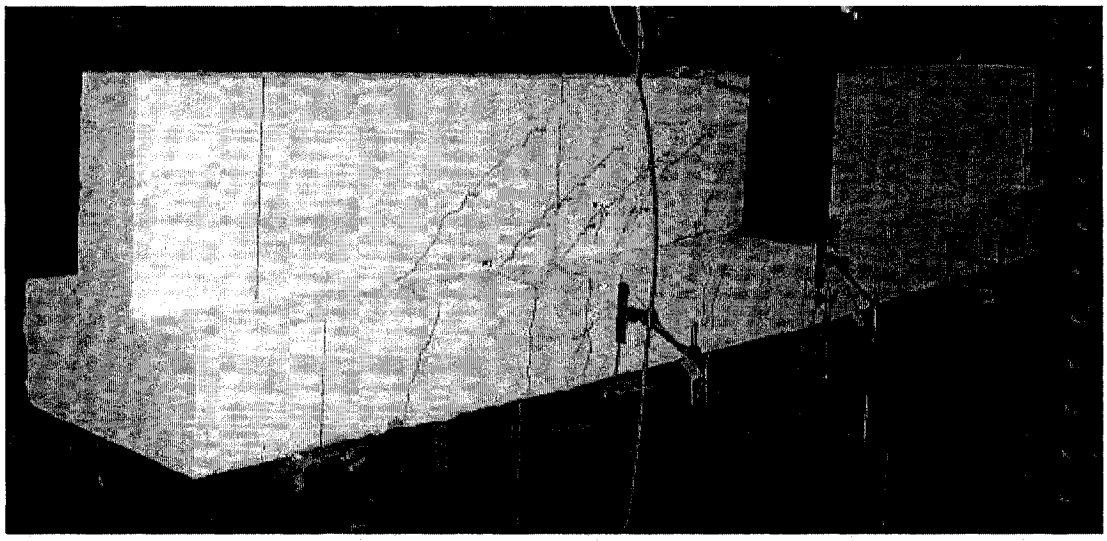

Figure 5.5 Shear-compression failure (girder IT-G1) in the web

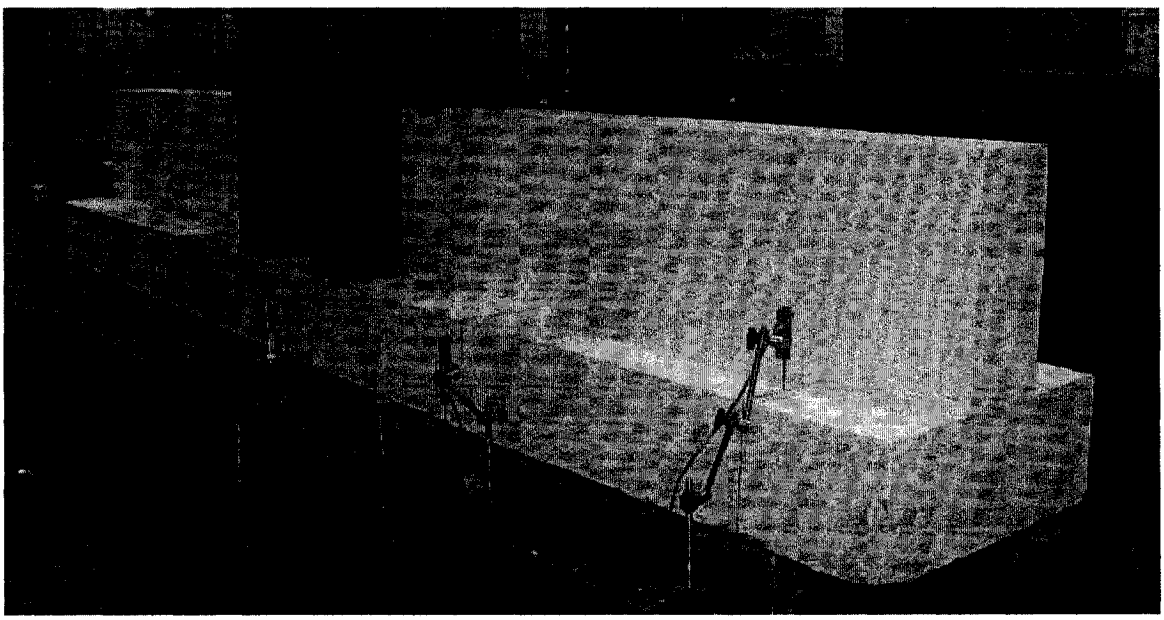

Figure 5.6 Girder IT-G2 before test

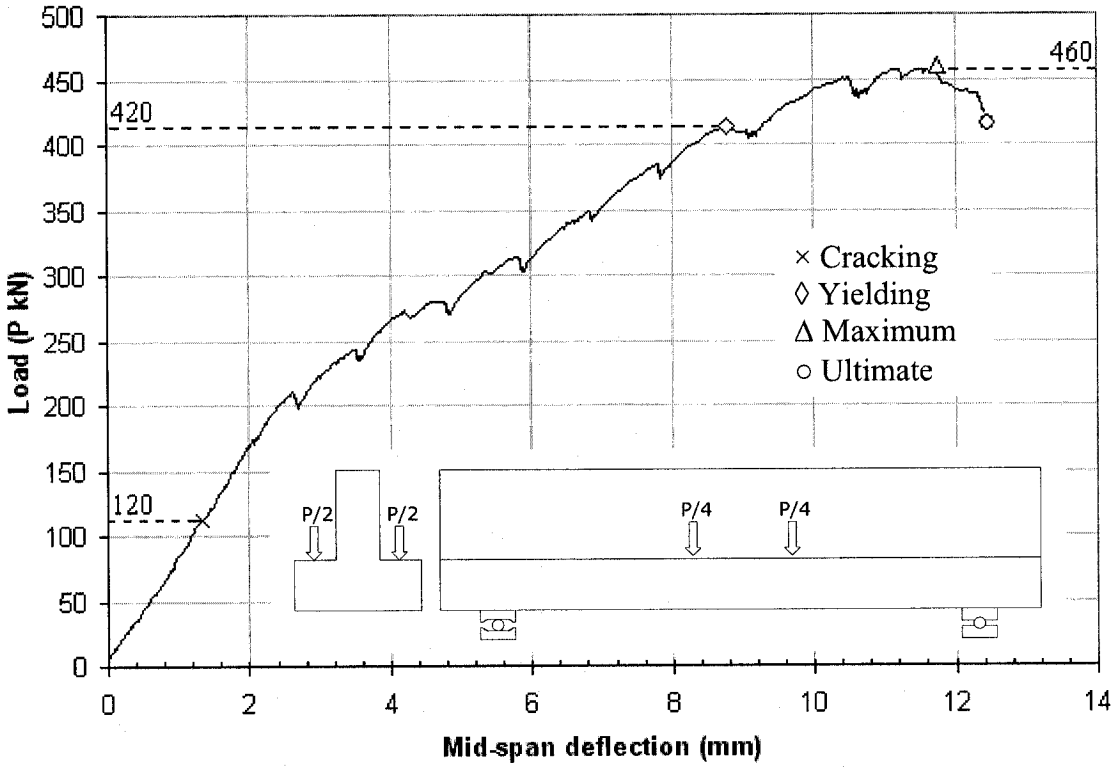

Figure 5.7 Load mid-span deflection of girder IT-G2

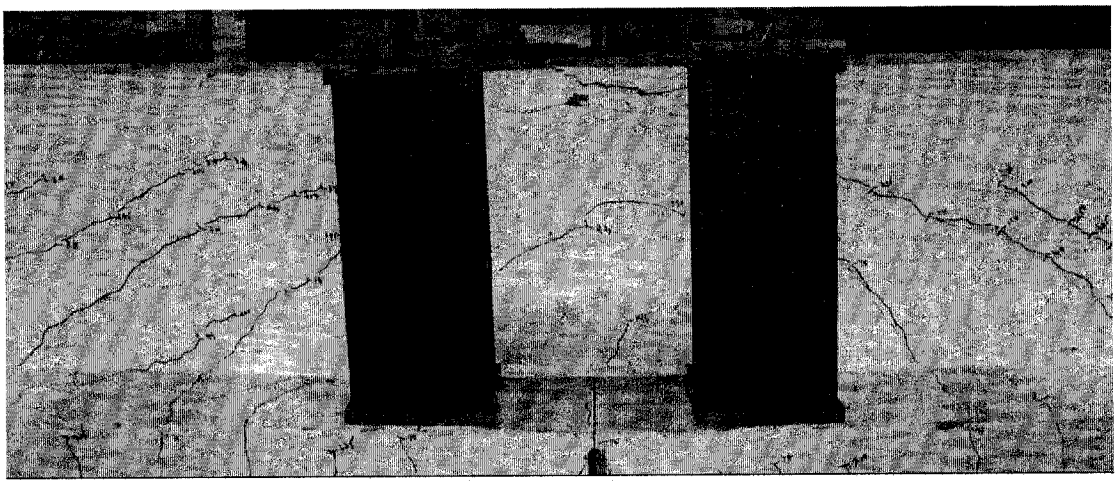

Figure 5.8 Hanger failure (girder IT-G2)

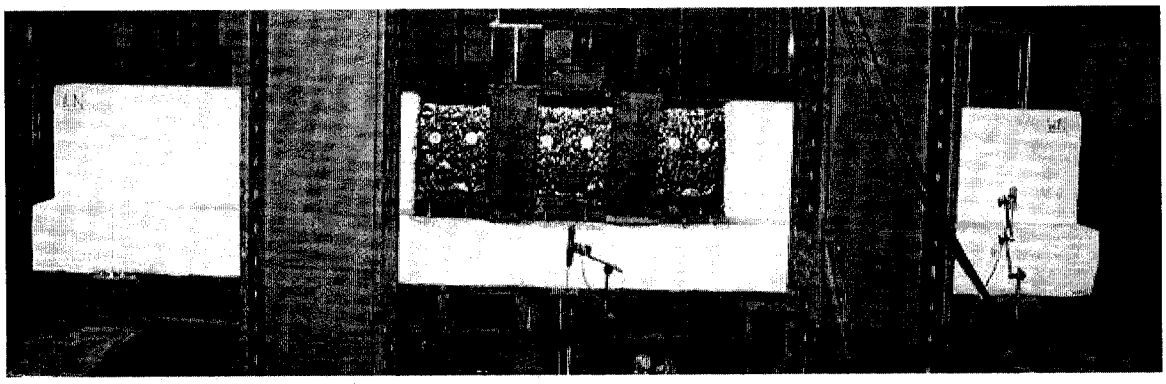

Figure 5.9 Rehabilitated girder IT-G1R before test

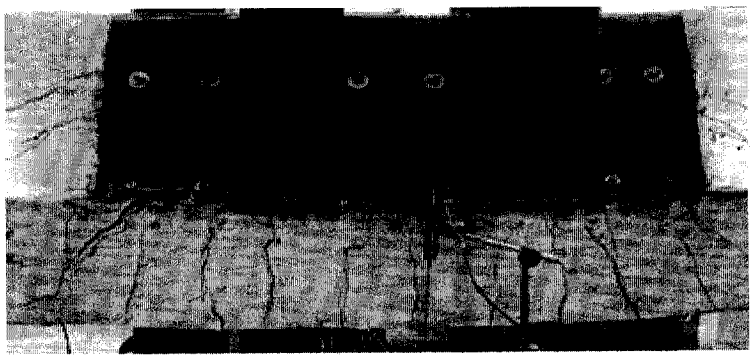

Figure 5.10 Rehabilitated girder IT-G1R at failure

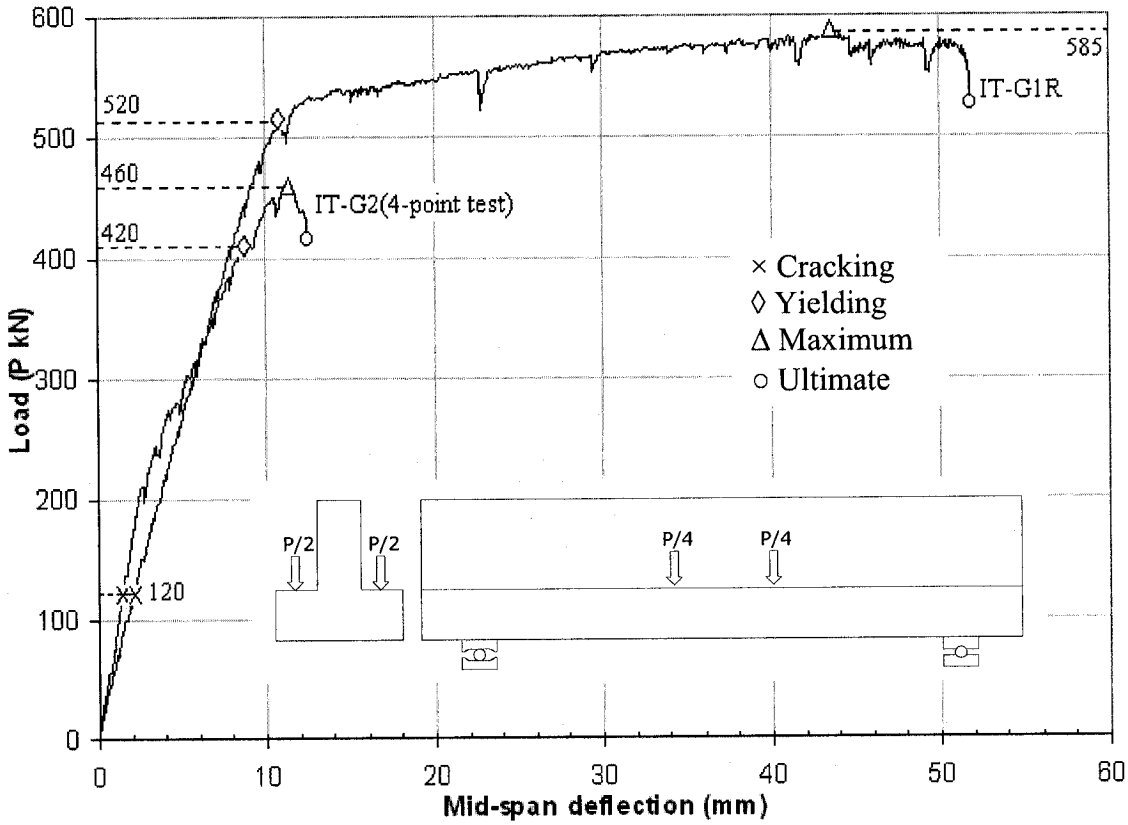

Figure 5.11 Load-deflection relationship for girders IT-G2 and IT-G1R

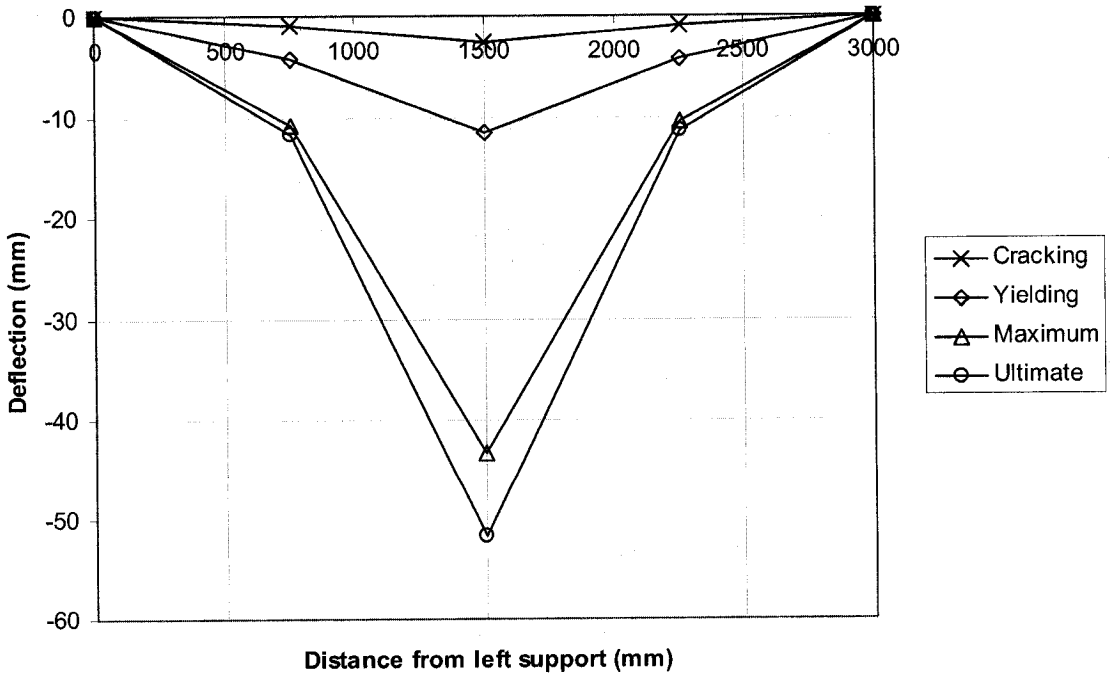

Figure 5.12 Deflected shape of IT-G1R at various performance levels

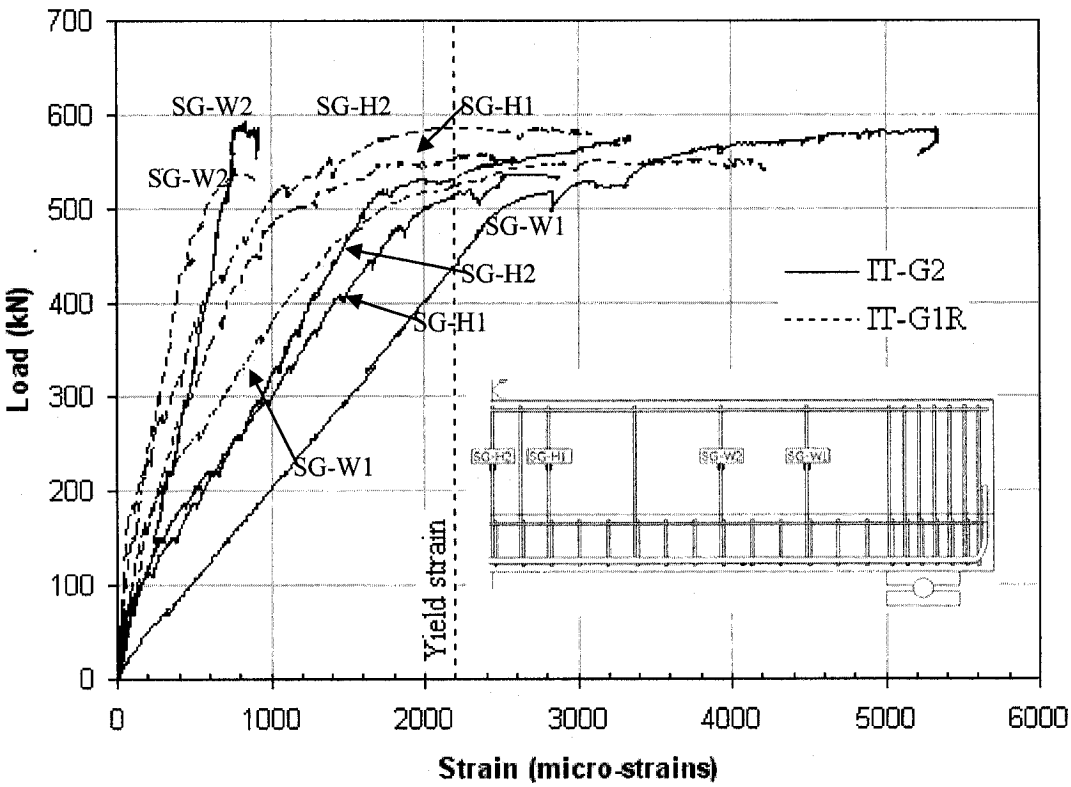

Figure 5.13 Load-strain relationship for web stirrups

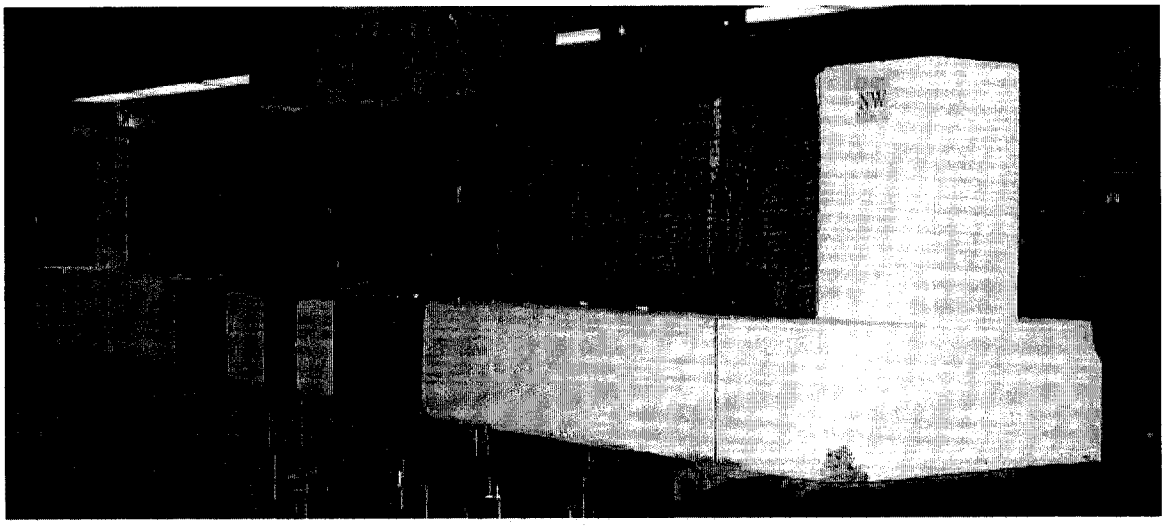

Figure 5.14 Rehabilitated girder IT-G2R before test

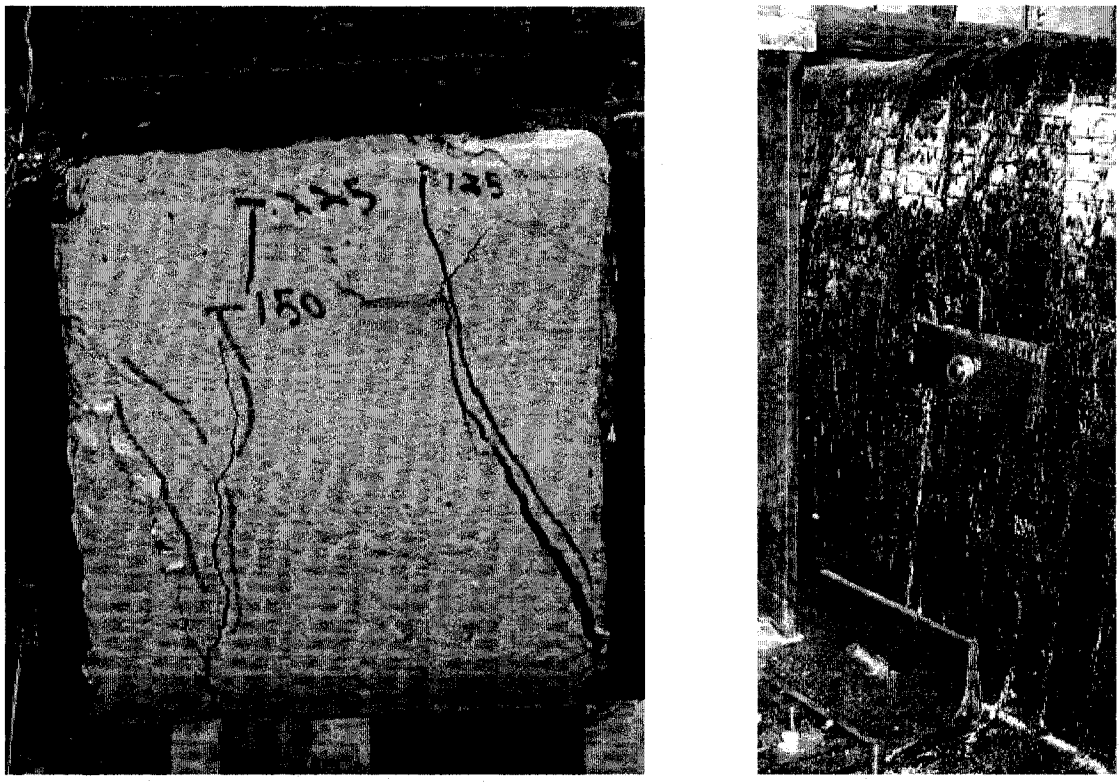

(a) (b)

Figure 5.15 Close up view of girder IT-G2R at failure

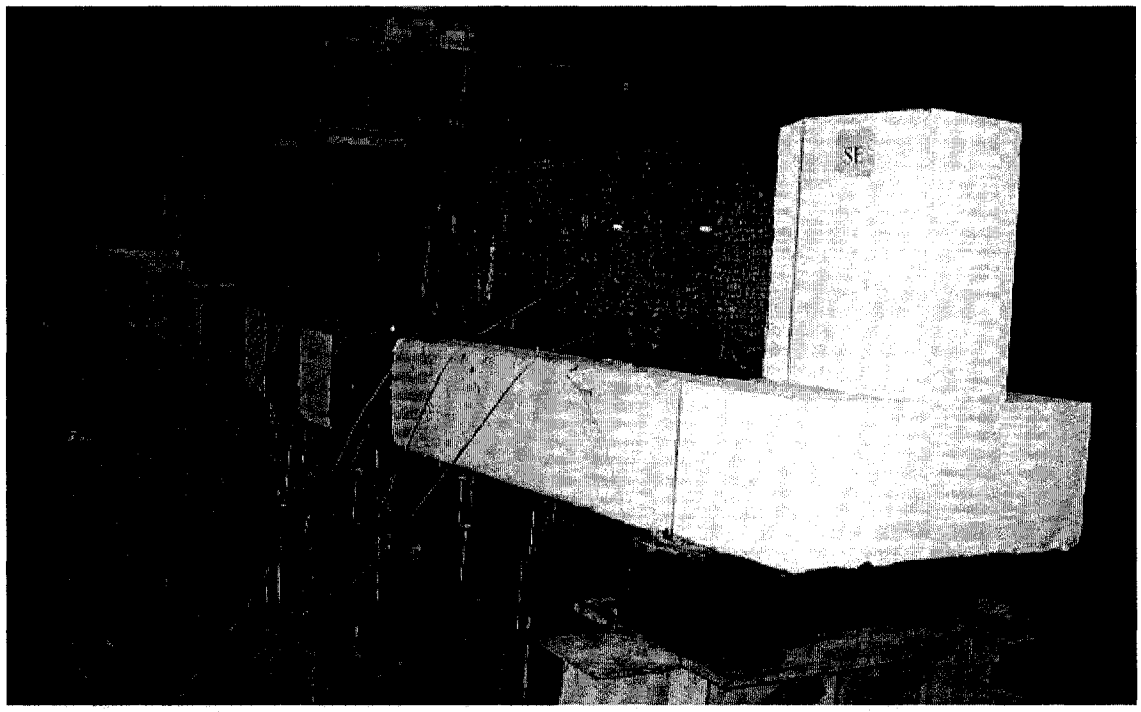

Figure 5.16 Rehabilitated girder IT-G2R at failure

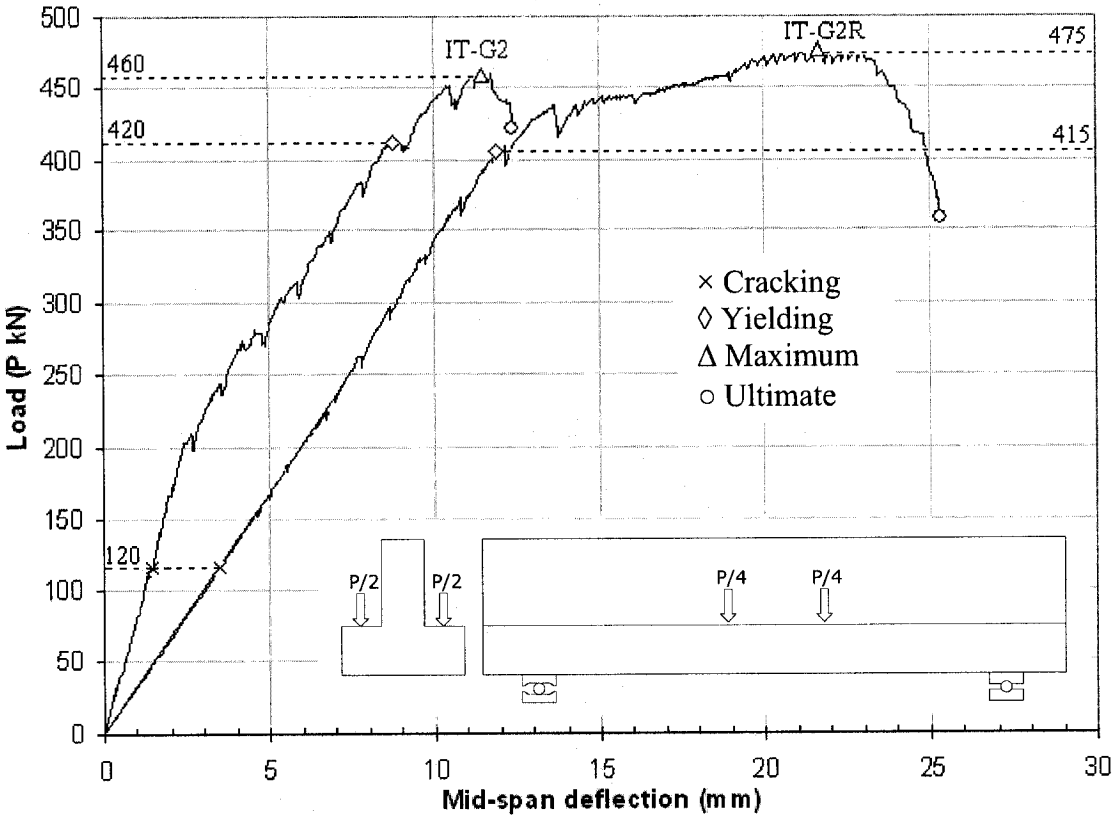

Figure 5.17 Load-deflection relationship for girders IT-G2 and IT-G2R

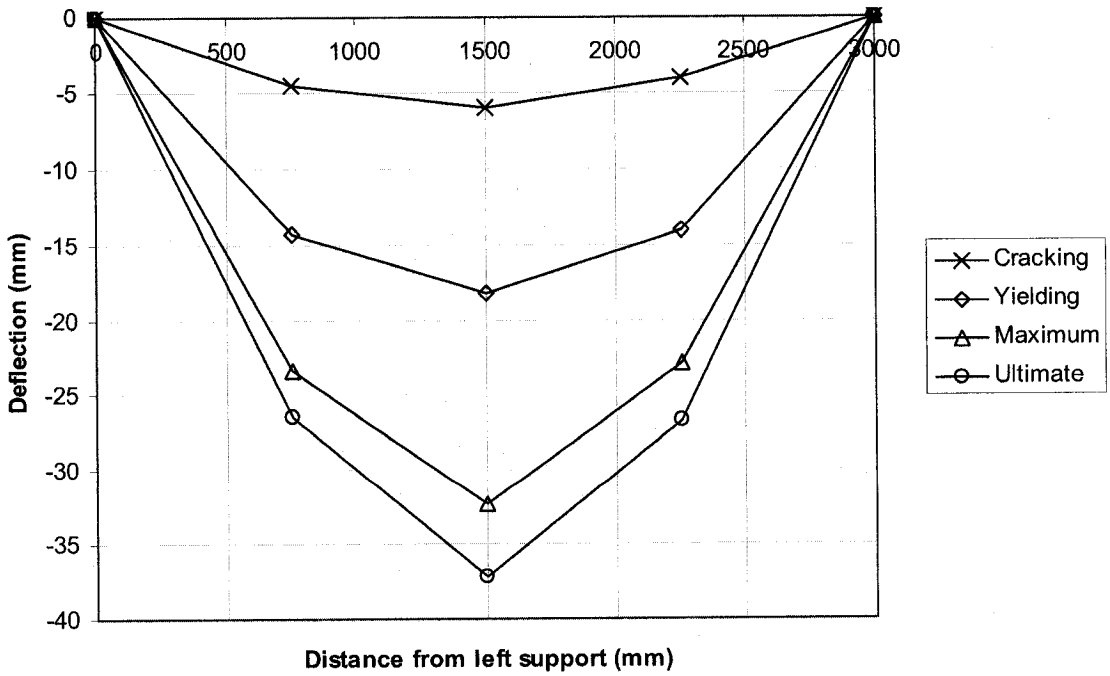

Figure 5.18 Deflected shape of IT-G2R at various load levels

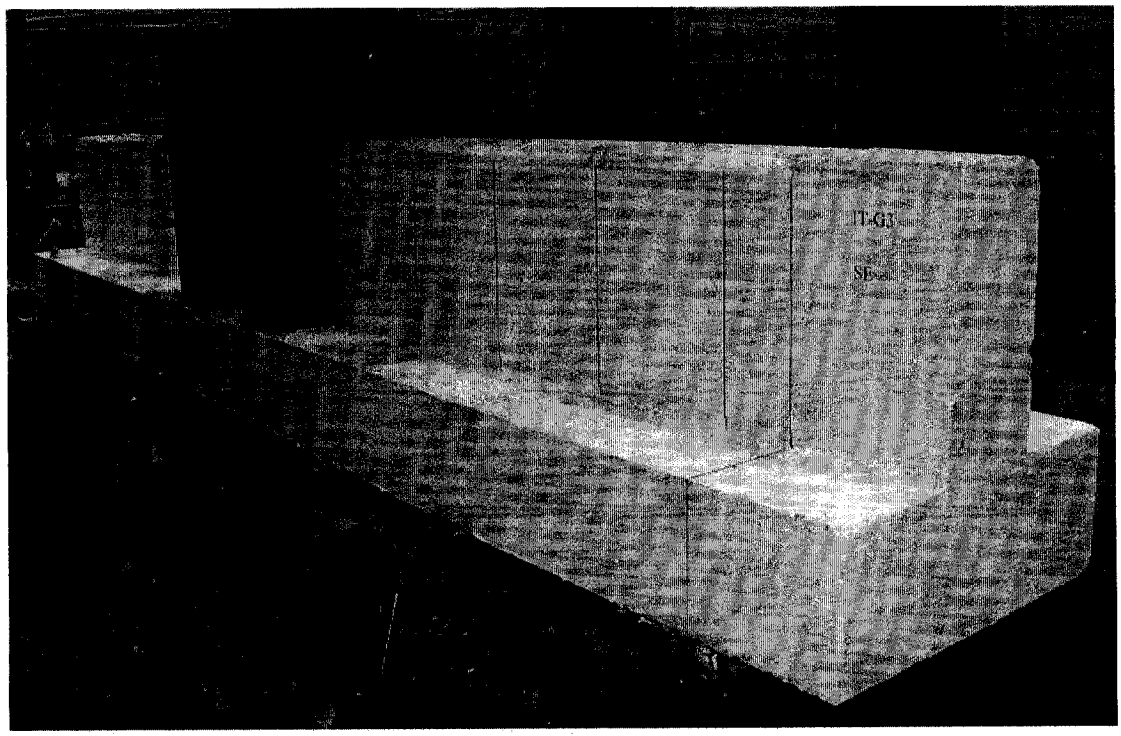

Figure 5.19 Girder IT-G3 before test

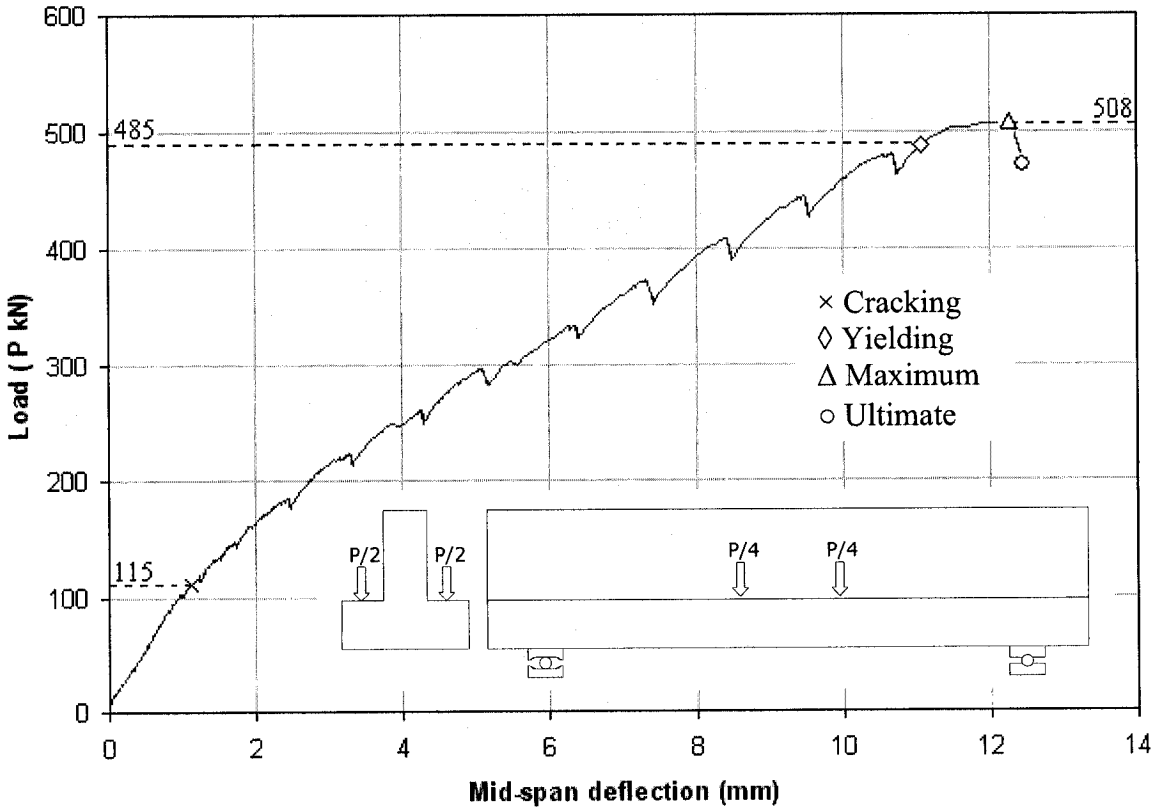

Figure 5.20 Load mid-span deflection of girder IT-G3

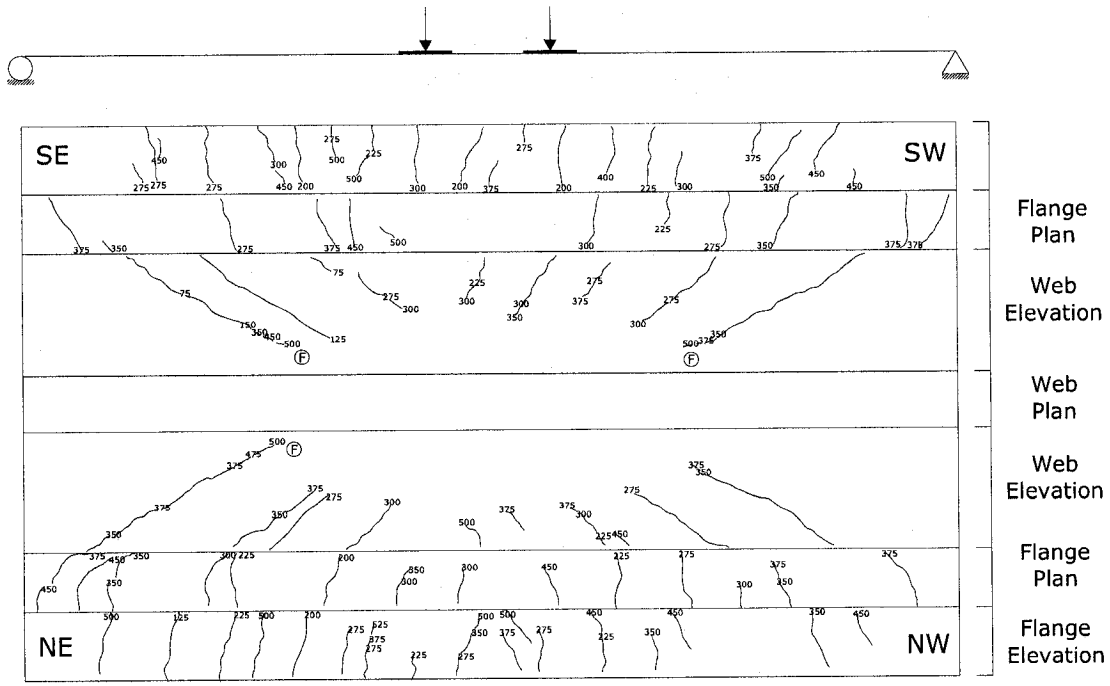

Figure 5.21 Crack pattern of girder IT-G3

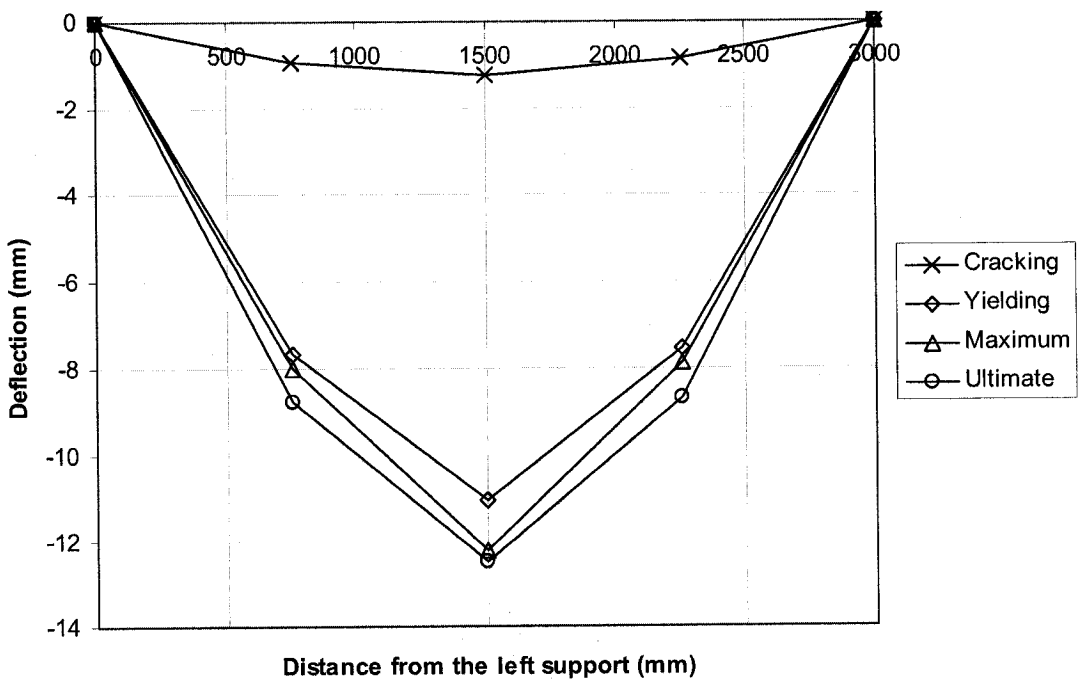

Figure 5.22 Deflected shape of IT-G3 at various load levels

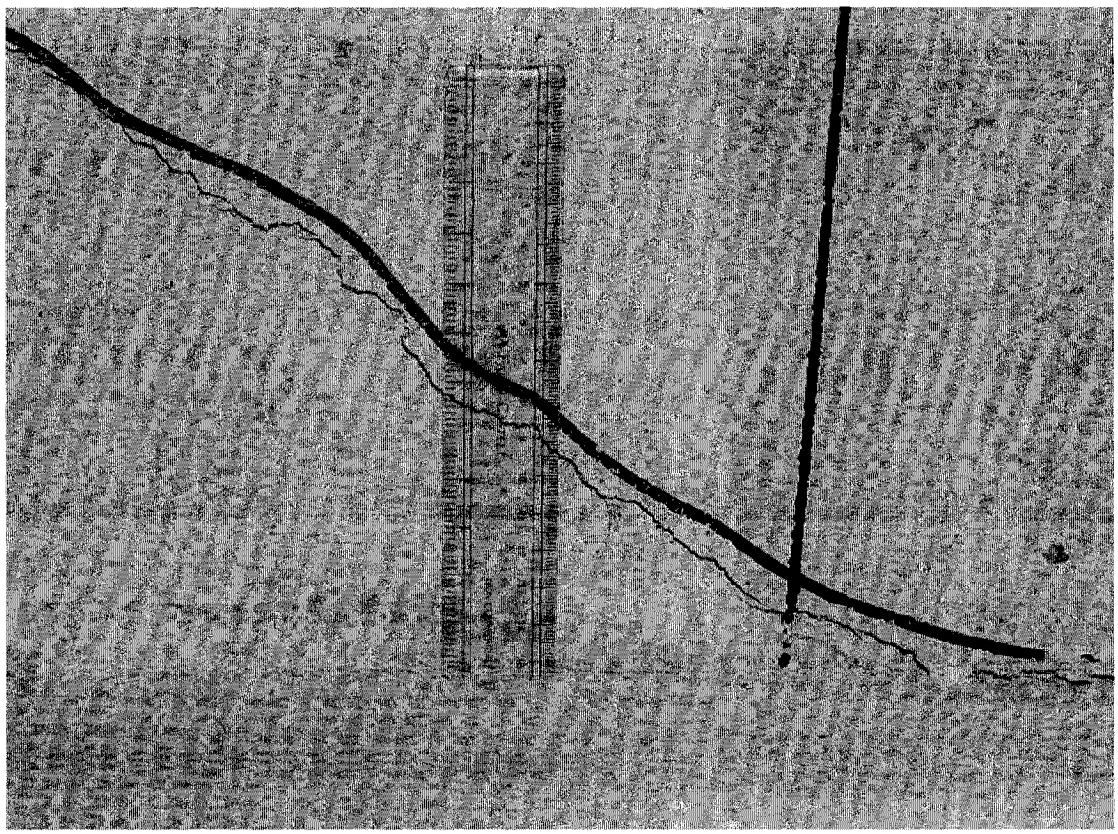

Figure 5.23 Close up view of girder IT-G3R at failure

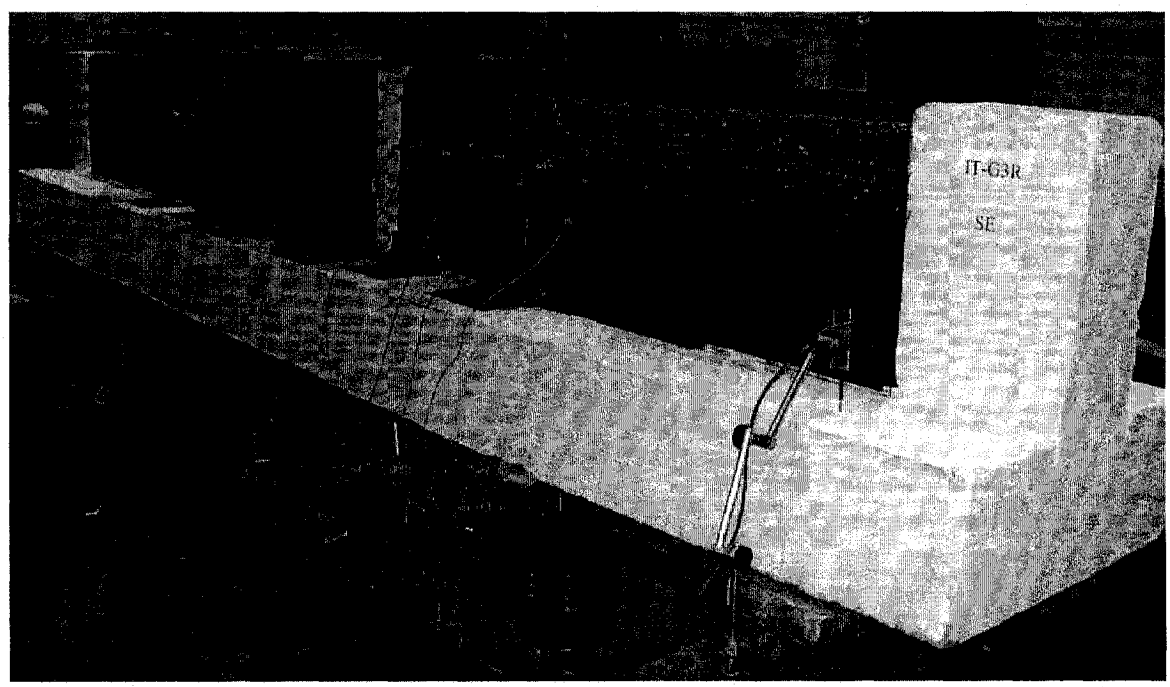

Figure 5.24 Rehabilitated girder IT-G3R before test

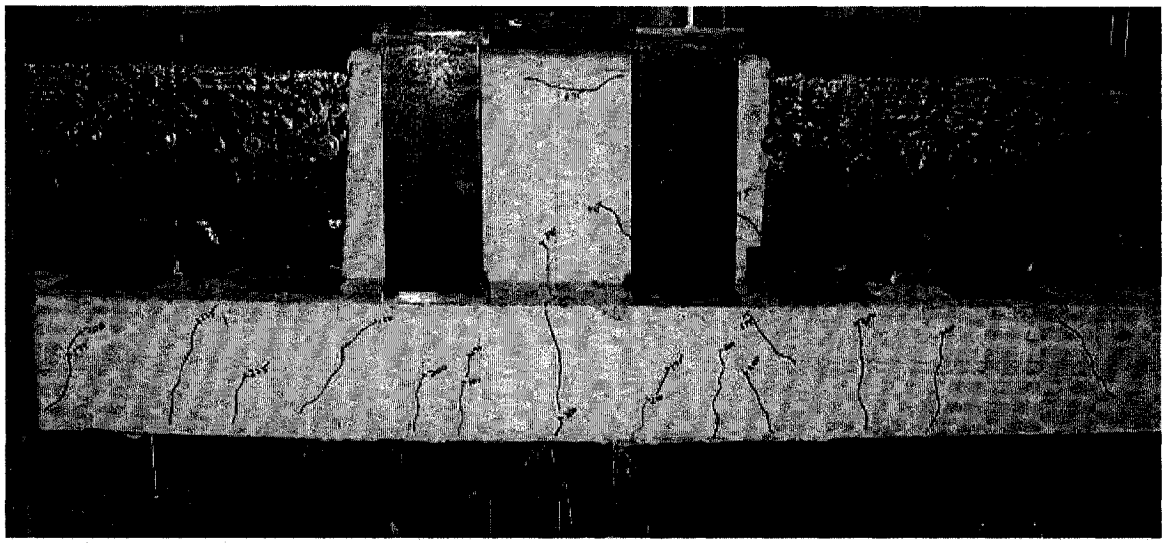

Figure 5.25 Close up view of rehabilitated girder IT-G3R at failure

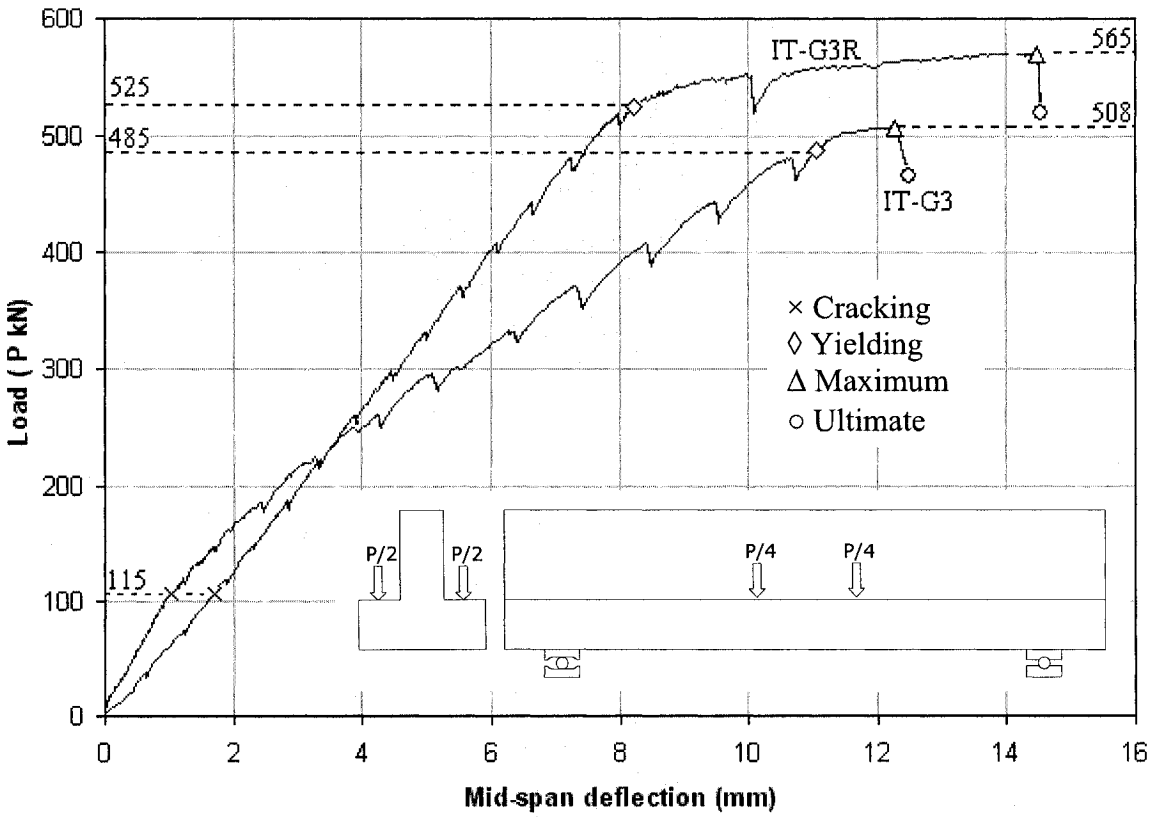

Figure 5.26 Load-deflection relationship for girders IT-G3 and IT-G3R

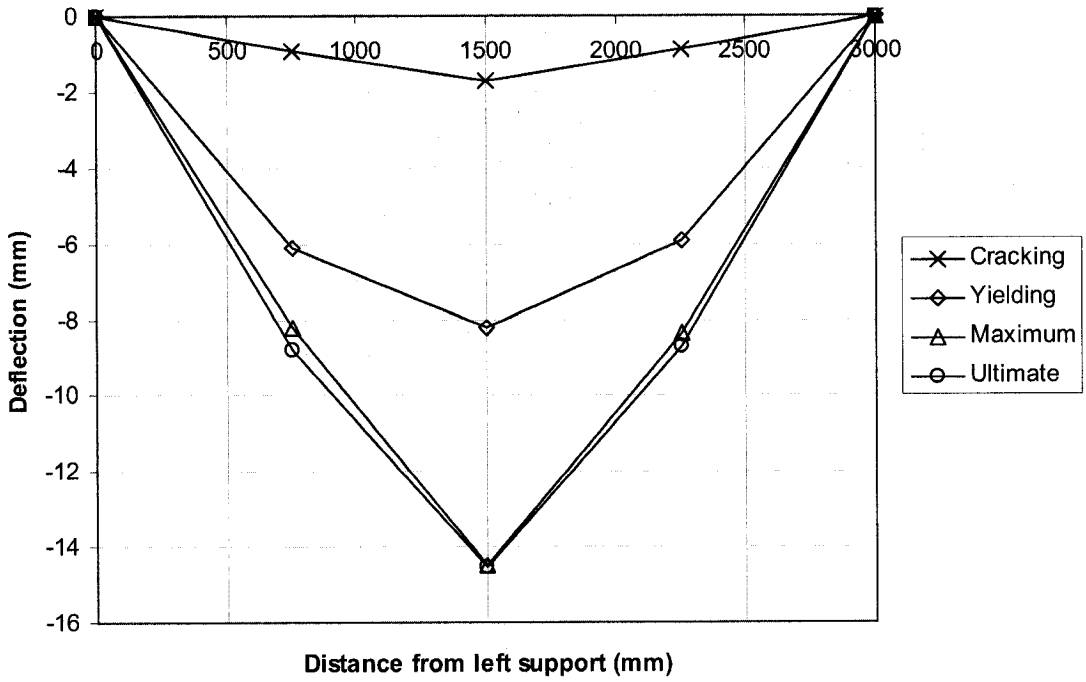

Figure 5.27 Deflected shape of IT-G3R at various load levels

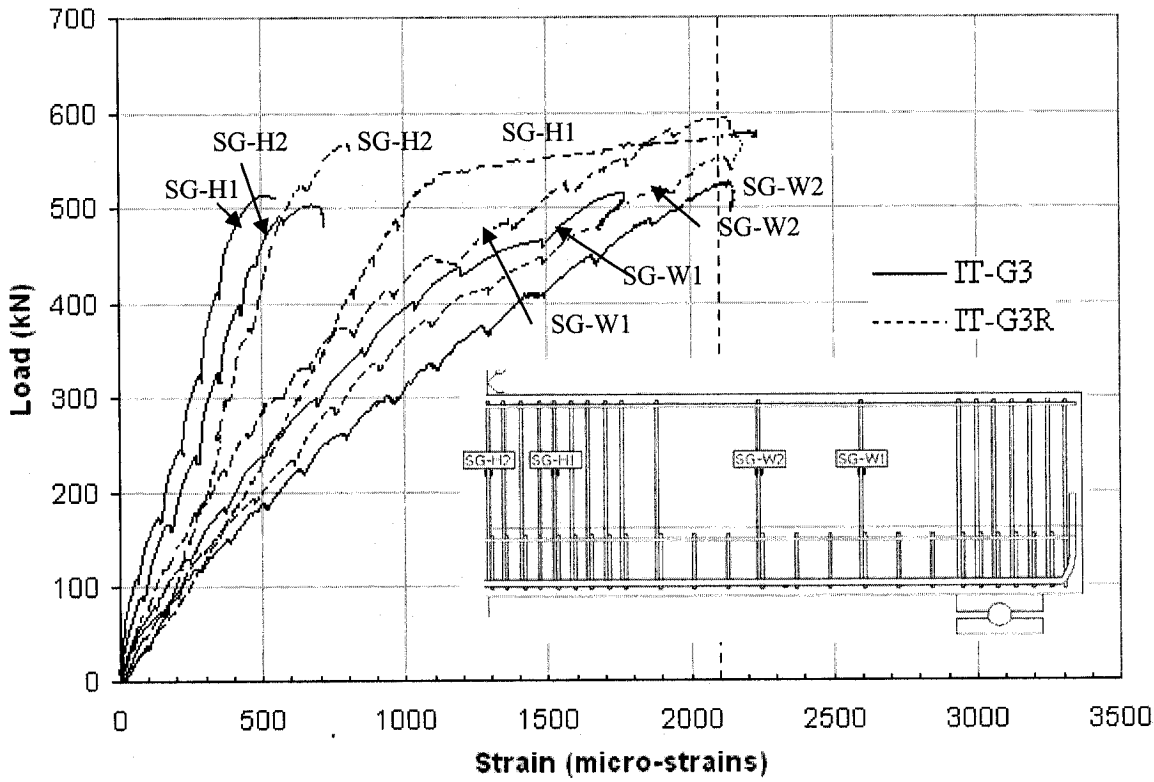

Figure 5.28 Load-strain relationship for web stirrups

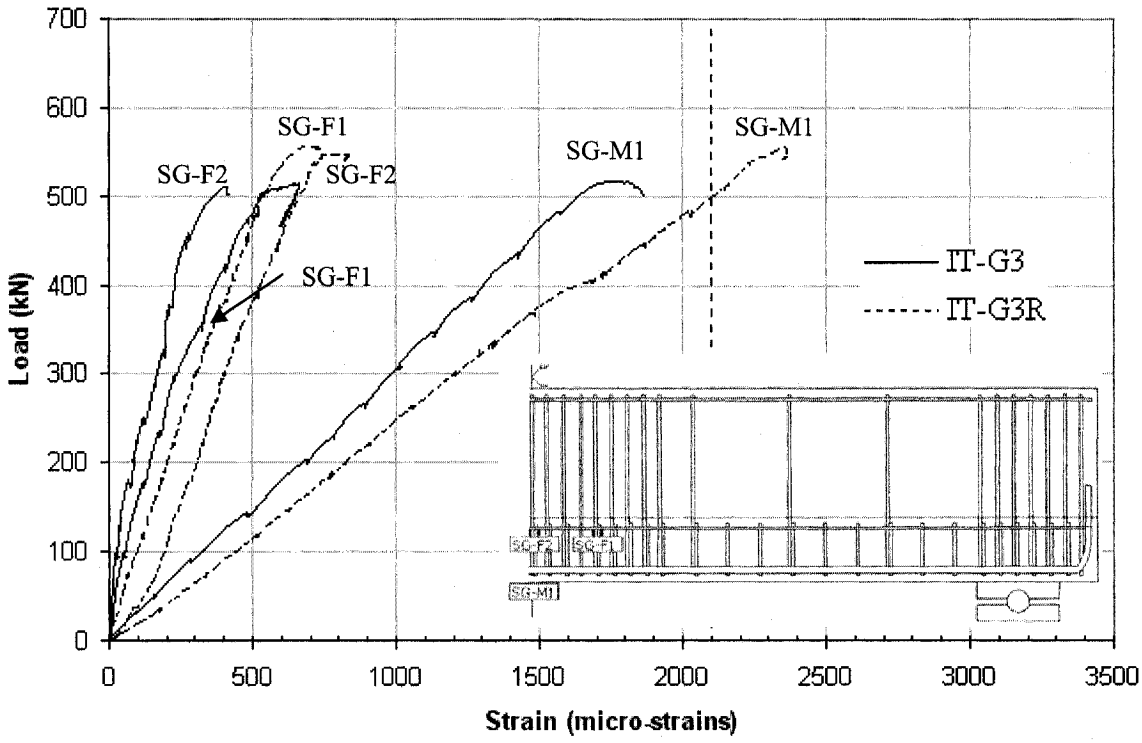

Figure 5.29 Load-strain realtionship for flange and flexural reinforcement

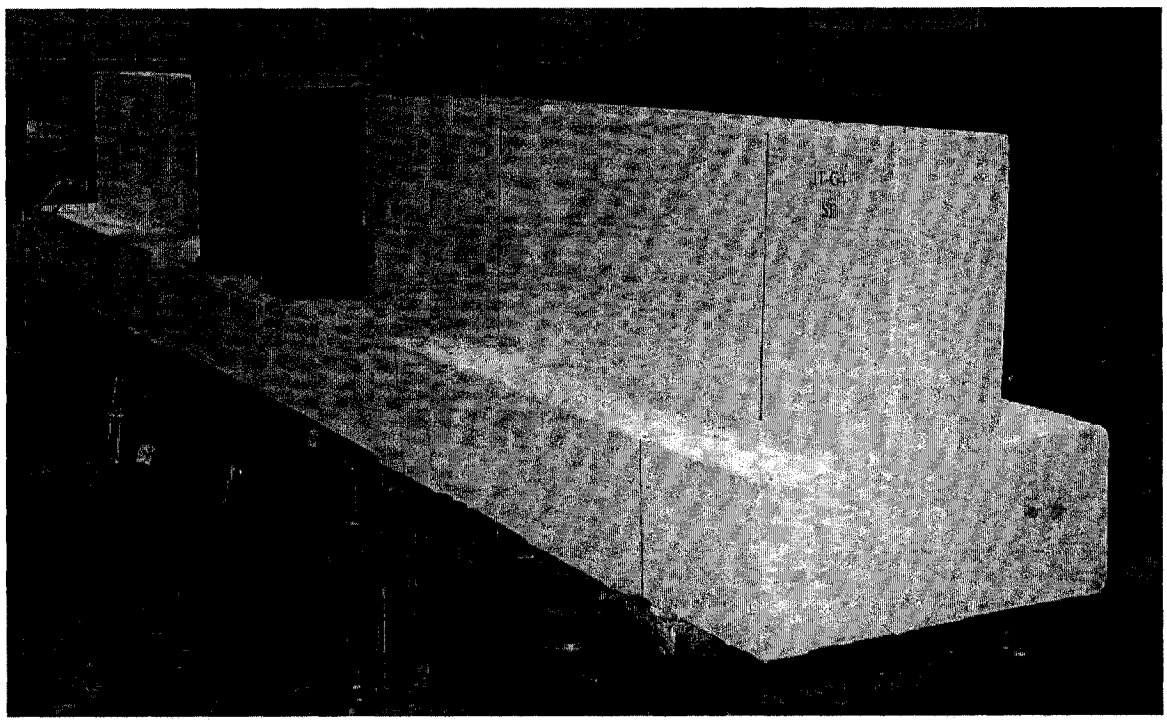

Figure 5.30 Girder IT-G4 before test

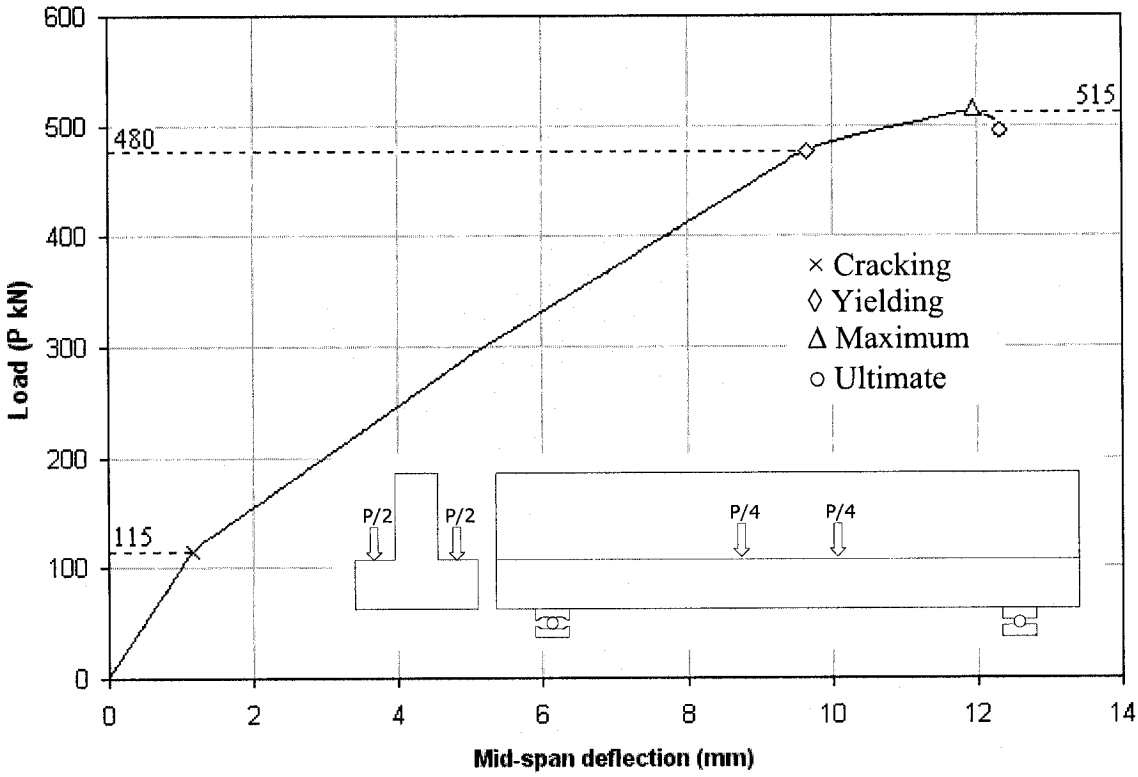

Figure 5.31 Load mid-span deflection of girder IT-G4

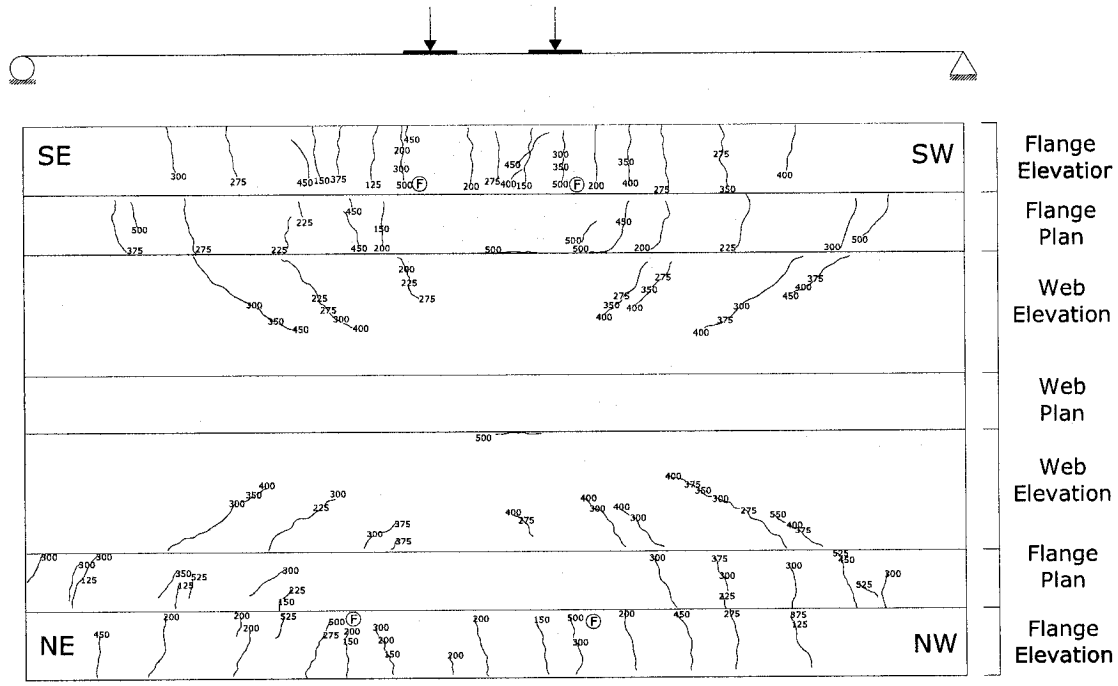

Figure 5.32 Crack pattern of girder IT-G4

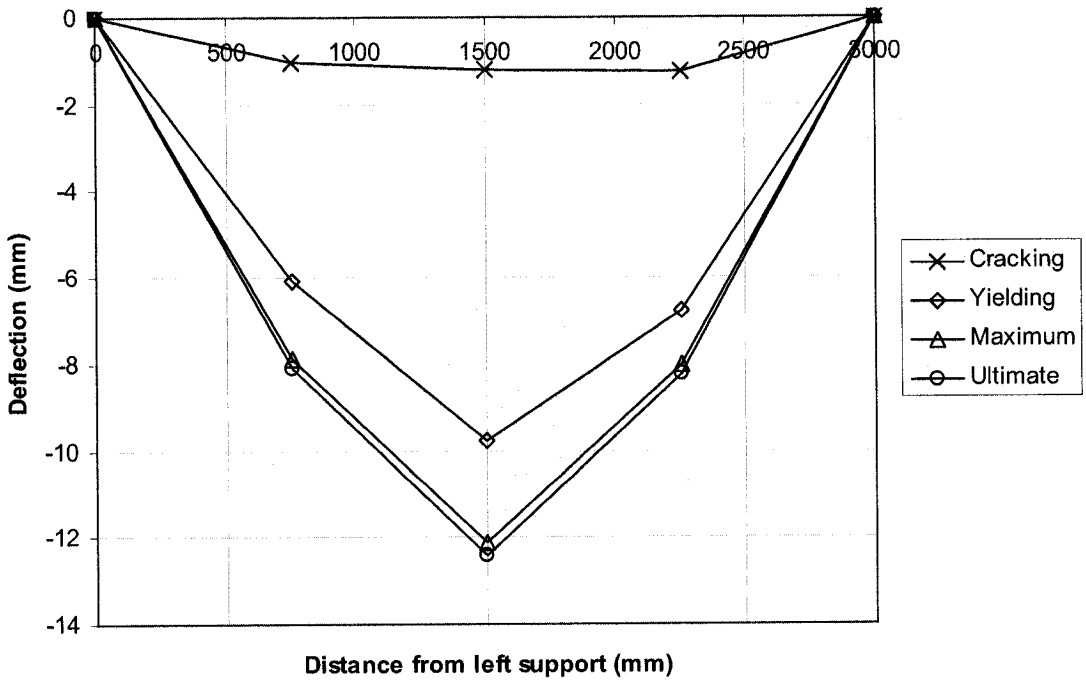

Figure 5.33 Deflected shape of IT-G4 at various load levels

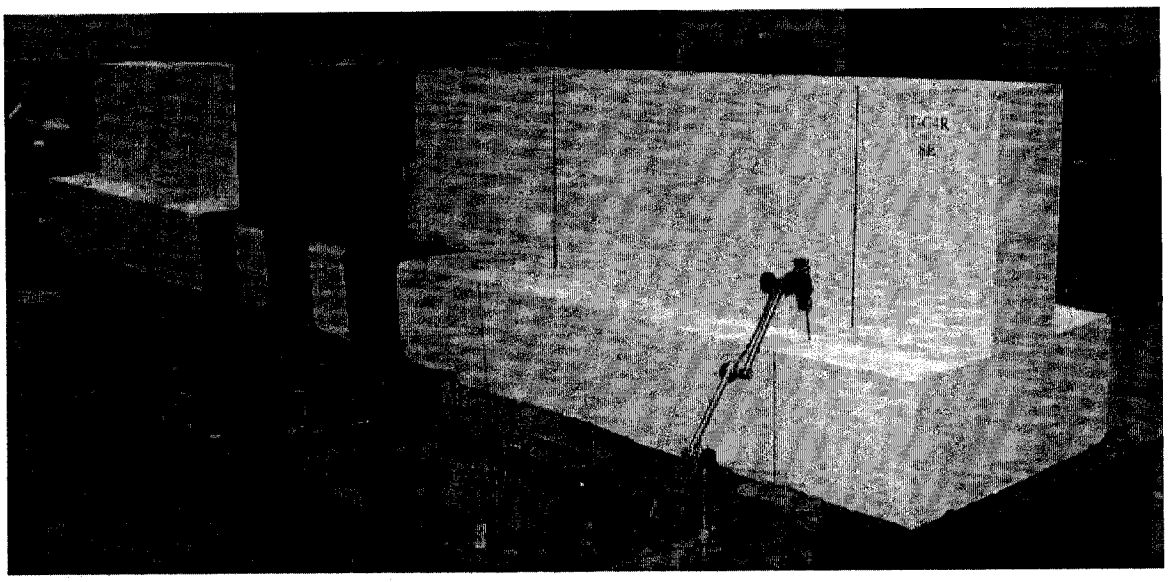

Figure 5.34 Rehabilitated girder IT-G4R before test

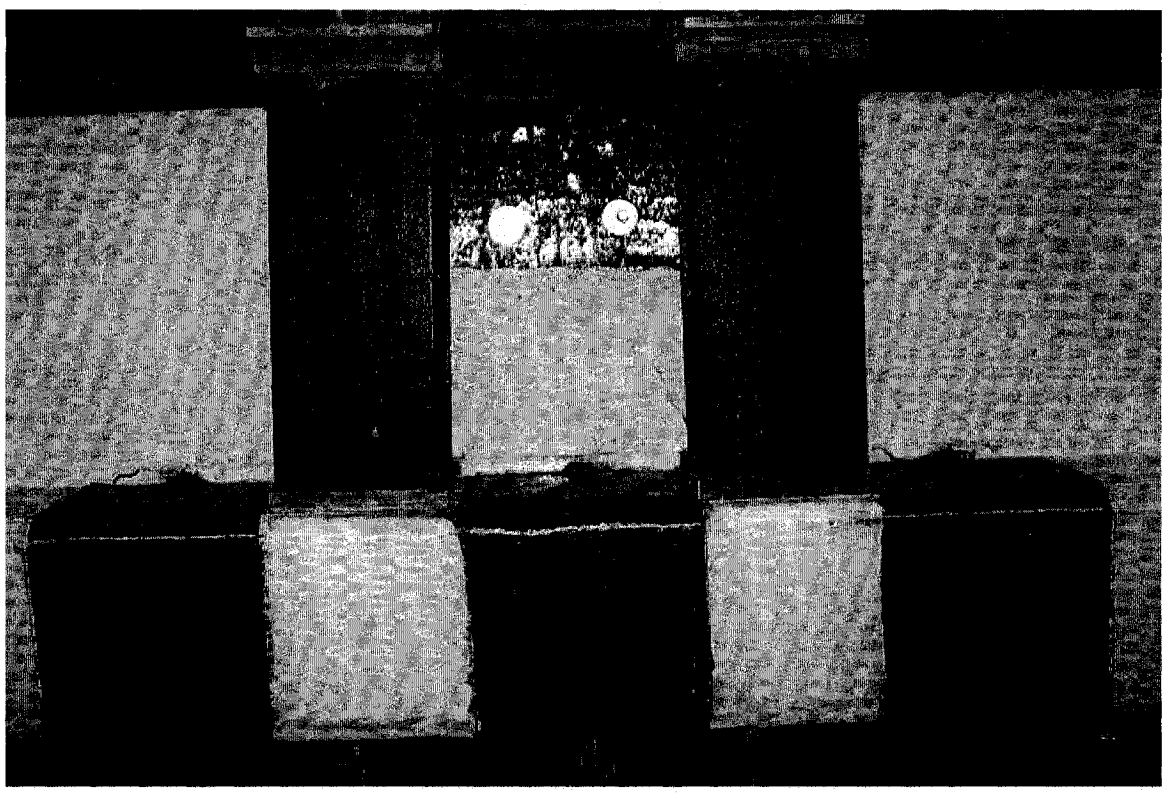

Figure 5.35 Close up view of the rehabilitated girder IT-G4R

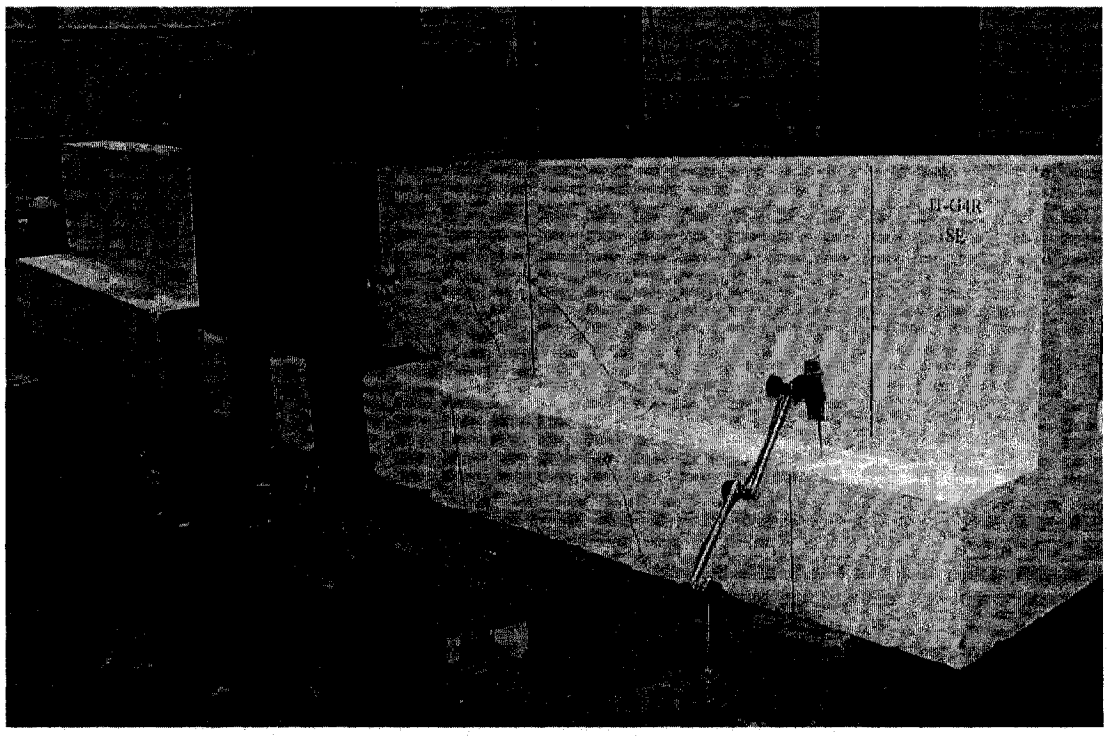

Figure 5.36 Rehabilitated girder IT-G4R at failure

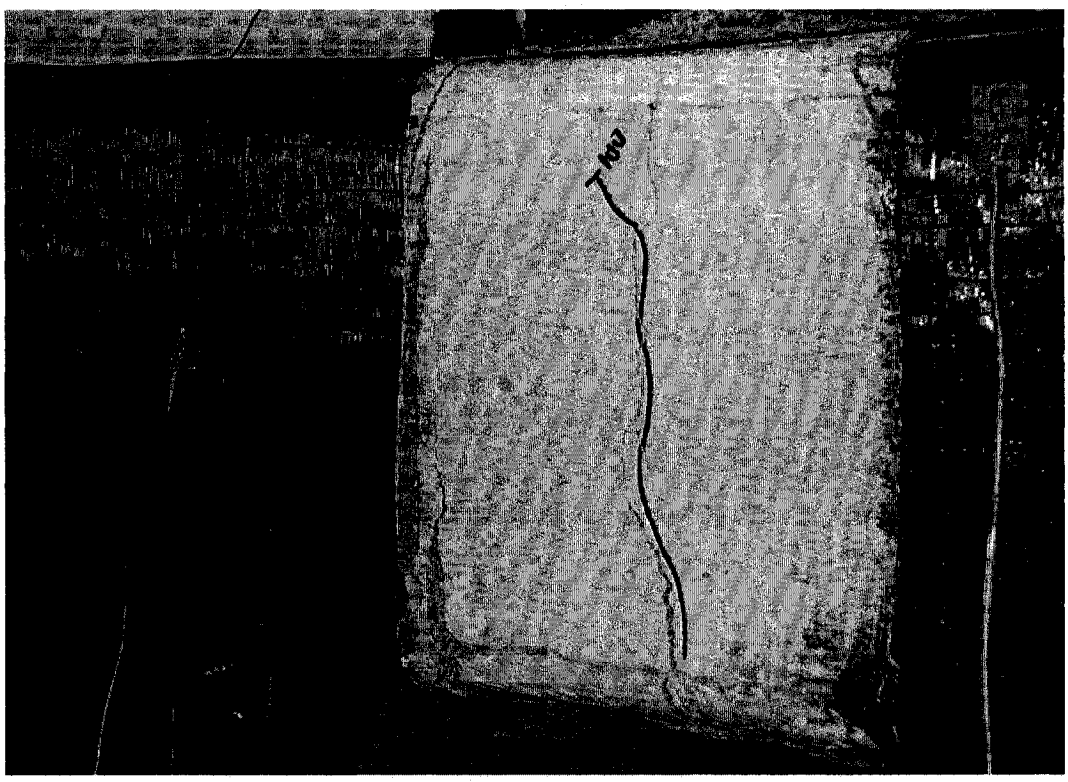

Figure 5.37 Close up view of rehabilitated girder IT-G4R at failure

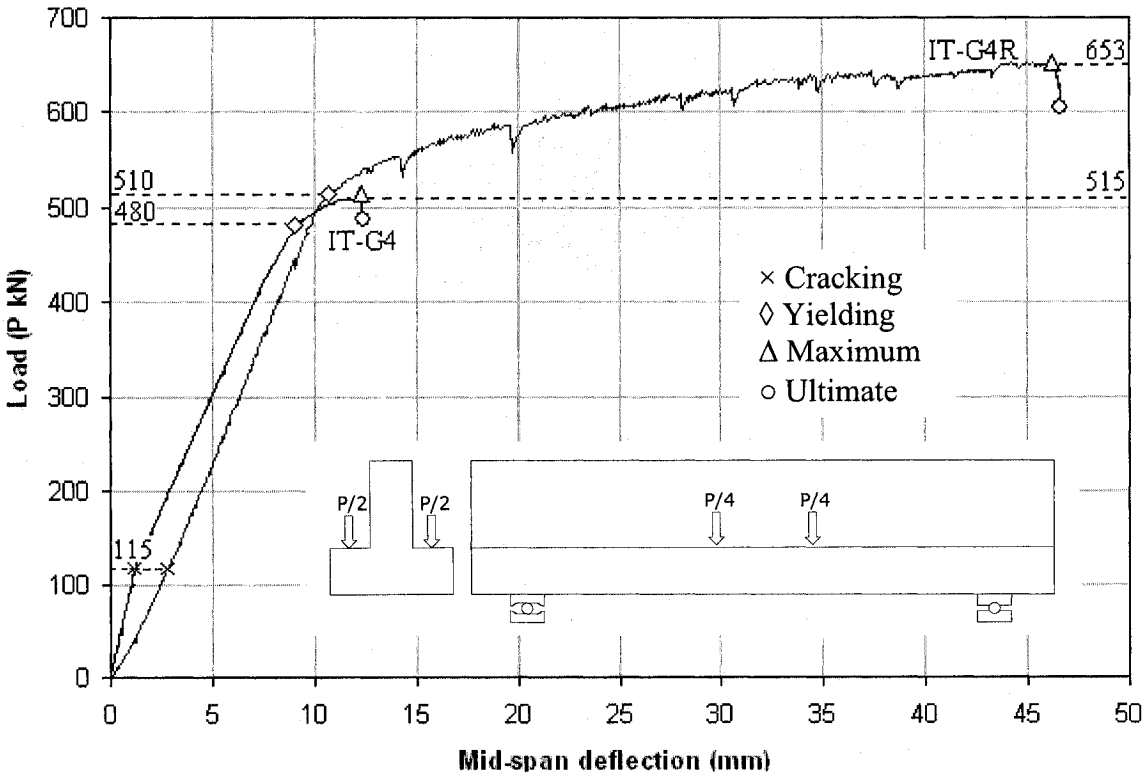

Figure 5.38 Load-deflection relationship for girders IT-G4 and IT-G4R

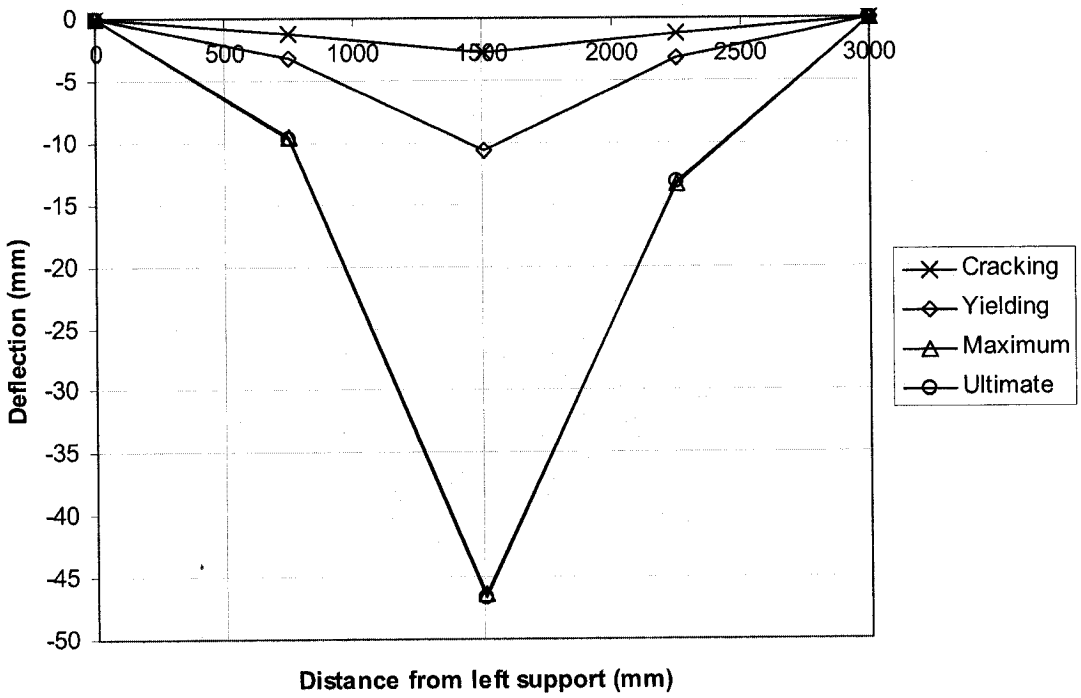

Figure 5.39 Deflected shape of IT-G4R at various load levels

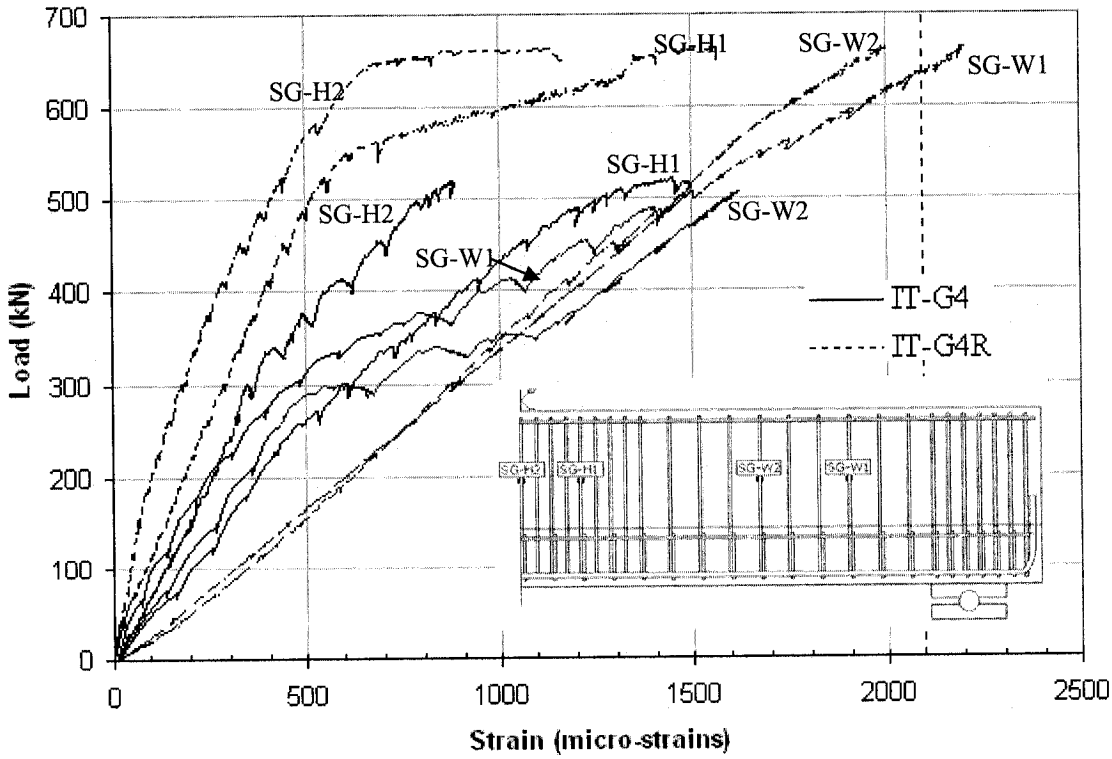

Figure 5.40 Load-strain relationship for web stirrups

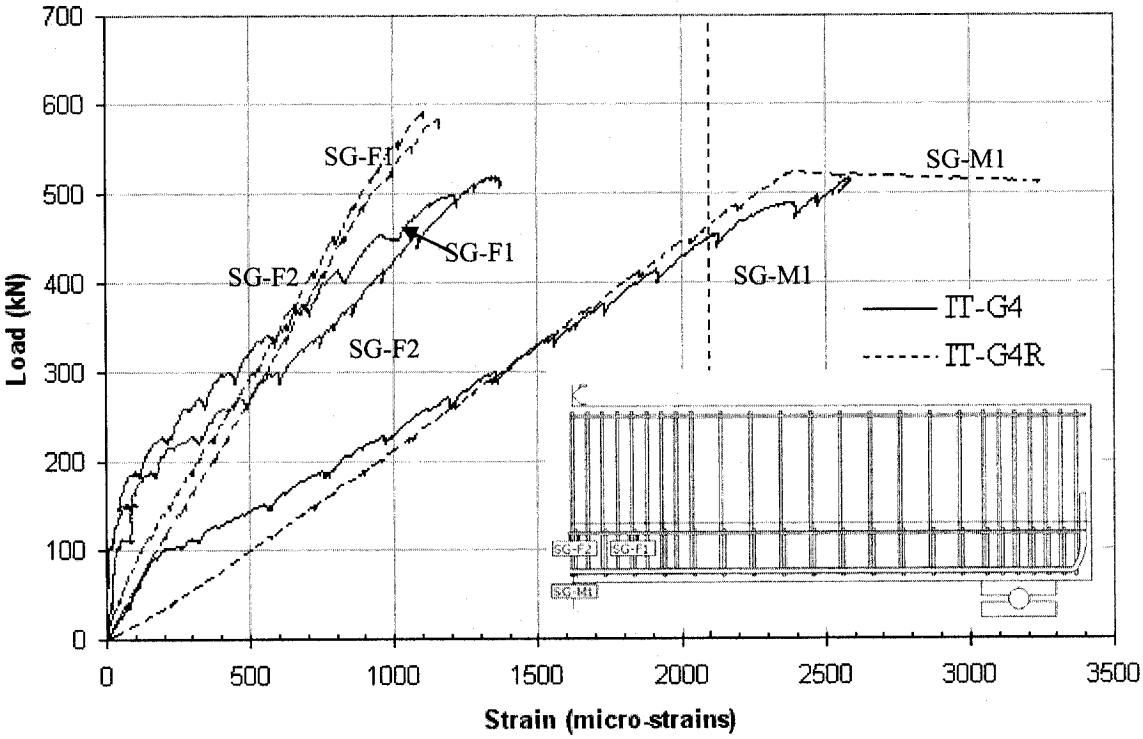

Figure 5.41 Load-strain realtionship for flange and flexural reinforcement

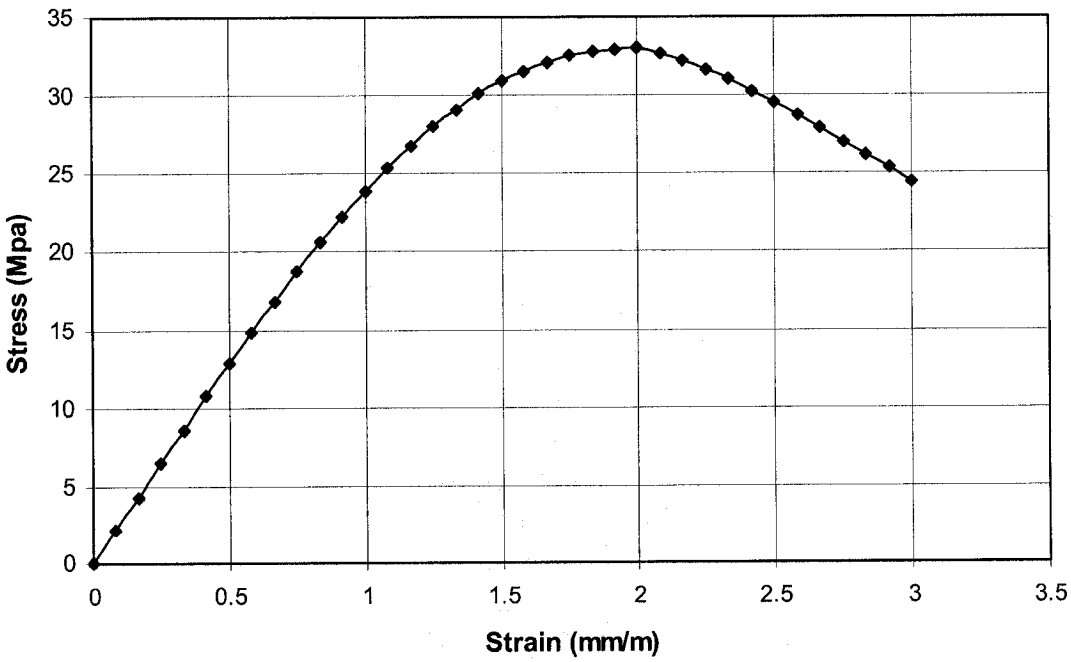

Figure 5.42 Compressive stress-strain curve of concrete used in model.

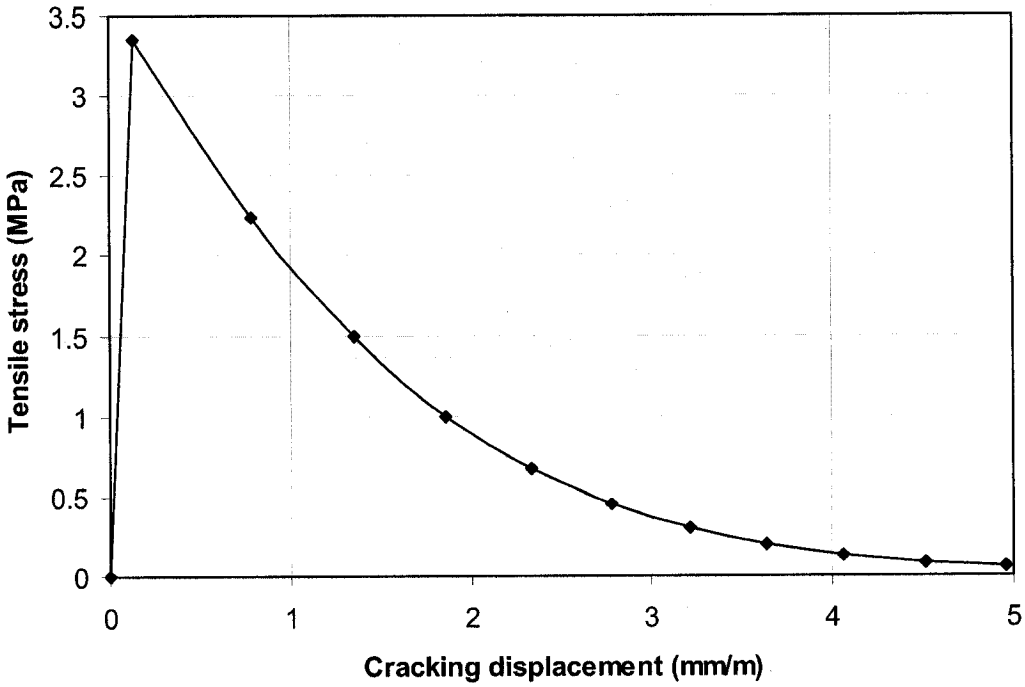

Figure 5.43 Tensile stress-strain curve of concrete used in model.

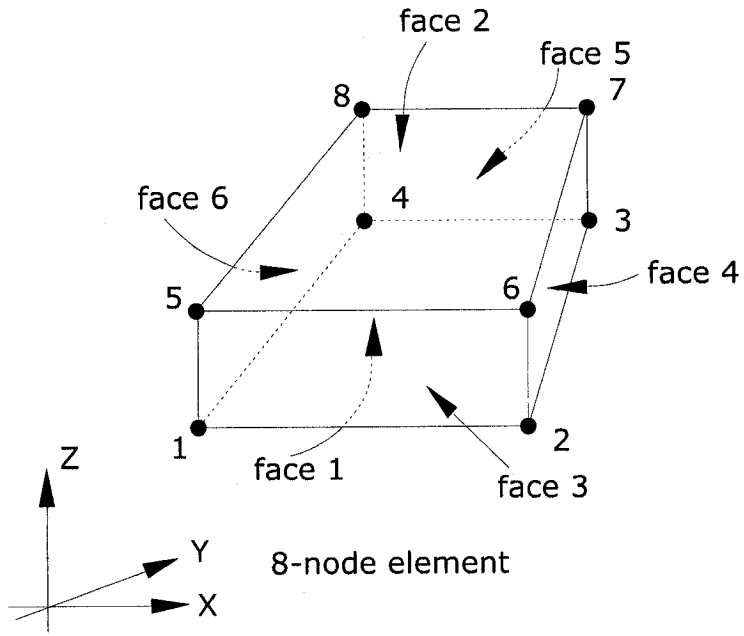

Figure 5.44 Solid 8-node concrete element

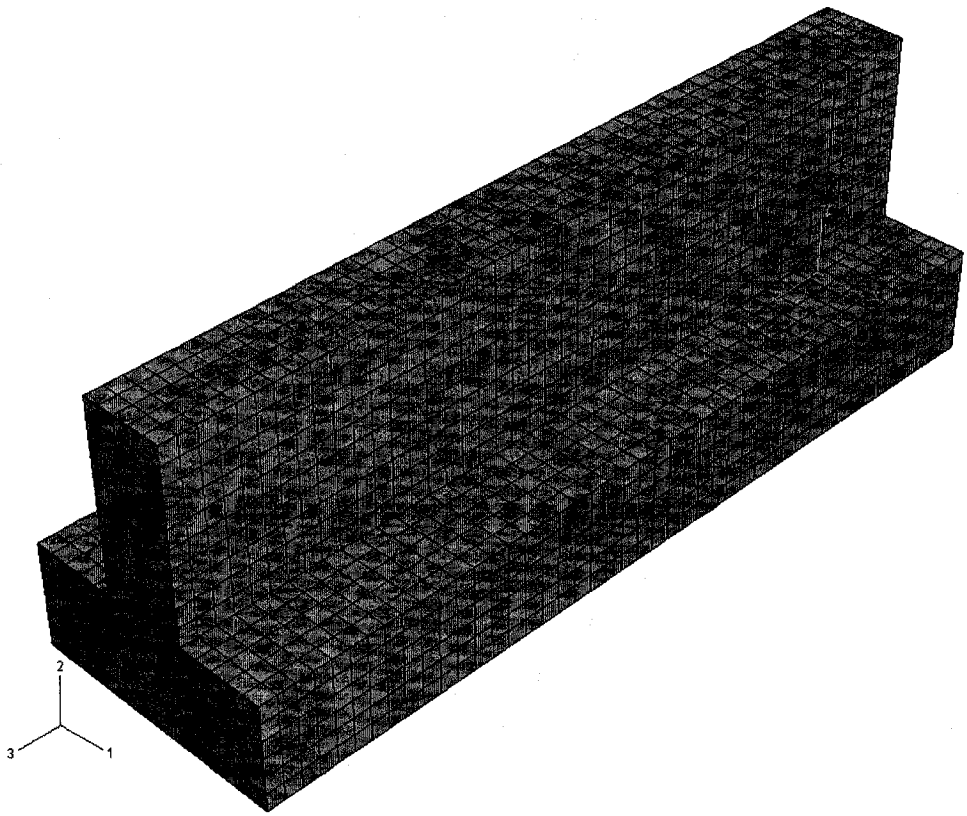

Figure 5.45 Finite element model for concrete

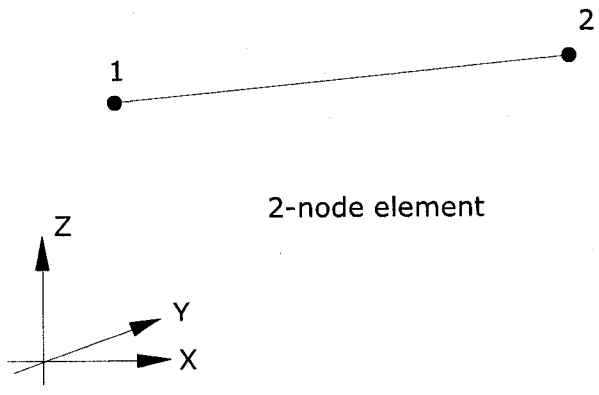

Figure 5.46 2-node uniaxial non-linear tension-compression steel element

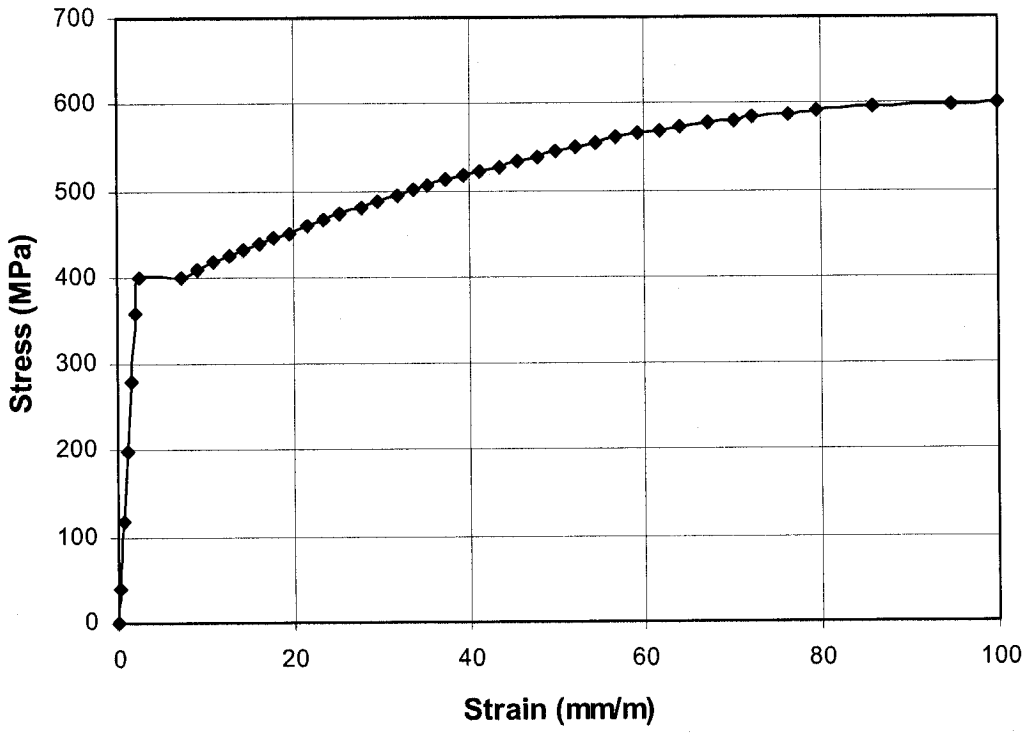

Figure 5.47 Tensile stress-strain curve of steel used in model

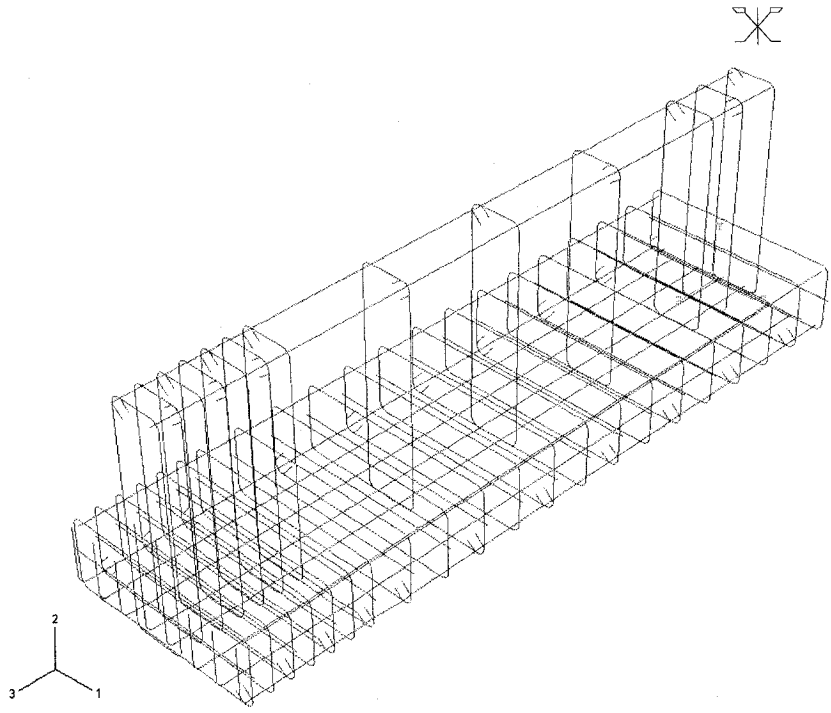

Figure 5.48 Finite element model – Steel reinforcement for girder IT-G1, IT-G2 (half specimen)

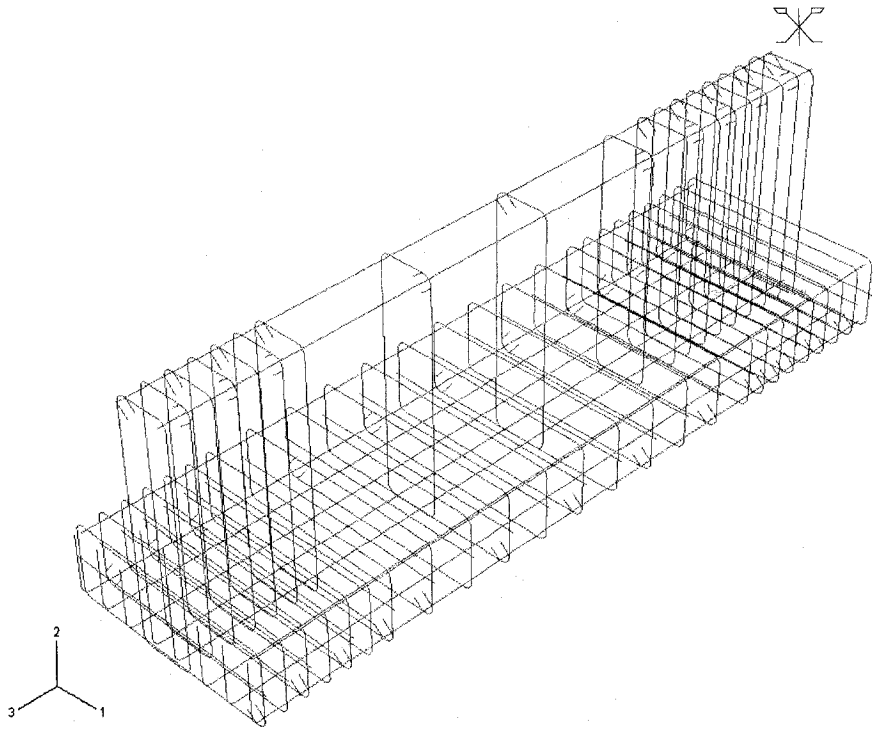

Figure 5.49 Finite element model – Steel reinforcement for girder IT-G3 (half specimen)

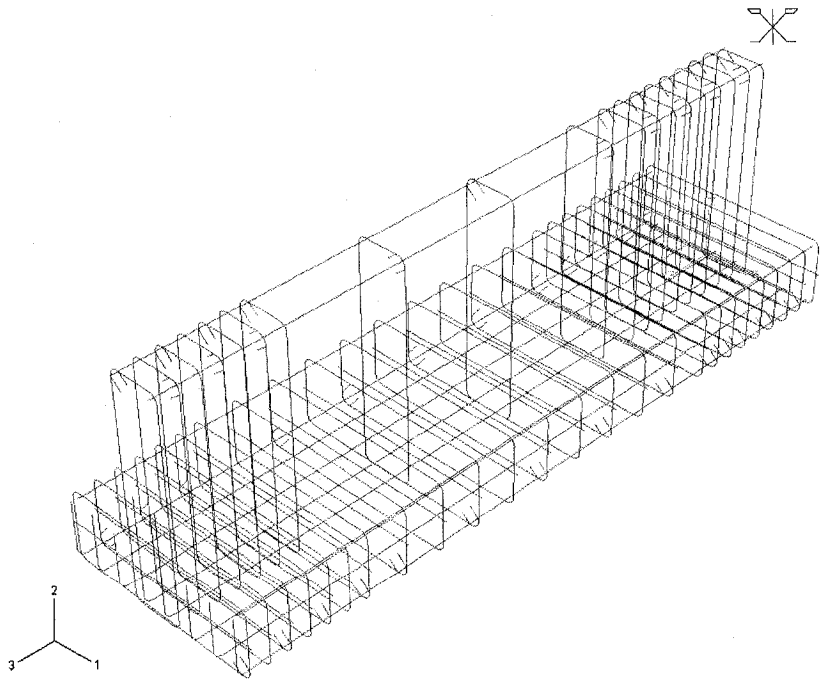

Figure 5.50 Finite element model – Steel reinforcement for girder IT-G4 (half specimen)

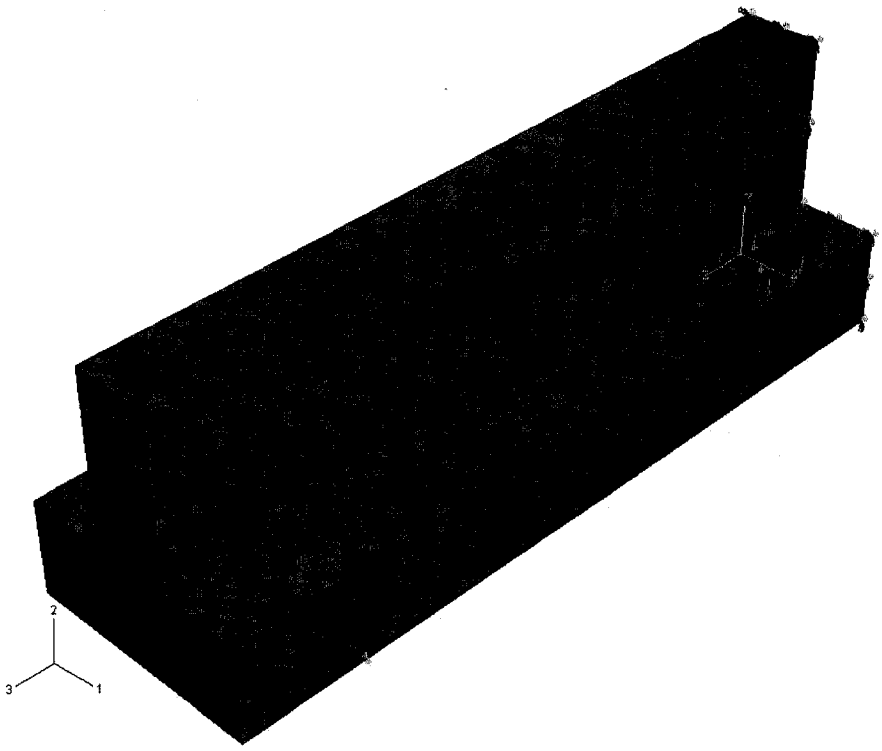

Figure 5.51 Finite element model with loading pattern and boundary conditions

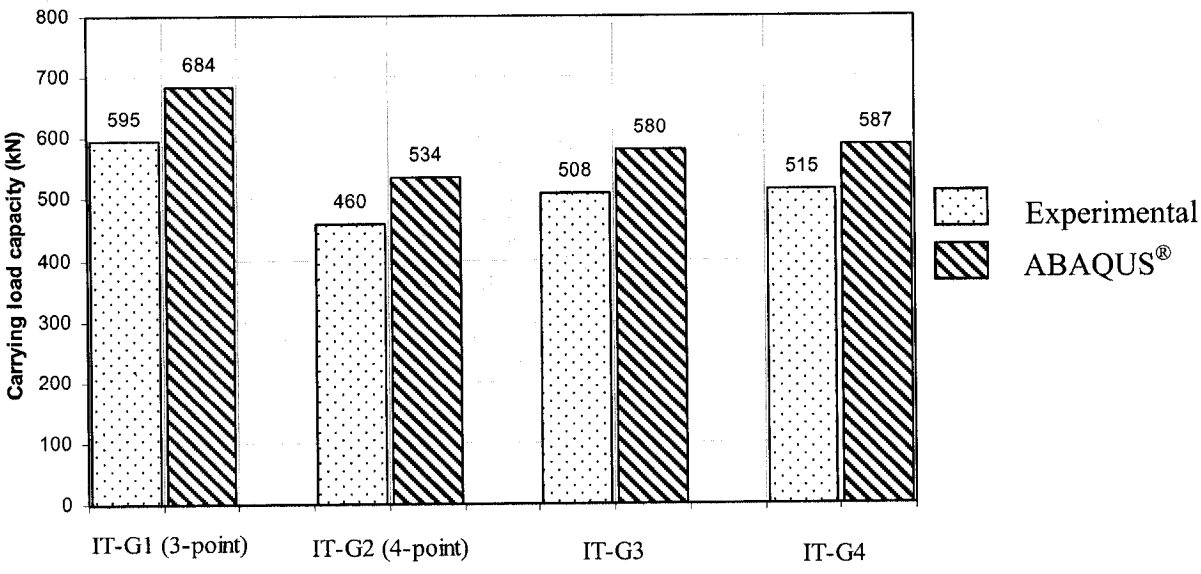

Figure 5.52 Comparison between the experimental and finite element model load carrying capacities of the four inverted-T girders

CHAPTER 6

CONCLUSIONS AND RECOMMENDATIONS

6.1 SUMMARY

This study focuses on eliminating non-ductile failure mechanisms of reinforced concrete (RC) inverted-T girders of existing bridge bentcaps and parking garages using externally bonded carbon fibre reinforced polymer (CFRP) sheets. Eight tests were conducted on four simply supported RC inverted-T girders before and after rehabilitation. New rehabilitation schemes to eliminate the non-ductile failure mechanisms in hanger zone, web, and flange were evaluated experimentally. The rehabilitation schemes proved to eliminate the abovementioned mechanisms, and increase the girder's strength and displacement ductility capacities. In addition, an analytical study was conducted in order to evaluate the effect of the design variables on the failure mechanisms of FRP-rehabilitated RC inverted-T bridge bentcap girders.

6.2 CONCLUSIONS

The following conclusions are drawn from the experimental study:

1. Rehabilitating a RC inverted-T girder that have inadequate hanger and web-shear reinforcement using 3 layers of anchored CFRP sheets in the hanger zone eliminates the non-ductile shear-compression failure mechanism, increases the

displacement ductility capacity up to 4, and increases the load carrying capacity of the girder by about 20%.

2. Rehabilitating a RC inverted-T girder that has inadequate web-shear reinforcement using 3 layers of anchored CFRP sheets in the web-shear zone eliminates the non-ductile web-shear failure mechanism, increases the displacement ductility capacity up to 1.7, and increases the load carrying capacity of the girder by about 10%.
3. Rehabilitating a RC inverted-T girder that has inadequate punching shear capacity of the flanges with 3 layers of anchored CFRP sheets in the punching and web-compression zones eliminates the non-ductile failure mechanism, increases the displacement ductility capacity up to 4, and increases the load carrying capacity by about 20%.
4. Confining the web-compression zone of RC inverted-T girders ensures the formation of the full flexural capacity of the girder.
5. Anchoring the CFRP sheets that are epoxied on the web or the flange into the girder using sandwiched (fan type) CFRP fiber anchors that are aligned with the CFRP sheets' fibers showed better performance compared to using anchored curved steel plates at the web-flange intersection in the hanger zone.

The following conclusions are drawn from the analytical study:

6. For targeted non-ductile capacity-to-flexure capacity, the required content of FRP wraps increases with the increase of Yield strength of reinforcement (f_y), Ratio of the effective depth-to-total girder depth (γ), Longitudinal steel ratio (ρ_f) and Punching force-to-shear force ratio $(PF/V)_{ratio}$.

7. For targeted non-ductile capacity-to-flexure capacity, the required content of FRP wraps increases with the decrease of Characteristic concrete compressive strength (f'_c), Ratio of flange over hang-to-width of the web (β), Ratio of flange depth-to-depth of the girder (α), Web transverse reinforcement ratio (ρ_{vw}), Flange transverse reinforcement ratio (ρ_{vf}) and Shear span-to-depth ratio $(a/t)_{ratio}$.

6.3 RECOMMENDATIONS FOR FUTURE RESEARCH

Further experimental studies should be conducted in order to refine the analytical model for the contribution of FRP on different non-ductile failure mechanisms proposed in this study. This can be achieved by varying the parameters discussed in Chapter 3. Consequently, design guidelines can be developed for the rehabilitation of RC inverted-T girders using FRP sheets based on both experimental results and analytical models.

Since FRP sheets are externally bonded to the concrete surface, a better understanding of the bond characteristics of the FRP and concrete interface is required. The current research was limited to reinforced concrete members, yet the rehabilitation scheme should also be extended to prestressed concrete girders.

The performance of FRP-rehabilitated inverted-T girders under fatigue and torsional loading should be studied. Finally, the long-term performance and the durability performance of FRP composite materials exposed to environmental effects should be studied.

REFERENCES

1. ABAQUS, *ABAQUS Version 6.2 User Manual*, ABAQUS Inc., 2003.

2. ACI 318-63, Proposed Revision, "Building Code Requirements for Reinforced Concrete" *ACI Journal Proceedings,* Vol. 67, No.2, Feb 1970.

3. ACI Manual of Concrete Practice, Structural design. Specifications, Structural analysis, Part-2, 1968.

4. ACI Committee 440, "Guide for the Design and Construction of Externally Bonded FRP Systems for Strengthening Concrete Structures (ACI 440.2R-02)," *American Concrete Institute*, Farmington Hills, Mich., pp. 45, 2002.

5. Al-Sulaimani, G.J., Sharif, A., Basunbul, I.A., Baluch, M.H., and Ghaleb, B.N., "Shear Repair for Reinforced Concrete by Fiberglass Plate Bonding." *ACI Structural Journal*, V.91, No.3, 458-464, July-August.1994.

6. An, W., Saadatmanesh, H., and Ehsani, M.R., "RC Beams Strengthened with FRP Plates. Part I: Experimental Study." *ASCE Journal of Structural Engineering*, 3417-3433, 1991.

7. ASTM.. "Standard test method for tensile properties of fiber-resin composites." *D3039-76*, West Conshohocken, Pa, 1989.

8. Bousselham, A. and Chaallal, O., "Shear Strengthening Reinforced Concrete Beams with Fiber-Reinforced Polymer: Assessment of Influencing Parameters and Required Research" *ACI Structural Journal*, V.101, No. 2, March-April 2004.

9. CCE, "Innovations in Bridge Engineering," *Canadian Civil Engineer Magazine*, pp.6, 2006.

10. Chajes, M.J., Januszka, T.F., Mertz, D.R., Thomson, T.A., Finch, W.W., "Shear Strengthening of Reinforced Concrete Beams using Externally Applied Composite Fabrics," *ACI Structural Journal*, V.92, No. 3, 295-302, May-June 1995.

11. Challal, O., Shahawy, M. and Hassan, M., "Performance of Reinforced Concrete T-girders Strengthened in Shear with Carbon Fiber reinforced Polymer Fabrics." *ACI Structural Journal*, V.99, No. 3, 335-343, May-June 2002.

12. Challal, O., Nollet, M.J., and Perraton, D., "Shear Strengthening of Beams by Externally Bonded Side CFRP Strips." *Journal of Composite Construction*, ASCE, V.2, No.1, 111-113, 1998.

13. CHBDC, "Canadian Highway Bridge Design Code", CSA-S6-00, Ontario, Canada, December 2000.

14. CSA., "Design of Concrete Structures" Standard A23.3-04, *Canadian Standards Association*, Mississauga, Ontario, 2004.

15. FIB bulletin No. 14 "Externally Bonded FRP Requirement for RC Structures." Technical Report, *Fédération International du Béton*, France, 2001.

16. Fyfe (2005). "www.fyfeco.com", retrieved September 2005.

17. Furlong, R.W., Ferguson M. and Ma, J.S., "Shear and Anchorage of Reinforcement in Inverted T-beam Bentcap Girders" Research report No. 113-4, *Center for Highway research*, The University of Texas at Austin, July 1971.

18. ISIS Canada. "Strengthening Reinforced Concrete Structures with Externally-Bonded Fiber Reinforced Polymers (FRPs)." University of Manitoba, 2001.

19. Karbhari, V. M., Seible, F., Burgueno, R., Davol, A., Wernli, M., and Zhao, L., "Structural characterization of fiber-reinforced composite short and medium-span bridge systems." *Applied Composite Materials*, 7(2), 151–182.

20. Karbhari, V. M., Zhao, L., "Use of Composites for 21st Century Civil Infrastructure." *Applied Composite Materials*, 433-454, 2000.

21. Khalifa, A., Gold., W.J., Nanni, A., and Aziz, A.M.I., "Contribution of Externally Bonded FRP to Shear Capacity of RC Flexural Members." *Journal of Composites for Construction*, ASCE, 195-202, 1998.

22. Ma, J.S. "Behaviour of Reinforced Concrete Inverted T-Beams" *Ph.D. Dissertation*, University of Texas at Austin, May 1971.

23. Mavichak, V., "Reinforced Concrete Inverted T-beams Loaded in Flexure and Torsion", *M.S. Thesis*, The University of Texas at Austin, Texas, August 1973.

24. Meier, U., "Carbon Fiber-Reinforced Polymers: modern Materials in Bridge Engineering." *Structural Engineering International*, 7-12, 1992.

25. Mirza, S.A. and Furlong, R.W., "Design Of Reinforced and Prestressed Concrete Inverted T Beams for Bridge Structures" *Journal of the Prestressed Concrete Institute*, v 30, n 4, 112-136, Jul-Aug 1985.

26. Mirza, S.A and Furlong, R.W., "Serviceability Behavior and Failure Mechanisms of Concrete Inverted T-Beam Bridge Bentcaps" *Journal of The American Concrete Institute*, v 80, 294-304, Jul-Aug 1983.

27. Mirza, S.A and Furlong, R.W., "Strength Criteria for Concrete Inverted T-Girders." *Journal of Structural Engineering*, v 109, n 8, 1836-1853, Aug 1983.

28. Ritter, W., The building method Hennebique, Schweiseri construction journal, Zurinch, Switzerland, 1899.

29. Teng, T.G., Chen, J.F., Smith, S.T., Lam, L., "RC Structures Strengthened with FRP Composites." Hong Kong, China: Hong Kong Polytechnic University, pp.134, 2000.

30. Triantafillou, T.C., and Antonopoulos, C.P., "Design of Concrete Flexural Members Strengthened in Shear with FRP." *Journal of Composites for Construction*, ASCE, V.4, No. 4, 198-205, 2000.

31. Triantafillou, T.C., "Shear Strengthening of Reinforced Concrete Beams using Epoxy-bonded FRP Composites." *ACI Structural Journal*, 107-115, March-April 1998.

32. Triantafillou, T.C., and Plevris, N., "Strengthening of RC Beams with Epoxy-Bonded Fiber Composite Materials." *Materials and Structures*, RILEM, V.25, 201-211, 1992.

33. Uji, K., "Improving Shear Capacity of Existing Reinforced Concrete Members by Applying Carbon Fiber Sheets." *Transactions of the Japan Concrete Institute*, V.14, 253-266, 1992.

34. Vecchio, F.J., and Collins, M.P., "Response of Reinforced Concrete to In-Plane Shear and Normal Stresses." Publication No. 82-03, Department of Civil Engineering, University of Toronto, pp. 332, March 1982.